

**International
Journal of
Engineering
Technologies
(IJET)**

**Printed ISSN: 2149-0104
e-ISSN: 2149-5262**

**Volume: 3
No: 4
December 2017**

© Istanbul Gelisim University Press, 2017
Certificate Number: 23696
All rights reserved.

International Journal of Engineering Technologies is an international peer-reviewed journal and published quarterly. The opinions, thoughts, postulations or proposals within the articles are but reflections of the authors and do not, in any way, represent those of the Istanbul Gelisim University.

CORRESPONDENCE and COMMUNICATION:

Istanbul Gelisim University Faculty of Engineering and Architecture
Cihangir Mah. Şehit P. Onb. Murat Şengöz Sk. No: 8
34315 Avcilar / Istanbul / TURKEY
Phone: +90 212 4227020 Ext. 221
Fax: +90 212 4227401
e-Mail: ijet@gelisim.edu.tr
Web site: <http://ijet.gelisim.edu.tr>
<http://dergipark.gov.tr/ijet>
Twitter: [@IJETJOURNAL](https://twitter.com/IJETJOURNAL)


Printing and binding:

Anka Matbaa
Certificate Number: 12328
Phone: +90 212 5659033 - 4800571
E-mail: ankamatbaa@gmail.com

International Journal of Engineering Technologies (IJET) is included in:



**International Journal of Engineering Technologies (IJET) is
harvested by the following service:**

Organization	URL	Starting Date	Feature
 The OpenAIRE2020 Project	https://www.openaire.eu	2015	Open Access



INTERNATIONAL JOURNAL OF ENGINEERING TECHNOLOGIES (IJET)
International Peer-Reviewed Journal
Volume 3, No 4, December 2017 Printed ISSN: 2149-0104, e-ISSN: 2149-5262

Owner on Behalf of Istanbul Gelişim University
Rector Prof. Dr. Burhan AYKAC

Editor-in-Chief

Prof. Dr. Mustafa BAYRAM

Associate Editors

Prof. Dr. A. Burak POLAT
Assoc. Prof. Dr. Baris SEVİM
Asst. Prof. Dr. Ahmet AKTAS
Asst. Prof. Dr. Yalcin CEKİC
Asst. Prof. Dr. Ali ETEMADI

Publication Board

Prof. Dr. Mustafa BAYRAM
Prof. Dr. Nuri KURUOĞLU
Prof. Dr. A. Burak POLAT
Asst. Prof. Dr. Ahmet AKTAS
Asst. Prof. Dr. Yalcin CEKİC
Asst. Prof. Dr. Mehmet Akif SENOL

Layout Editor

Asst. Prof. Dr. Ahmet AKTAS

Copyeditor

Res. Asst. Mehmet Ali BARISKAN

Proofreader

Asst. Prof. Dr. Ahmet AKTAS

Contributor

Ahmet Senol ARMAGAN

Cover Design

Mustafa FİDAN
Tarık Kaan YAGAN

Editorial Board

Professor Abdelghani AISSAOUI, University of Bechar, Algeria

Professor Gheorghe-Daniel ANDREESCU, Politehnica University of Timișoara, Romania

Associate Professor Juan Ignacio ARRIBAS, Universidad Valladolid, Spain

Professor Goce ARSOV, SS Cyril and Methodius University, Macedonia

Professor Mustafa BAYRAM, Istanbul Gelisim University, Turkey

Associate Professor K. Nur BEKIROGLU, Yildiz Technical University, Turkey

Professor Maria CARMEZIM, EST Setúbal/Polytechnic Institute of Setúbal, Portugal

Professor Luis COELHO, EST Setúbal/Polytechnic Institute of Setúbal, Portugal

Professor Filote CONSTANTIN, Stefan cel Mare University, Romania

Professor Mamadou Lamina DOUMBIA, University of Québec at Trois-Rivières, Canada

Professor Tsuyoshi HIGUCHI, Nagasaki University, Japan

Professor Dan IONEL, Regal Beloit Corp. and University of Wisconsin Milwaukee, United States

Professor Luis M. San JOSE-REVUELTA, Universidad de Valladolid, Spain

Professor Vladimir KATIC, University of Novi Sad, Serbia

Professor Fujio KUROKAWA, Nagasaki University, Japan

Professor Salman KURTULAN, Istanbul Technical University, Turkey

Professor João MARTINS, University/Institution: FCT/UNL, Portugal

Professor Ahmed MASMOUDI, University of Sfax, Tunisia

Professor Marija MIROSEVIC, University of Dubrovnik, Croatia

Professor Mato MISKOVIC, HEP Group, Croatia

Professor Isamu MORIGUCHI, Nagasaki University, Japan

Professor Adel NASIRI, University of Wisconsin-Milwaukee, United States

Professor Tamara NESTOROVIĆ, Ruhr-Universität Bochum, Germany

Professor Nilesh PATEL, Oakland University, United States

Professor Victor Fernão PIRES, ESTSetúbal/Polytechnic Institute of Setúbal, Portugal

Professor Miguel A. SANZ-BOBI, Comillas Pontifical University /Engineering School, Spain

Professor Dragan ŠEŠLIJA, University of Novi Sad, Serbia

Professor Branko SKORIC, University of Novi Sad, Serbia

Professor Tadashi SUETSUGU, Fukuoka University, Japan

Professor Takaharu TAKESHITA, Nagoya Institute of Technology, Japan

Professor Yoshito TANAKA, Nagasaki Institute of Applied Science, Japan

Professor Stanimir VALTCHEV, Universidade NOVA de Lisboa, (Portugal) + Burgas Free University, (Bulgaria)

Professor Birsen YAZICI, Rensselaer Polytechnic Institute, United States

Professor Mohammad ZAMI, King Fahd University of Petroleum and Minerals, Saudi Arabia

Associate Professor Lale T. ERGENE, Istanbul Technical University, Turkey

Associate Professor Leila PARSA, Rensselaer Polytechnic Institute, United States

Associate Professor Yuichiro SHIBATA, Nagasaki University, Japan

Associate Professor Kiruba SIVASUBRAMANIAM HARAN, University of Illinois, United States

Associate Professor Yilmaz SOZER, University of Akron, United States

Associate Professor Mohammad TAHA, Rafik Hariri University (RHU), Lebanon

Assistant Professor Kyungnam KO, Jeju National University, Republic of Korea

Assistant Professor Hidenori MARUTA, Nagasaki University, Japan

Assistant Professor Hulya OBDAN, Istanbul Yildiz Technical University, Turkey

Assistant Professor Mehmet Akif SENOL, Istanbul Gelisim University, Turkey

Dr. Jorge Guillermo CALDERÓN-GUIZAR, Instituto de Investigaciones Eléctricas, Mexico

Dr. Rafael CASTELLANOS-BUSTAMANTE, Instituto de Investigaciones Eléctricas, Mexico

Dr. Guray GUVEN, Conductive Technologies Inc., United States

Dr. Tuncay KAMAS, Eskişehir Osmangazi University, Turkey

Dr. Nobumasa MATSUI, Faculty of Engineering, Nagasaki Institute of Applied Science, Nagasaki, Japan

Dr. Cristea MIRON, Politehnica University in Bucharest, Romania

Dr. Hiroyuki OSUGA, Mitsubishi Electric Corporation, Japan

Dr. Youcef SOUFI, University of Tébessa, Algeria

Dr. Hector ZELAYA, ABB Corporate Research, Sweden

From the Editor

Dear Colleagues,

On behalf of the editorial board of International Journal of Engineering Technologies (IJET), I would like to share our happiness to publish the twelfth issue of IJET. My special thanks are for members of editorial board, publication board, editorial team, referees, authors and other technical staff.

Please find the twelfth issue of International Journal of Engineering Technologies at <http://ijet.gelisim.edu.tr> or <http://dergipark.gov.tr/ijet>. We invite you to review the Table of Contents by visiting our web site and review articles and items of interest. IJET will continue to publish high level scientific research papers in the field of Engineering Technologies as an international peer-reviewed scientific and academic journal of Istanbul Gelisim University.

Thanks for your continuing interest in our work,

Professor Mustafa BAYRAM
Istanbul Gelisim University
mbayram@gelisim.edu.tr

<http://ijet.gelisim.edu.tr>
<http://dergipark.gov.tr/ijet>

Printed ISSN: 2149-0104

e-ISSN: 2149-5262

International Journal of
Engineering Technologies
IJET

Table of Contents

	<u>Page</u>
<i>From the Editor</i>	<i>vii</i>
<i>Table of Contents</i>	<i>ix</i>
• A Multi-Objective Approach For The In-Plant Milk-Run in a Furniture Factory /	186-189
Erhan Baran	
• Nonlinear Analysis of a Multiple Story Building Under Uniform Blast Loading /	190-195
Namata Saidou Sabiou, Ali Koçak	
• The Investigation of Wear Behaviour of Dual Phase Steel DP600 /	196-201
Yasin Aygül, İsmail Ovalı	
• Binding Energy and Stability Calculations on Hydrogenated Forms of Substituted Carbazoles as Hydrogen Storage Materials /	202-206
Mustafa Karakaya, Fatih Uçun	
• A New Multilevel Inverter Based Parallel Active Power Filter /	207-212
Korhan Karaarslan, Birol Arifoglu, Ersoy Beser, Sabri Camur	
• Effects of Arc Voltage and Welding Current on the Arc Length of Tungsten Inert Gas Welding (TIG) /	213-221
Ikpe Aniekan E., Owunna Ikechukwu, Ememobong Ikpe	
• Interactive Fuzzy Decision Making Algorithm for Two Level Linear Fractional Programming Problems /	222-229
Hasan Dalman	
• Innovative Design for A Ball Worm Gear Mechanism /	230-234
Sait Koçak	

International Journal of Engineering Technologies, IJET

e-Mail: ijet@gelisim.edu.tr

Web site: <http://ijet.gelisim.edu.tr>

<http://dergipark.gov.tr/ijet>

Twitter: [@IJETJOURNAL](https://twitter.com/IJETJOURNAL)

A Multi-Objective Approach for The In-Plant Milk-Run in A Furniture Factory

Erhan Baran*‡

*Industrial Engineering Department, Faculty of Engineering, Hitit University, 19030

(erhanbaran@hitit.edu.tr)

‡Erhan Baran, Industrial Engineering Department, Hitit University, Tel: +90 364 227 4533,

Fax: +90 364 227 4535,erhanbaran@hitit.edu.tr

Received: 18.07.2017 Accepted: 13.12.2017

Abstract- Today, facility optimization is one of the most important decision for the firms while establishing a new factory. It is necessary to carry work-in-process products between the production lines in firms. Many firms use trains to carry these items. In this study, an application is made in a furniture manufacturing factory. Firstly, the routes which the train can use in the firm are created. The alternative routes are compared with each other. The routes contain all of the production lines in the factory. Our aim is to route the train with minimum distance and minimum amount of cargo carrying. In this study, one train is used in the firm. It is also necessary to use minimum train for carrying the work-in-process products. The optimal route is determined by using some of the methods in the literature for multi-objective models.

Keywords Facility logistic, In-plant Milk-Run, Multi-Objective Programming, Vehicle Routing Problem, Tow Train.

1. Introduction

In this study, one of the leading furniture suppliers of the world is investigating a cargo transportation route that can be integrated with the production line and the loading of these trains. It is aimed to develop this process with a systematic viewpoint. In the system studied, it is aimed to optimize the transportation of the materials in the production line between the units in the factory. Today, it is very important to minimize the time loss for factories. In order to be able to compete with the big companies in the sector, it is always necessary to carry out the best works. In this context, it is very important that the trains used in cargo transportation are used regularly on a certain route in a systematic manner with a minimum waiting time between units. In this study, appropriate routes are determined for trains owned by the company, and then a route to reach the whole point was determined with minimum distance in the most appropriate way. It is necessary to design the optimal route in a facility. The sequence and the time is very important. Next section literature review about this study is given. And in other sections, an application is made and the solution is compared with the current situation of the facility. Optimal route means, carrying the items with minimum distance and minimum time.

2. Literature Review

It is necessary to design the optimal route in a facility. The sequence and the time is very important. In this study, multi-objective approach is used for vehicle routing for a firm. In the literature, it is called in-plant milk-run when routing is planned in the firm. In Du et al.'s study, there is a milk-run application between suppliers and customers. Best fit algorithm and 2-exchange algorithm is used for vehicle-dispatching [1]. In Jafari-Eskandari et al.'s study, the milk-run between the supplier and the manufacturer has been studied. A model has been developed that takes account of the advantages and disadvantages of this method. First, a complex mathematical model has been developed. Then the robust optimization approach is used [2]. In Sadjadi et al.'s study, the milk-run is between the suppliers. A mixed number model has been established. However, a meta-intuition was needed because the computation time was too long. Then a genetic algorithm was used [3]. In Nemoto et al.'s study, the milk-run is between the suppliers. The milk-run application of an automobile company in Thailand is explained [4]. In Kovac's study, the milk-run is in stock within the firm. A mixed integer model has been developed. Solved with ILOG CPLEX [5]. In Brar et al.'s study, the literature review for the milk-run is made [6]. In Kilic et al's study, in-plant milk-run is made. 0-1 mixed

integer mathematical model has been developed [7]. In Arvidson’s study, the milk-run is between distribution center and customers. During the milk-run application, different routes (clockwise, counter clockwise) were compared and it was investigated which is better in terms of fuel consumption and time [8]. In Gyulai et al.’s study, a literature review is made for vehicle routing and milk-run [9]. In Ma et al.’s study, the milk-run is between the suppliers. A mutated ant colony algorithm is used [10]. In Hosseini et al.’s study, the milk-run is between the suppliers. The harmony search and annealing simulation algorithm is used [11]. In Hanson et al.’s study, the in-plant milk-run is made. A study has been made on how effective the unit load is in the factory supply [12]. In Novaes et al.’s study, the milk-run is between customers. The dynamic tooling procedure has been developed. Genetic algorithm is used [13]. In Lin et al.’s study, the milk-run is between suppliers. Greedy has developed a two-step heuristic algorithm, which is an intuitive and tabu search algorithm [14]. In Lin et al.’s study, the milk-run is between the suppliers. A two-step heuristic algorithm, greedy heuristic and annealing simulation algorithm, has been developed [15]. In Klenk et al.’s study, in-plant milk-run is made. Various strategies have been developed in order to make the ship better, and 4 different algorithms have been developed for these strategies [16]. In Korytkowski et al.’s study, the in-plant milk-run is made. A milk-run is simulation application was carried out in an assembly line [17]. In this study, an in-plant milk-run application is made by using multi-objective programming in. The difference from the literature is to obtain the route under these objectives.

3. In-Plant Milk-run

There are many types of problems in the literature for carrying the items from somewhere to the target place. In material flow system, items are transferred to the workstations from the warehouse or several supermarkets. And this transfer can be accomplished using tigger trains or forklifts. These trains show that transferring workstations in one trip of the train. This is called “in-plant milk-run” which will decrease the transportation costs [18]. This method is different from the other milk-run application because of the train’s capacity and the demand patterns. Just in time is very important for these problems.

4. Application

In this study, an application is made in a furniture manufacturing factory. In this factory, there is a problem for carrying the items from one cell to another cell in the factory. The tigger train is used to carry the items. In this study an optimal route for the train is obtained by using multi-objective mathematical programming. To solve the multi-objective problems, there are many methods presented in the literature. In this study, ϵ -Constraint Scalarization Method, Weighted-Sum Scalarization and The Augmented Weighted Thebycheff Scalarization Method is compared for this problem. The best of these method is used. There are 6 cells in the factory in this study. The demands of these cells are given below in Table 1.

Table 1. Results for the weighted sum method

<i>Solutions</i>	<i>Objective (F₁,F₂)</i>	<i>Route</i>
1-8	520,350	1-5-3-4-6-2-1
9-16	450,390	1-5-3-4-6-2-1
16-20	420,470	1-5-4-3-2-6-1
21	420,550	1-6-2-3-4-5-1

5. Mathematical Model

In this study, the mathematical model has two objectives. These are; minimizing of total carrying distance and minimizing the amount of cargo carrying. The second objective means that some packages contain more than the target cell needs. So only demand of the cells can be carried by the train. The mathematical model for this problem is given below.

5.1. Notations

i, j : Transportation node index, $i=1,2,3,\dots,6$ and $j=1,2,3,\dots,6$ cell nodes and $i, j=1$ is delivery center or depot node.

d_{ij} : Carrying distance from node i to node j .

R : A set of intermediate nodes.

u_i : It has any real value of node i .

l_{ij} : Carrying amount of item from the way i to node j .

5.2. Objective Functions

$$\min F1 = \sum_{i=1}^6 \sum_{j=1}^6 d_{ij} x_{ij} \tag{1}$$

$$\min F2 = \sum_{i=1}^6 \sum_{j=1}^6 l_{ij} x_{ij} \tag{2}$$

5.3. Constraints

$$\sum_{i=0}^{N_k} x_{ij} = 1 \quad \forall j=1,2,\dots,6 \tag{3}$$

$$\sum_{j=0}^{N_k} x_{ij} = 1 \quad \forall i=1,2,\dots,6 \tag{4}$$

$$u_i - u_j + n. x_{ij} \leq n - 1 \quad \forall i \neq j \in R \tag{5}$$

The equations (1) and (2) are the objective functions of the mathematical model. (3) and (4) constraints are pacified to visit each node at least once. Equation (5) denotes the sub-tour elimination constraint. This type of sub-tour elimination constraints, using Gomory cutting planes approach developed by Miller, Tucker and Zemlin in 1960[19]. These constraints took the tour of the state model to inhibit the formation of approximately (n^2-3n+2) lead to the addition of one constraint [20]. In particular, the use of this Miller, Tucker and Zemlin constraints in oversized model is much easier and routing problems is one of the constraints to improved well-received tour blocking.

6. Computational Results

In this study, there are two objective functions. Firstly, combining these objectives process is made. Three of leading methods in the literature applied. These methods are; The

Weighted-Sum Scalarization Method, The ϵ -Constraint Scalarization Method and The Augmented Weighted Tchebycheff Scalarization Method. For the weighted-sum scalarization method, the mathematical model is solved and the results are given in Table 1.

Second method to combine the objectives is the epsilon-constraint method. In the epsilon-constraint method, one of the objective function is written as a constraint. According to this situation, objective function and constraints have to be written below. Epsilon values are changing between 350-430. The results for the epsilon-constraint method is given in Table 2.

Table 2. Results for the epsilon-constraint method

<i>Solutions</i>	<i>Objective (F₁,F₂)</i>	<i>Route</i>
1-8	420,550	1-6-2-3-4-5-1
9-16	420,470	1-5-4-3-2-6-1
17-19	420,550	1-6-2-3-4-5-1
20-21	420,470	1-5-4-3-2-6-1

The augmented weighted tchebycheff function method is based on the minimization of distance from ideal point. The results for the augmented weighted tchebycheff function method is given in Table3.

Table 3. Results for the augmented weighted tchebycheff function method

<i>Solutions</i>	<i>Objective (F₁,F₂)</i>	<i>Route</i>
1-3	520,350	1-5-3-4-6-2-1
4	490,380	1-5-2-6-4-3-1
5-11	450,390	1-5-6-4-3-2-1
12-21	420,470	1-5-4-3-2-6-1

6. Conclusion

In this study, a multi-objective mathematical is created for the in-plant milk-run problem. The objectives of the problem are combined by three of leading methods in the literature. Then it is examined which method is more effective. According to the results that calculated by GAMS 24.7.1 program, the most efficient scalarization method for the in-plant milk-run problem is ‘Augmented Weighted Tchebycheff Scalarization Method.’. It has the pare to efficient point more in many place number of these places are higher than the other methods have. The optimal point for both objective function is (F₁=420, F₂=470). And also optimal route for this in-plant milk-run is determined. The route must be 1-5-4-3-2-6-1.

References

[1] Timon Du, F.K. Wang, Pu-Yun Lu, “A real-time vehicle-dispatching system for consolidating milk-runs”, *Transportation Research Part E: Logistics and Transportation Review*, 43, 565-577, 2007.

[2] M. Jafari-Eskandari, S.J. Sadjadi, M.S. Jabalameli, A. Bozorgi-Amiri, “A robust optimization approach for the milk-run problem (an auto industry supply chain case industry)”, *Computers & Industrial Engineering*, 6-9 July 2009.

[3] S.J. Sadjadi, M. Jafari, T. Amini, “A new mathematical modelling and a genetic algorithm search for milk-run problem (an auto industry supply chain case study)”, *The International Journal of Advanced Manufacturing Technology*, 44, 194, 2009.

[4] Nemoto, T., Hayashi K., Hashimoto M., “Milk-run logistics by Japanese aotumobile manufactures in Thailand”, *Procedia-Social and Behavioral Sciences*, 2(3), 5980-5989, 2010.

[5] Kovacs, A., “Optimizing the storage assignment in a warehouse served by milk-run logistics”, *International Journal of Production Economics*, 133(1), 312-318, 2011.

[6] Brar, G.S., Saini, G., “Milk-run logistics: literature review and directions”, *Proceedings of the World Congress on Engineering*, 1, WCE 2011, July 6-8 2011.

[7] Kilic, H.S., Durmusoglu, M.B., Baskak, M., “Classification and modelling for in-plant milk-run distribution systems”, *The International Journal of Advanced Manufacturing Technology*, 62(9-12), 1135-1146, 2012.

[8] Arvidsson, N., “The milk-run revisited: a load factor paradox with economic and environmental implications for urban freight transport”, *Transportation Research Part A: Policy and Practice*, 51, 56-62, 2013.

[9] Gyulai, D., Pfeiffer A., Sobottka, T., Vancza, J., “Milk-run vehicle routing problem approach for shop-floor logistics”, *Procedia CIRP*, 7, 127-132, 2013.

[10] Ma, J., Sun, G., “Mutation ant colony algorithm of milk-run vehicle routing problem with fastest completion time based on dynamic optimization”, *Discrete Dynamics in Nature and Society*, 2013.

[11] Hosseini S.D., Shirazi, M.A., Karimi, B., “Cross-docking and mil-run logistics in a consolidation network: a hybrid of harmony search and simulated annealing approach”, *Journal of Manufacturing Systems*, 33(4), 567-577, 2014.

[12] Hanson R., Finnsgard, C., “Impact of unit load size on in-plant materials supply efficiency”, *International Journal of Production Economics*, 133(1), 312-318, 2011.

[13] Novaes, A.G.N., Bez, E.T., Burin, P.J., Aragao Jr., D.P., “Dynamic milk-run OEM operations in over-congested traffic conditions”, *Computers & Industrial Engineering*, 88, 326-340, 2015.

- [14] Lin, Y., Xu, T., Bian, Z., "A two-pahse heuristic algorithm for the common frequency routing problem with vehicle type choice in the milk-run", *Mathematical Problems in Engineering*, 2015.
- [15] Lin, Y., Bian, Z, Shuijing, S., Xu, T., "A two-stage simulated annealing algorithm for the many-to-many milk-run routing problem with pipeline inventory cost", *Mathematical Problems in Engineering*, 2015.
- [16] Klenk, E., Galka, S., Günthner, W.A., "Operating strategies for in-plant milk-run systems", *IFAC-Papers On Line*, 48(3), 1882-1887, 2015.
- [17] Korytkowski, P., Karkoszka,R., "Simulation-based efficiency analysis of an in-plant milk-run operator under disturbances", *The International Journal of Advanced Manufacturing Technology*, 82(5-8), 827-837, 2016.
- [18] Alnahal, M., "In-plant milk-run", *Transportsysteme Und*, Duisburg, Essen University, 2014.
- [19] Bellmore, M., Nemhauser, G.L., "The travelling salesman problem: a survey", *Operations Research*, 16(3), 538-558, 1968.
- [20] Kulkarni, R.V., Bhave, B.R., "Integer programming formulations of vehicle routing problems", *European Journal of Operational Research*, 20(1), 58-67, 1985.

Nonlinear Analysis of a Multiple Story Building Under Uniform Blast Loading

Namata Saidou Sabiou*, Ali Koçak***†

* Department of Civil Engineering, Yıldız Technical University, 34210 Istanbul, Turkey

** Department of Civil Engineering, Yıldız Technical University, 34210 Istanbul, Turkey

(sabiouaidounamata@yahoo.fr, akocak@yildiz.edu.tr)

† Namata Saidou SABIU; Ali KOÇAK, Postal address, Tel: +90 (212) 383 5217,

Fax: +90 (212) 383 5102, namata.saidou@std.yildiz.edu.tr

Received: 22.07.2017 Accepted: 13.12.2017

Abstract- The design of structures to critical can be heavily modified by explosions or shocks effects; in reality, intentional disruptions, blasts, or impacts have unfortunately become part of the possible load scenarios that could act on construction structures during their lifetime. The use of vehicle bombs to attack city centers or bombs intentionally put on construction facilities has been a feature of campaigns by terrorist organizations around the world. A bomb explosion within or immediately nearby a building can cause catastrophic damage on the building's external and internal structural frames, collapsing of walls, blowing out of large expanses of windows, and shutting down of critical life-safety systems. Loss of life and injuries to occupants can result from many causes, including direct blast-effects, structural collapse, debris impact, fire, and smoke. The response of reinforced concrete structures subjected to blast loads can be studied numerically using commercial finite element programs. This paper, hence, to get the structural response of structural elements within a 6 storeys building, which is composed a concrete frame a simulation using the finite element programs ABAQUS.

Keywords: Blast, load, structure, finite element, building.

1. Introduction

A number of analytical and numerical models have been published in the international literature using software's for Scientifics and engineering designs. Blast loads have received more attention in recent years because of accidental or intentional events (terrorist attacks) affected important structures. Traditionally, little research on the blast resistance of structures has appeared in the open literature. Enrin et al. [1] and Ishikawa et al. [2], Studied the performance of prestressed concrete beams when subjected to impact loading, bounded and unbounded prestressed beams were tested experimentally and analytically. It was found that, while static loading resulted in failure of the compression concrete for both the bonded and unbounded specimens, the higher load rate induced by impact resulted in the breaking of the prestressed tendon. Compared to prestressed concrete, reinforced concrete has received much more attention

from researchers over the years. Magnusson and Hallgren [3], in their study revealed that concrete beams show an increased load capacity for blast loading relative to static loading. Luccioni and Luege [4], by analysing the behaviour of concrete pavements subjected to blast loads produced by the detonation of high explosives, performed the tests to assess the concrete pavement slab under blast loads, as a result, the maximum vertical displacement obtained with the finite element model was significantly lower than the one measured experimentally for the third explosion using a 12.5 kg charge.

However, due to the high cost, it is almost impossible to investigate the response of the multi- storey buildings against blast loads with full-scale experimental tests. The analysis and design of structures subjected to blast loads require a detailed understanding of blast phenomena and the dynamic response of various structural elements. Luccioni, Ambrosini and Danesi [5], performed a detailed analysis of the structural failure of a reinforced concrete building caused by

a blast load. However, most of the current numerical modeling research is involved with massive computational time and the model is difficult to build due to its complexity. Therefore, for designers, it is imperative to establish a simple modeling method to study the detailed behavior of the building after the blast denotation. Techniques developed by Feng Fu [6], with ABAQUS, a 3-D finite element model representing a 20-storey building was built to perform the blast analysis, a simplified direct simulation method of blast load is applied, the nonlinear material behavior and dynamic effects are also included in the simulation.

The collapse of a tall building under blast loading can also affect the adjacent buildings. Alex et al. [7], provided an accurate prediction of the effects of adjacent structures on the blast loads on a building in urban terrain. In the paper, a tentative attempt has been made to characterize the blast environment by considering a simple urban configuration with a relatively long, straight street segment and a T-junction at the far end. Numerical simulations using a computational Fluid dynamics (CFD) code Air3D has been used to determine the blast effects on building in a typical urban terrain. Each simulation provided the variation with distance of peak overpressure and impulse. When compared with the corresponding variations for a surface burst of a hemispherical charge in a free-field environment, these variations in the calculation of the pressure and impulse enhancement factors at each scaled distance from the charge. The resulting enhancement factors effectively modify the blast parameters obtained from simplified analytical techniques.

Blast load parameters are reasonably easily determined for rectangular columns and can be derived from either the literature or numerous utility programs. Qasrawi et al. [8], investigated the pressure distribution around a circular column constructed in AUTODYN a numerical model. The model was verified and showed good agreement with established values.

It was found that the column radius increased the maximum reflected pressure at the point closest to the blast approached a maximum of approximately 0.9 of the design value quickly. It was also found that the pressure varied sinusoidal from this maximum to a minimum at the side of the column approximately equal to the incident pressure. The used a sinusoidal function to fit the distribution around the column with good results and this curve fit can be used to find an equivalent design value. A 3-D dynamic analysis of an entire structure is used to determine the effects of an explosion and the response of the structure. D. Makavicka [9], discussed about the methodology for dynamic response assessment and its application to the new RC building. The authors used a specific building as an example to illustrate the problem of an explosion and the threat to the safety of the structure due to the explosion of a rather large terrorist charge installed in a car and initiated on a road adjacent to the building. The structure response was assessed on the basis of the results of 3D dynamic calculation using the

magnitudes of the internal forces and deflections and rotation of the central line of beam or plate sections of the structure. Evaluating a structure on the basis of the rotation of its sections is a methodology under development at present, and is in accordance with recent research trends. The authors have used limit rotation values (failure angle) determined experimentally on the basis of the explosion load of masonry, reinforced concrete and window glass plates, comparing their own results with results published by other authors.

2. Blast Loading

An explosion is a rapid release of stored energy characterized by a bright flash and an audible blast. Part of the energy is released as thermal radiation (flash); and part is coupled into the air as air blast and into the soil (ground) as ground shock, both as radials expanding shock waves. The rapid expansion of hot gases resulting from the detonation of an explosive charge gives rise to a compression wave called a shock wave, which propagates through the air. The blast wave instantaneously increases to a value of pressure above the ambient atmospheric pressure. This is referred to as the positive phase that decays as the shock wave expands outward from the explosion source. After a short time, the pressure behind the front may drop below the ambient pressure, Fig.1. During such a negative phase, a partial vacuum is created and air is sucked in. This is also accompanied by high suction winds that carry the debris for long distances away from the explosion source.

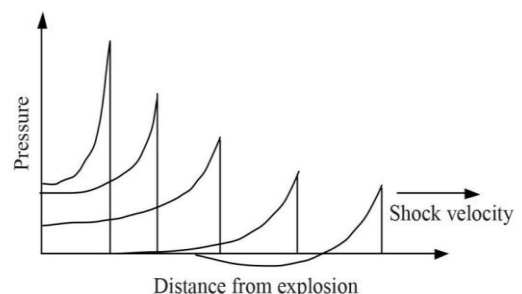


Fig. 1. Blast wave propagation (Abaqus 6.10)

As the shock wave travels outward from the charge, the pressure in the front of the wave, called the peak pressure, steadily decreases as shown in Fig. 2. At great distances from the charge, the peak pressure is infinitesimal, and the wave can be treated as a sound wave. The observed characteristics of air blast waves are found to be affected by the physical properties of the explosion source. At the arrival time t_A , following the explosion, pressure at that position suddenly increases to a peak value of overpressure, P_{so} , over the ambient pressure, P_o . The pressure then decays to ambient level at time t_d , then decays further to an under pressure P_{so}^- (creating a partial vacuum) before eventually returning to ambient conditions at time $t_d + t_d^-$. The quantity P_{so} is usually referred to as the peak side-on overpressure, incident peak overpressure or merely peak overpressure, TM 5-1300 [10].

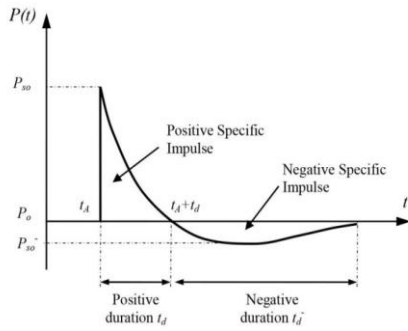


Fig. 2. Blast wave pressure – Time history (Abaqus 6.10)

2.1. Blast Wave Scaling Laws

All blast parameters are primarily dependent on the amount of energy released by a detonation in the form of a blast wave and the distance from the explosion. A universal normalized description of the blast effects can be given by scaling distance relative to $(E/P_0)^{1/3}$ and scaling pressure relative to P_0 , where E is the energy release (kJ) and P_0 the ambient pressure (typically 100 kN/m²). For convenience, however, it is general practice to express the basic explosive input or charge weight W , as an equivalent mass of TNT. Results are then given as a function of the dimensional distance parameter (scaled distance) $Z = R/W^{1/3}$, where R is the actual effective distance from the explosion. W is generally expressed in kilograms. Scaling laws provide parametric correlations between a particular explosion and a standard charge of the same substance.

2.2. Prediction of Blast Pressure

Blast wave parameters for conventional high explosive materials have been the focus of a number of studies during the 1950's and 1960's. Estimations of peak overpressure due to spherical blast based on scaled distance $Z = R/W^{1/3}$ was introduced by Brode (1955) as:

$$P_{SO} = \frac{6.7}{Z^3} + 1bar(P_{SO}) \tag{1}$$

$$P_{SO} = \frac{0.975}{Z} + \frac{1.455}{Z^2} + \frac{5.85}{Z^3} - 0.019 bar \tag{2}$$

$$(0.1 < P_{SO} < 10bar)$$

Newmark and Hansen (1961) introduced a relationship to calculate the maximum blast overpressure, P_{so} , in bars, for a high explosive charge detonates at the ground surface as:

$$P_{SO} = 6784 \frac{W}{R^3} + 93 \left(\frac{W}{R^3} \right)^{1/2} \tag{3}$$

Another expression of the peak overpressure in kPa is introduced by Mills (1987), in which W is expressed as the equivalent charge weight in kilograms of TNT and Z is the scaled distance, as follow:

$$P_{SO} = \frac{1772}{Z^3} - \frac{114}{Z^2} + \frac{108}{Z} \tag{4}$$

In this paper the author used Mills formula shown in the Eq. 4, to calculate the peak overpressure. So the value of pressure calculated for 1m and 2m of stand points are respectively $P_{so} = 1.766MPa$ and $P_{so} = 0.25MPa$.

3. MODELLING

3.1. Numerical Analyze

The structure selected for this study is a 6-storey reinforced concrete building at the height of 18.5m. The length arranged as 6m in the longitudinal direction, and 6m span in the transverse direction. The storey height is 3.5 m for the first storey and a standard storey beyond the first storey is 3.0m. The plan view and structural configuration of the building are shown in Fig.3. The structural system of the building was made up of R.C Frames and Infill frames. The typical beam size used is 350x250mm; the size of the columns is 300 x 300 mm. The rebar used for the concrete beam section are 2φ16 and 2φ14 and for the column are 4φ16. Columns are spaced at 5 m in X direction and 6m in Y direction and are connected with beams and thickness of the slabs is 175mm. Computer Modeling of the building was performed using the finite element software ABAQUS. The 6 storey reinforced concrete building were frame structure of columns, beams, and slabs. The columns and beams were modeled as frame elements while the slabs were modeled as plate elements. The building model was assigned fixed bottom Support condition while a rigid diaphragm constraint was allotted to all floors.

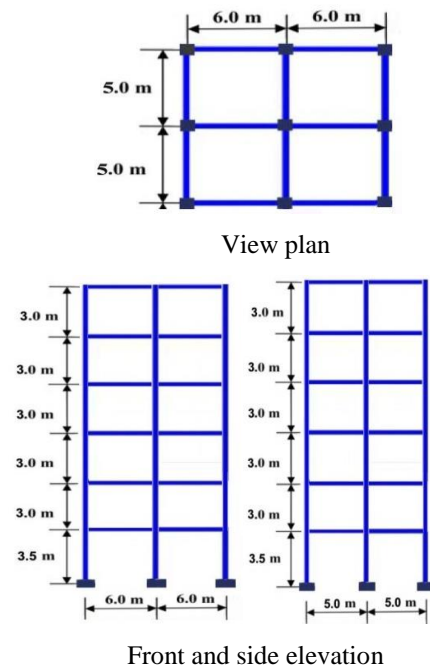


Fig. 3. 6-storey building model

3.2. Analytical model

In this paper, finite element analysis is performed using

the general purpose finite element package ABAQUS /Explicit version 6.10 ABAQUS /Explicit solves dynamic response problems using an explicit direct-integration procedure. In an implicit dynamic analysis, the integration operator matrix must be inverted and a set of nonlinear equilibrium equations must be solved at each time increment. In an explicit dynamic analysis displacements are calculated in terms of quantities that are known at the beginning of an increment; therefore, the global mass and stiffness matrices need not be formed, which means that each increment is relatively inexpensive compared to the increments in an implicit integration (Simulia, [11]). Therefore, explicit method is more efficient than the implicit integration method for solving extremely short-term events such as blast, explosion and impact. Solid elements in 3D were used to model the deformable structure presented in this paper. In this case, C3D8R: 8-node linear brick, reduced integration, hourglass control, 3D Stress explicit was used to model frame Where the influence of mesh size has been studied and is sufficiently fine to ensure the accuracy of Models.

The general approach for solving the non-linear modal analysis, for most realistic results a very small time step is required to obtain a stable solution. In this paper a time step of 0.05ms has been used to make the simulation. The building is designed to resist lateral loads due to wind and seismic ground motion specified by Turkish Regulations on Building. The Fig.4 shows the attack phenome at the structural configuration of the blast attack.

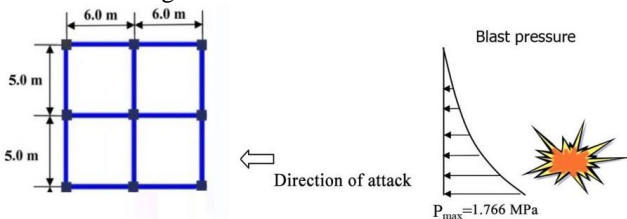


Fig.4. Structural configuration

4. Material Property

a) Concrete

There are several models available for modelling the adhesive based on different criteria for plastic deformation of concrete. Predictions of joint performance at large strains close to joint failure depend on the model used. For the prediction of failure, stress and strain distributions in the adhesive need to be accurately calculated and a failure criterion for the adhesive needs to be established.

In this studies Drucker Prager has been used which is defining as follow:

The Drucker–Prager yield criterion (DP) is a pressure-dependent model for determining whether a material has failed or undergone plastic yielding. The yielding surface of the DP criterion may be considered depending on the internal friction angle of the material and its cohesion. In the space defined by the principal stresses, it is expressed as:

$$-\frac{2 \cdot \text{sen}\phi}{(3 - \text{sen}\phi)} J_1 + \sqrt{1/2 [(\sigma_1 - \sigma_2)^2 + (\sigma_1 - \sigma_3)^2 + (\sigma_2 - \sigma_3)^2]} - \frac{6 \cdot c \cdot \text{cos}\phi}{(3 - \text{sen}\phi)} = 0 \quad (5)$$

Where, $I_1 = \sigma_1 + \sigma_2 + \sigma_3$, $c =$ cohesion, $\phi =$ internal friction angle.

With the purpose of obtaining the classical representation, this yielding surface can be expressed in the following way:

$$(\sigma_1 - \sigma_2)^2 + (\sigma_1 - \sigma_3)^2 + (\sigma_2 - \sigma_3)^2 - A^2 (I_1 + B)^2 = 0 \quad (6)$$

Where:

$$A = \frac{2\sqrt{2} \text{sen}\phi}{3 - \text{sen}\phi}, \quad B = \frac{3c \text{cos}\phi}{\text{sen}\phi} \text{ and } \text{compression}$$

stresses are considered positives in the main stress space.

Fig.5 represents the classical quadric surface for a conventional concrete ($f_c = 25$ MPa) with $c = 4.47$ MPa, $\phi = 30^\circ$. The axis of the cone takes the direction of the vector (1, 1, 1).

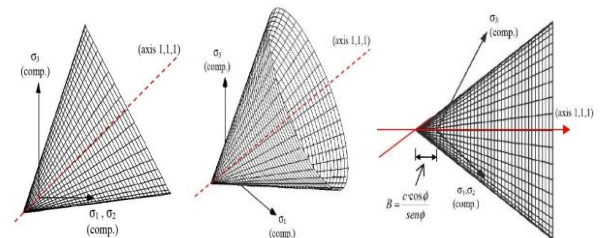


Fig. 5. Graphic representation of the DP criterion

The properties used for the concrete are as shown in the Table 1.

Table 1. Reinforced concrete mechanical properties

Density (kg/m ³)	Elastic modulus (MPa)	Poisson's ratio	Compression Strength (MPa)	Tension Strength (MPa)
2400	2.6000	0.20	25	4

b) Steel

The properties used for the steel are as shown in the Table 2.

Table 2. Reinforcement steel mechanical properties

Density (kg/m ³)	Elastic		Plastic	
	Young's modulus (MPa)	Poisson's ratio	Yield Stress (MPa)	Plastic Strain (MPa)
7.85E-009	210.000	0.30	350	0

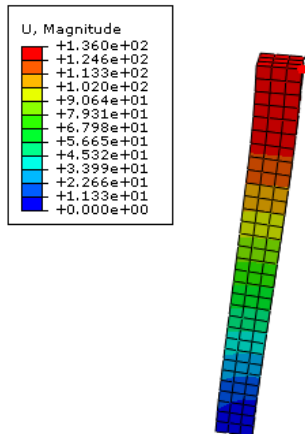
5. Results and discussions

In this study the attack has been occurred outside of the structure so the type of the explosion is classified as the open air explosion, Tehnički vjesnik (2012), which causes a wave that spreads from the source of detonation to the structure without any wave amplification. Due to the blast source's distance and height is away from the structure, the explosion provoked a wave increase due to the reflection of the ground before it contacts the structure. Also the explosion occurred on the ground and the initial pressure is immediately increased as a result of refraction on the ground.

Due to the evolving of high nonlinear behavior and the complexity of the model, to analyses the effect of blast loading, the column located on the left side of the attack at the ground floor has been selected. The Fig.6 illustrated the blast loading after the explosion and selected column deflection.



a) 3D model after the attack



b) A column displacement expressed in mm

Fig. 6. 6- Storey building modelled in ABAQUS

The analysis has done according to the peak pressure and standpoint calculated above. For each peak pressure and stand point the model has been simulated. It can be seen in the Fig.7 that there is a significant difference between two graphics in which the maximum value of displacement in the nodal shown above in the Fig. 6 (b) is: 0.136m for the case $P_{os} = 1.766\text{MPa}$ (standoff distance of 1m) and 0.037 for the case $P_{os} = 0.25\text{MPa}$ (2m).

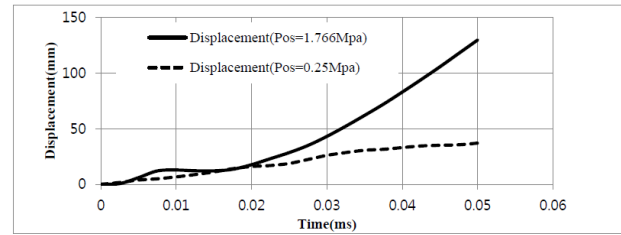


Fig. 7. Nodal displacement curve

After 0.125 ms the strain energy reached the maximum value of 0.146 MPa, in the case: $P_{os} = 1.766\text{MPa}$ (standoff distance of 1m) and got decrease till the failure point as shown in the Fig.8 in color blue. Also the same observation has been made on second curve which also increased from 0.006 MPa at 0.025ms and remain virtually constant.

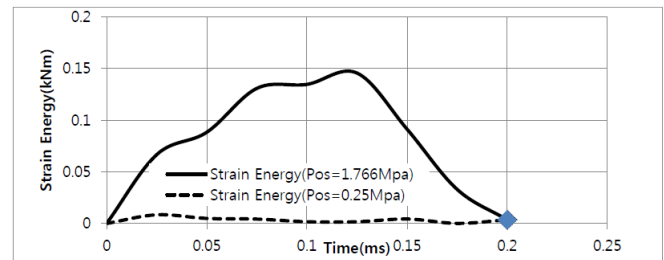


Fig. 8. Strain energy

The stress reach the peak value of 28, 9617 MPa at 0,01ms in the case: $P_{os} = 1.766\text{MPa}$ (standoff distance of 1m) and only at 0.015 reach the peak value of 25.7434 MPa in the second case as shown in the Fig. 9.

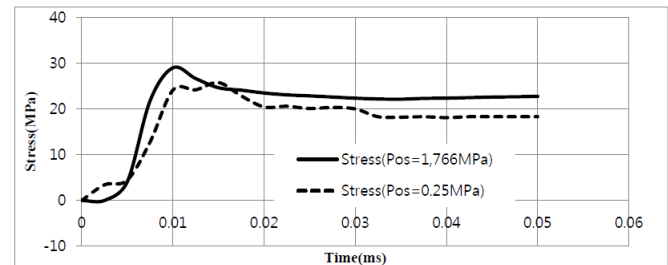


Fig. 9. Stress

The energy release after the explosion for the whole model reached the maximum value of 0. 4 E10 J, after 0.0085 ms as shown in the Fig.10, from zero and at the same moment started decaying till the end of the simulation.

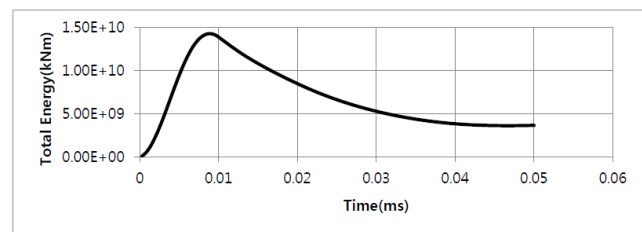


Fig. 10. Total energy.

6. Conclusion

According to the results the system affects significantly when the peak pressure (which is proportional to the charge

weight) increases and standoff distance decreases respectively.

So the standoff distance is the key parameters that determines the blast pressure which decrease so far the effect of blast loading on the structure can be reduce by keeping or prevent the bomb attack as far away as possible by maximizing the standoff distance.

Blast has a characteristic of high amplitude, the results shows that columns subjected to high pressure they could cause big deformation and exceed the support reaction so the columns which are close to explosion are damaged and can be lost. Ones the critical load bearing columns lost which leads to sudden changes in the building geometry and load path which initiates a chain reaction of structural elements failure

The value of the strain energy is higher in the case of major peak pressure because of the higher lateral deflection presented, which shows better energy absorption.

References

- [1] N. Ishikawa, H. Enrin, S. Katsuki and T. Ohta (1998), "Dynamic Behaviour of Prestressed Concrete Beams under Rapid Speed Loading". Department of Civil Engineering, National Defence Academy, 1-10-20 Hashirimizu Yokosuka 239, Japan.
- [2] N Ishikawa, S Katsuki & K Takemoto (2002), "Incremental Impact Test And Simulation Of Prestressed Concrete Beam", Structures Under Shock and Impact VII, N Jones, CA Brebbia and AM Rajendran , ISBN 1-85312-911-9(63),10.
- [3] J. Magnusson & M. Hallgren (2004). "Reinforced High Strength Concrete Beams Subjected to Air Blast Loading", WIT Transactions on The Built Environment, ISSN: 1743-3509(73), 10.
- [4] Luccioni, B.M. and Luege, M. (2006). "Concrete Pavement Slab under Blast Loads", International Journal of Impact Engineering 32(8): 1248-1266.
- [5] B.M. Luccioni, R.D. Ambrosini and R.D. Danesi, (2004). "Analysis of Building Collapse under Blast Loads", Engineering Structures 26 (2004) 63–71.
- [6] Feng Fu, (2009). "Advanced Modeling Techniques in Structural Design", Wiley Blackwell, City University London.
- [7] Alex M. Remennikov and Timothy A. Rose (2005), "Modelling blast loads on buildings in Complex city geometries", Computers & Structures, 83 (27), 2197-2205.
- [8] Y. Qasrawi, P. J. Heffernan & A. Fam (2010). "Numerical Determination of Reflected Blast Pressure Distribution on Round Columns", WIT Transactions on the Built Environment, Vol 113, SN 1743-3509.
- [9] Daniel Makovicka, Daniel Makovicka, Jr. (2010). "Simplified Evaluation of a Building Impacted by a terrorist Explosion", WIT Transactions on The Built Environment, vol. 113, 93-103.
- [10] TM 5-1300 Structures to Resist the Effects of Accidental Explosions, US Army, November 1, 1990.
- [11] ABAQUS User's Manual, Version 6.10, Simulia 2010.

The Investigation of Wear Behaviour of Dual Phase Steel DP600

Yasin Aygül*, İsmail Ovalı**‡

*Department of Manufacturing Engineering, Faculty of Technology, Affiliation of Pamukkale University,
yasin_aygul@yahoo.com

** Department of Manufacturing Engineering, Faculty of Technology, Affiliation of Pamukkale University,
iovali@pau.edu.tr

(yasin_aygul@yahoo.com, iovali@pau.edu.tr)

‡ İsmail Ovalı; Yasin Aygül, iovali@pau.edu.tr, yasin_aygul@yahoo.com, Tel: +90 258 296 4138,

Fax: +90 258 296 41 96, iovali@pau.edu.tr

Received: 23.07.2017 Accepted: 13.12.2017

Abstract- Dual phase steels have been widely used in many applications in the automotive industry. In this study, the wear behaviour of commercially available DP600 steel with dual-phase structure are investigated. The wear rate, volume loss and friction coefficient are used to optimize wear resistance of DP600 steel with dual-phase. Abrasive and Adhesive wear tests were carried out to determine the abrasive friction coefficient of the DP600 steel.

Experimental studies show that the ferrite and martensite phases based on microstructures of the DP600 steel with dual-phase structure have an effect on tensile and wear tests. The wear resistance of DP600 steel can be controlled and optimized with wear condition (the wear rate, volume loss and friction coefficient).

Keywords Dual Phase Steel, Rolling, Flat Product, Wear, Abrasive, Adhesive.

1. Introduction

With the aim of meeting the needs and expectations of the industrial area, many new researches are made by the material engineers day by day in the steel industry. As a result of these studies, steel materials with a light, suitable strength, good deformation ability and high forming ability are foregrounded [1,2].

Dual-phase steels are produced by the critical annealing-quenching process of High Strength Low Alloy (HSLA) steels. It is a low-alloy or non-alloy high-strength steel type containing martensite phase dispersed in ferrite in microstructure. Microstructures also contain trace amounts of austenite, bainite and pearlite. Basic dual phases; Ferrite phase and martensite phase. These steels show many ideal properties when compared to HSLA steels. These; High strength, homogenous forming, percent elongation properties [1,2].

Coldren and Cornford have experimented to produce double-phase steel during ingot hot rolling. Chemical

composition of test samples; 0,065% C, 1-1,2% Mn, 0,9-1% Mo, and 0,05% Al. As a result of the experiment; Samples containing martensite in high amounts showed dual-phase steel properties. Also, contrary to what is expected, they showed double-phase steel properties in samples having 70-90% polygonal ferrite, 0-25% bainitic ferrite and martensite volume above 10% of the steel they produced. The study shows that microstructures having the above-mentioned characteristics can be produced when appropriate cooling conditions are met. As a result of the experiment, there is no significant relationship between residual austenite and mechanical properties [2,3].

Hansen and Bramfitt investigated two different experiments to produce dual phase steel. Critical annealing heat treatment and hot rolling. The chemical composition of the test sample; 0,04-0,11C, 0,80-1,2Mn, 0,51-1,45Si, 0,05-0,65Cr, 0,27-0,62Mo. The Dual-phase steels produced shows similar tensile properties except yield strengths. The yield strength of hot rolled steels is higher. This is caused by the presence of spherical bainite, which forms the third phase, except polygonal ferrite and martensite, which are found in the microstructure. They stated that the

coiling temperature should be below 610 ° C in order to produce martensite without pearlite formation [2,4].

In this study; Abrasive and adhesive wear behaviours of dual phase DP600 steel produced for industrial purposes were investigated. In addition, the yield stress, tensile stress and elongation properties of selected specimens of different orientations of DP600 Steel (Orientation) were examined.

2. Experimental Studies

2.1. Material

In the experimental work, DP600 dual-phase steel with a thickness of 4.5 mm produced by Hot Rolling was selected. The chemical composition of steel is given in Table 1.

Table 1. Chemical composition of the sample (%Wt)

Chemical composition (%Weight)							
%C	%Mn	%Si	%P	%S	%Al	%V	%Ti
0,079	0,82	0,23	0,039	0,0013	0,031	0,001	0,002
%Nb	%Mo	%Ca	%N	%Cu	%Ni	%Cr	%Ti/N
0,000	0,002	0,0011	0,0067	0,02	0,04	0,66	0,3

2.2. Rolling

Production of DP600 steel with dual phase structure used as test samples were carried out by Hot Rolling method. The production line is given in Fig.2.1. Dual-phase steel production in the Hot Rolling process is more economical than other production methods [2,3].

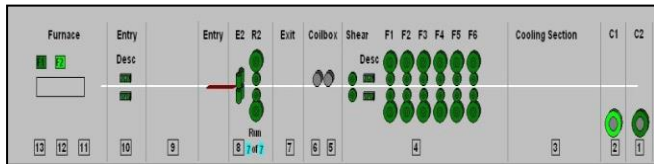


Fig. 1. Hot Rolling process

Production of flat rolled products by hot rolling is carried out as a result of applications at different stations in Figure 2.1. It is annealed to hot shaping temperature in slab. After the annealing process, the slab enters the reaction with oxygen. The oxide layer formed in this reaction is called descaling. Pressurized water is sprayed onto the slab to break the resulting oxide layer. The slab, which is cleaned from the oxide layer on the surface, is first sent to the coarse rolling process and then to the coil box to prevent temperature loss. The slab is subjected to strip rolling according to the order sizes. The slab is then cooled down continuously in the shower tables controlled by the automation system to create the desired microstructure. The strip is then coiler at the appropriate temperature [5].

The rate of cooling of material during rolling is too slow to bring ordinary carbon steels to normal dual-phase steel. At slow cooling rates after rolling, suitable alloying elements should be used to form an ideal dual-phase steel structure. In the production of dual-phase steel by the hot

rolling method, the formation of the structure is difficult to follow. CCT diagrams are used for this [2,3].

The recommended alloying elements are Mn, Cr, Ni and Mo. If quenching is carried out after hot rolling, double-phase steel structure is obtained with less alloy addition [2,3].

2.3. Tensile Test

To make the tensile test, the drawing sample is prepared according to the standards from the material. In this study, test specimens were prepared according to TS 138 EN 100008 standards and experiments were carried out. The selection direction of samples is given in Fig. 2.2. Sheet metal materials exhibit different mechanical properties in different directions (isotropic and anisotropic) The samples are angularly removed from the plate. (R₀, R₄₅, R₉₀) Angular samples are prepared and necessary calculations are made [6].

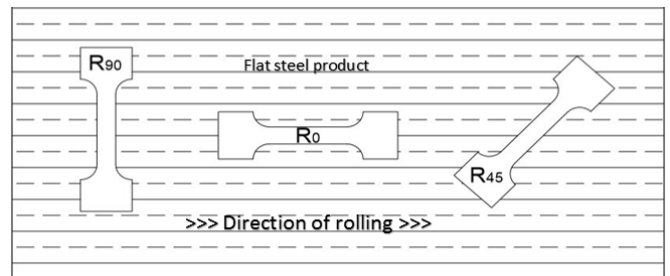


Fig. 2. Tensile test sample selection

2.4. Wear Test

Load on the sample is recorded during wear test in order to get data for calculation of friction coefficient. Eq. (1) was used for defining friction coefficient.

$$\text{The coefficient of friction is, } \mu = \left(\frac{F}{P} \right) \tag{1}$$

Where F is the frictional force measured by the load cell and P is the normal load on the specimen [7].

The volume loss was calculated from the weight loss according to the following Eq. (2).

$$\text{Volume Loss (m m}^3\text{)} = \left(\frac{\text{WeightLoss(g)}}{\text{Density} \left(\frac{\text{g}}{\text{mm}^3} \right)} \right) \times 1000 \tag{2}$$

The wear tests were conducted five times for every sample. The wear rate was calculated from the following Eq. (3) [7]:

$$\text{Wear Rate (mm}^3\text{/m)} = \left(\frac{\text{Volume Loss (mm}^3\text{)}}{\text{Sliding Distance (m)}} \right) \times 1000 \quad (3)$$

Abrasive and adhesive wear tests were carried out on the TURKYUS Pin-On-Disc. The weights and densities during the test were measured on the RADWAG electronic scale [7].

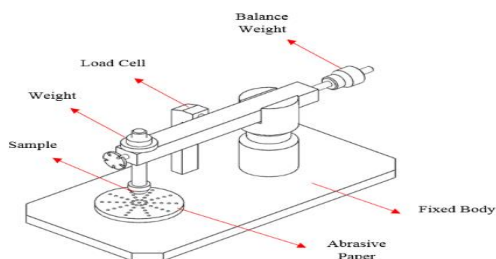


Fig. 3. Pin-On-Disk Wear Device

2.4.1. Abrasive Wear Test

Experiments have been carried out on a pin on disk abrasive wear device designed according to ASTM G99-05 as standard. The wear tester used in the wear tests is given in Figure 5. The surfaces to be abraded of all samples were sanded with 220 mesh SiC abrasive before testing to obtain the same surface quality. The wear tests were carried out at a speed of 3.16 m / s with 5, 10 and 15 N loads. 220 mesh SiC was used as the abrasive disc. Experimental times were determined as 95,190 and 285 meters. The specimens were moved perpendicular to the abrasive disc surface. The weight loss of the samples was also measured with an electronic balance of ± 0.001 g precision. Furthermore, in order to determine the friction coefficient, the frictional forces were measured with the load sensor mounted on the device and the friction coefficients were determined. Before and after the wear test, the samples were cleaned with ethyl alcohol and dried. All samples were subjected to wear test twice as shown in Table 2 and weight loss, volume losses, friction coefficients and wear rates were calculated using the formulas (1,2,3) indicated by the averages of these values [7].

Table 2. Abrasive test parameters

Sample Numbers	Sliding Distance (m/s)	Applied Load (N)	Sliding Distance (m)
DP-600	3,16	5	95
DP-600	3,16	5	190
DP-600	3,16	5	285
DP-600	3,16	10	95
DP-600	3,16	10	190
DP-600	3,16	10	285
DP-600	3,16	15	95
DP-600	3,16	15	190
DP-600	3,16	15	285

2.4.2. Adhesive Wear Test

Load Experiments have been carried out on a pin on disk abrasive wear device designed according to ASTM G99-05 as standard. The wear tester used in the wear tests is given in Figure 5. The surfaces to be abraded of all samples were sanded with 220 mesh SiC abrasive before testing to obtain the same surface quality. The wear tests were carried out at a speed of 3.16 m / s with 5, 10 and 15 N loads. In the experiment; AISI 52100 Bearing Steel material is used as abrasive. AISI 52100 bearing steel has 60 HRC hardness. Experimental times were determined as 95,190 and 285 meters. The specimens were moved perpendicular to the abrasive disc surface. The weight loss of the samples was also measured with an electronic balance of ± 0.001 g precision. Furthermore, in order to determine the friction coefficient, the frictional forces were measured with the load sensor mounted on the device and the friction coefficients were determined. Before and after the wear test, the samples were cleaned with ethyl alcohol and dried. All samples were subjected to wear test twice as shown in Table 3 and weight loss, volume losses, friction coefficients and wear rates were calculated using the formulas (1,2,3) indicated by the averages of these values [7].

Table 3. Adhesive test parameters.

Sample Numbers	Sliding Distance (m/s)	Applied Load (N)	Wear Distance (m)
DP-600	3,16	30	475
DP-600	3,16	30	575
DP-600	3,16	30	665
DP-600	3,16	40	475
DP-600	3,16	40	575
DP-600	3,16	40	665
DP-600	3,16	55	475
DP-600	3,16	55	575
DP-600	3,16	55	665

3. Experimental Results

3.1. Tensile Test Results

The results of three different tensile tests of the two-phase DP600 steel specimen taken in three different directions are given in Table 4.

Table 4. Tensile Test Results

Sample	DP600 R ₀	DP600 R ₄₅	DP600 R ₉₀
Thickness (mm)	4,19	4,16	4,20
Width (mm)	25,37	25,13	25,19
Yield Strength (MPa)	347	359	341
Tensile Strength (MPa)	579	575	572
Elongation (%)	% 34	% 31	% 32

Tensile test results show that there are very similarities in the yield, tensile break results of three differently prepared (R0, R45, R90) samples. The microstructure formed in the sample produced by hot rolling shows the same behaviour in all the sections as isotropic regardless of direction.

Tensile testing of flat steel products produced by hot rolling; It is related to deformation rates, annealing, supply and winding temperatures [8].

The most important parameters determining the yield and tensile strengths in the double-phase steels are the proportions of the ferrite and martensite phases present in the microstructures. The equivalent strength of low-alloy steels, which are used equivalently for dual-phase steels, exhibit approximately the same behaviour as the yield and draw characteristics.

3.2. Wear Test Results

To characterize the wearing behavior of the DP600 Steel; Volume loss, wear rate and coefficient of friction were evaluated.

3.2.1. Volume Loss of Abrasive Sample

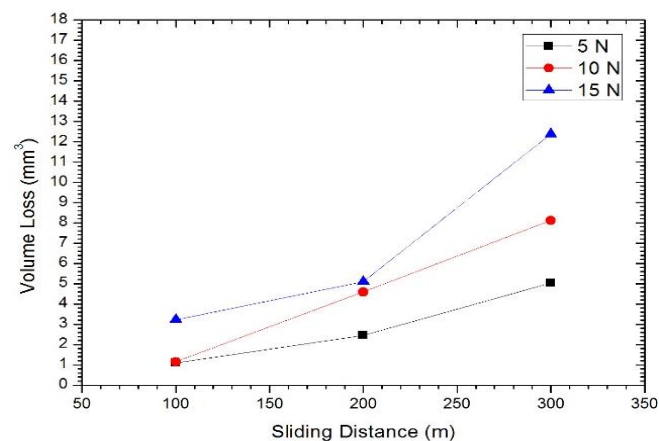


Fig. 4. Volume Loss of Abrasive samples

Volume loss of the abrasive wear test of DP600 Steel under different loads (5N, 10N, 15N) are given in Fig.3.1. The volume loss resulting from the increase in load also increased significantly in the Fig. 6. It can be seen clearly that abrasive wear tests have higher volume loss rates than adhesive wear tests due to abrasives. 5N, 10N and 15N test specimens have similar volume losses up to 200 m. In the range of 200-300 m there is no similarity in volume losses of the samples. The result shows the good correlation of literature study [9].

3.2.2. Volume Loss of Adhesive Sample

In The Fig.3.2 shows the volume loss adhesive wear test of DP600 Steel under different loads (30N, 40N, 55N) Figure 7 shows that volume loss during the test increases significantly at the end of the load increase Similarly, the increase in sliding distance has led to an increase in volume

loss. 40N, 55N test specimens show similarities in volume losses throughout the test period. However, it can be seen that the weight loss profile of 30N test sample is less than the other samples. Our test sample of 55N and 40N showed a noticeable difference from the other sample at 500m, since the force applied by the abrasive was higher. Adhesive wear tests have less volume losses than abrasive wear tests due to abrasive.

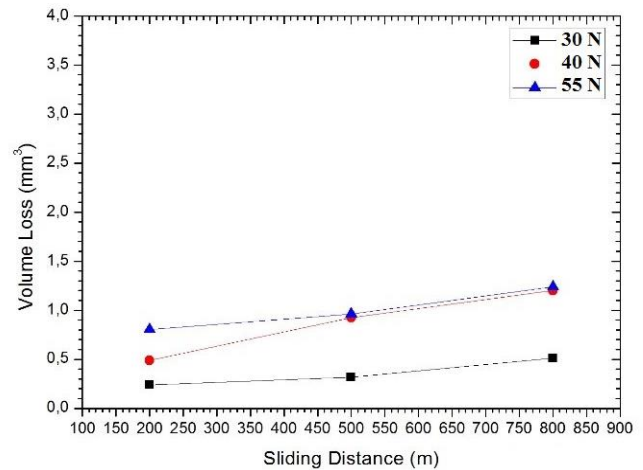


Fig. 5. Volume Loss of Adhesive samples

The volume of adhesive sample in Fig. 6 show good correlation within the literature [9].

3.2.3. Wear Rate of Abrasive Sample

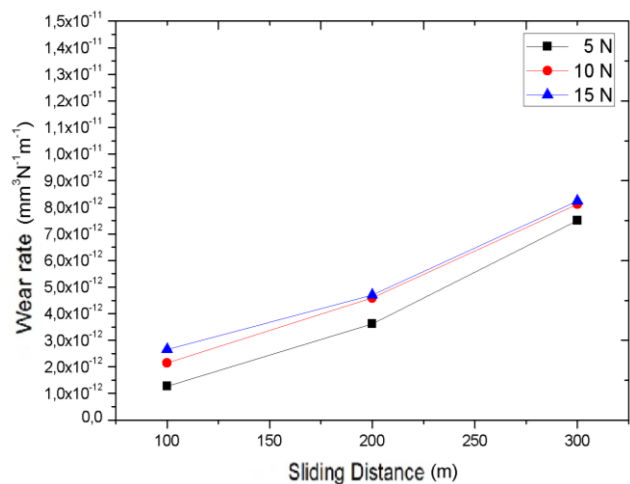


Fig. 6. Wear rate of Abrasive Samples

In the characterization of wear behaviour of steel, the volume losses are not enough alone. In order to determine the effect of sliding distance on wear behaviour, wear rate data should be evaluated.

Fig 6 exhibits abrasive wear test wear rates of the DP600 Steel under different loads (5N, 10N, 15N). 10N and 15N samples showed a similar wear rate at the 300 m sliding distance. In other words, the high sliding distance does not have a significant effect on the 10N and 15N samples. 5N, 10N and 15N samples showed higher wear rates than the

adhesive wear test. This is due to the use of 220 mesh SiC discs which are used as abrasive [7].

3.2.4. Wear Rate of Adhesive Sample

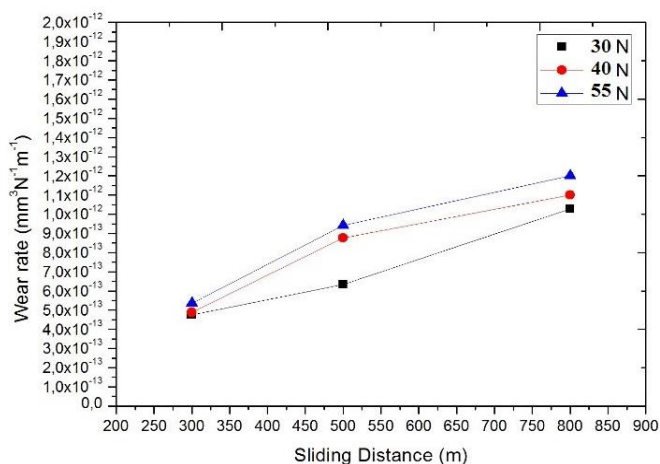


Fig. 7. Wear rate of Adhesive Samples

Wear test were carried out on the graph with different loads (30N, 40N, 55N). Fig. 8 illustrates the of wear rates of adhesive samples. It can be seen that the wear rates obtained as a result of the adhesive wear tests are lower than the abrasive wear rates. This result; Is an abrasive disk type used in adhesive wear tests. 40N and 55N samples exhibit similar wear rates between 300-500 m sliding distances. 35N test sample showed a proportional increase between 300-500 m. Showed a remarkable increase in the range of 500-800 m.

3.2.5. The Friction Coefficient of Abrasive Sample

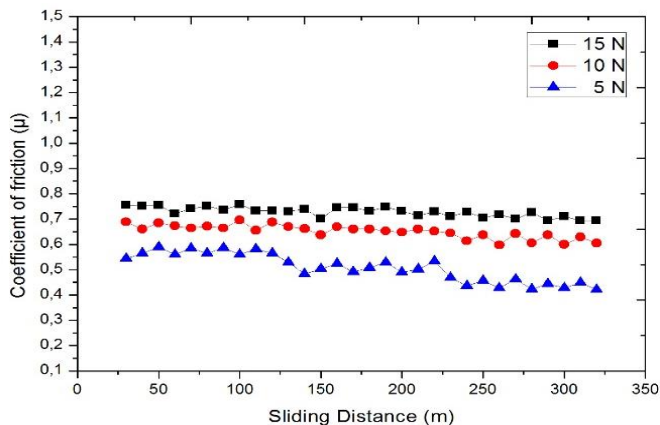


Fig. 8. Friction Coefficient of Abrasive Samples

The most important parameter used in studying the wear behaviour of metals is the friction coefficient. The coefficient of friction is used to characterize how the metals exhibit resistance during wear.

It can be related the coefficient of friction to the force of breaking a piece from a material. If it is easy to break off the material surface, the friction coefficient decreases. If the applied force increases, it should be easier to break the piece.

Tests were carried out on the graph with different loads (5N, 10N, 15N). As a result of the abrasive wear test of the DP600 Steel, the friction coefficient was plotted depending on the sliding distance. In Figure 9 it has been observed that the friction coefficient decreases considerably with increasing force. This result is parallel to the studies in the literature. The highest coefficient of friction was obtained at ~ 0.8 to 5N. The lowest coefficient is seen in the ~ 0.4 to 15N sample.

3.2.6. The Friction Coefficient of Adhesive Sample

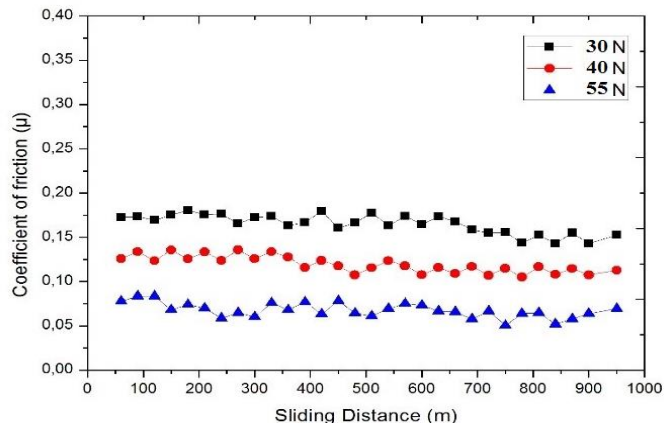


Fig. 9. Friction Coefficient of Adhesive Samples

The friction coefficient of adhesive samples is given in Fig. 9. It can be clearly understood that the friction coefficient is affected by sliding distance. Although the loads on the adhesive wear test are higher than those on the abrasive wear test, there is a significant reduction in their resistance. This is because; The disc used as an abrasive has a metallic structure. All of the samples are beginning to test with a significant increase before 50 mm sliding distance. A decrease in the coefficient of friction is seen with increasing force.

4. Conclusions

In this study; The mechanical properties of commercially available dual phase DP600 steel; Tensile and yield strengths, abrasive, adhesive wear behaviors were investigated. The results obtained are given below.

- Tensile tests were carried out by extracting tensile samples in different rolling directions of the flat test specimen produced after rolling. Tensile strength, tensile strength and breaking elongation of the specimens selected depending on the direction of orientation were determined at the end of the tensile test.
- All samples (isotropic) showed the same behavior regardless of the direction of the sample used as a result of tensile tests.
- As a result of the wear test, volume loss, wear rate and friction coefficients were determined under the slip distance and different loads. In the results of wear obtained; The volume losses and wear rates found in the

abrasive wear differ from the results of the adhesive wear.

- The highest abrasive rates as a result of abrasive wear tests; High sliding distance distance and 15 N load.
- The highest Adhesive rates as a result of abrasive wear tests; High sliding distance distance and 55 N load.

References

[1] Rashid M.S., “GM980X – A Unique High Strenght Sheet Steel with Superior Formability”, SAE, Preprint 760206, (1976).

[2] Demir, B., “Ereğli Demir ve Çelik Fabrikaları Sürekli Tavlama Hatlarında Çift-Fazlı Çelik Üretilirliğinin İncelenmesi”, Doktora Tezi, Gazi Üniversitesi, Fen Bilimleri Enstitüsü, 159 s., Ankara, 2003.

[3] Coldren A.P. & Eldis T., “Using CCT Diagrams to Optimize the Compositions of an as-Rolled Dual Phase Steels”, *Jornal of Metals*, vol:4, no:4, pp:41-48, 1980.

[4] Hansen S.S. & Bramfitt B.L., “Hot Strip Mill Processing of Dual-Phase Steels” *int Conf. On steel Rolling, Sci, and Tech. Of flat Roolled Products*, ISIJ, vol:4, no:7, pp:1297-1308, Tokyo, 1980.

[5] İSDEMİR Sıcak Haddeleme Tesisleri, Hatay (2016)

[6] Gavas, M., Aydın, M., Yaşar, K., Altunpak, Y., “Üretim Yöntemleri ve İmalat Teknolojileri”, Ankara, 2013.

[7] Ovalı, İ., “Küresel Grafitli Dökme Demirlerin Yüzeyinde Çil Oluşumu ve Östemperleme Isıl İşleminin Mikroyapı ve Mekanik Özellikler Üzerine Etkisi”, Gazi Üniversitesi Fen Bilimleri Enstitüsü Doktora Tezi, Ankara, 2012.

[8] Çapan, L., “Metallere Plastik Şekil Verme ” Çağlayan Kitapevi İstanbul, 2003.

[9] Andres, M,R., “Tribological behaviour of DP600 dual phase steel on uni- and bi-directional discontinuous sliding wear”, Madrid, 2015.

Binding Energy and Stability Calculations on Hydrogenated Forms of Substituted Carbazoles as Hydrogen Storage Materials

Mustafa Karakaya*[‡], Fatih Uçun**

*Department of Energy Systems, Faculty of Engineering & Architecture, Sinop University, Sinop 57000, Turkey

**Department of Physics, Faculty of Arts and Sciences, Süleyman Demirel University, 32260 Isparta, Turkey

(mkarakayafizik@hotmail.com, fatihucun@sdu.edu.tr)

[‡] Corresponding Author; Mustafa Karakaya, Sinop University, Sinop 57000, Turkey, Tel.: +90 368 2715516 Fax: +90 368 2714152, mkarakayafizik@hotmail.com

Received: 15.08.2017 Accepted: 13.12.2017

Abstract- The aim of this work is to explore the stable hydrogenated forms of carbazole and 9-methylcarbazole molecules by using M06-2X density functional as computational method. Binding energies per hydrogen atom in these hydrogenated forms were calculated by the counterpoise correction procedure. Relative energies, complexation and binding energies for the conformers of dodecahydrocarbazole were also calculated. Stabilities of all the hydrogenated forms were discussed by the analysis of the frontier molecular orbitals.

Keywords: Hydrogen energy technologies; hydrogenation; M06-2X theory; binding energy.

1. Introduction

Hydrogen is an important energy source that is shield to the global climate changes against the ever-increasing energy demands [1]. Hydrogen technologies relates to development of new methods in areas such as obtain the hydrogen, storage and processing. Also these technologies give very effective results in science to prevent negative environmental impacts and create green energy sources. Hydrogen storage methods are classified as pressurized hydrogen, carbonaceous materials, metal and complexation hydrides, organic liquids according to storage capacity (wt%), safety, stability and transaction costs [2–6].

Carbazole structures in liquid organic hydrides are noteworthy with reversible hydrogen sorption characteristics as hydrogen storage materials [7]. Liquid organic hydrides have significant advantages in hydrogen storage as access to high gravimetric hydrogen storage level, lack of carbon monoxide and carbon dioxide emissions as by-products [7, 8]. Hydrogenation and dehydrogenation techniques are used in the process of hydrogen storage and releasing,

respectively, for the organic liquid hydrides [2, 9–11]. Hydrogenation is the process of adding hydrogen under pressure with the aid of a catalyst. The aim of this procedure is that the hydrogen atoms attend to multiple bonds. In the hydrogenation reaction, alkene is converted to alkane condition by addition of the hydrogen to the unsaturated carbon chemical bond. The dehydrogenation process is the opposite of this. Hydrogenation and dehydrogenation kinetics and catalysis of carbazole derivatives and influences of the reaction temperature and pressure have been experimentally studied in the literature [12–14].

In this study we have theoretically aimed to investigate and interpreted the hydrogen binding energies, complexation energies and energy gaps between frontier (highest occupied and lowest unoccupied) molecular orbitals on the hydrogenated forms of substituted carbazoles as hydrogen storage materials via computational methods. Before anything else, we have determined the optimized molecular forms of carbazole (S1), 9-methylcarbazole (S2) and octahydro-, dodecahydro- structures as their hydrogenated forms. The next phase of our study consists of the

evaluations about the relationship between hydrogen binding energies, frontier molecular orbitals and hardness of all the S1-S2 hydrogenated forms to determine their chemical reactivity and stability.

2. Computational details

All the quantum calculations on the structural optimizing processes and molecular orbitals were performed by using M06-2X theory combined with 6-31+G (d,p) basis set level. Inputs on the atomic coordinates for all the geometry optimizations were created by Gauss View program [15]. Optimizations and computations on the S1, S2 hydrogenated forms and the atomic hydrogen binding energies were obtained by using Gaussian 09W software database [16]. Basis set superposition error (BSSE) corrections,

complexation and binding energies were calculated by the counterpoise correction procedure (CP) [17].

3. Results and discussion

Fig.1 is inclusive the optimized molecular structures of S1, S2 and their hydrogenated forms obtained by the output of quantum computing. In the figure the hydrogens of which the binding energies will be calculated, are located in the green zone. The minimum-energy structures of S1 and S2 have -517.280 and -556.571 a.u. of energies at M06-2X calculation method and 6-31+G (d,p) basis set, respectively. Calculated relative energies and hydrogen binding energies which bind to carbons have been reported in Table 1 for the substituted carbazoles and their hydrogenated forms.

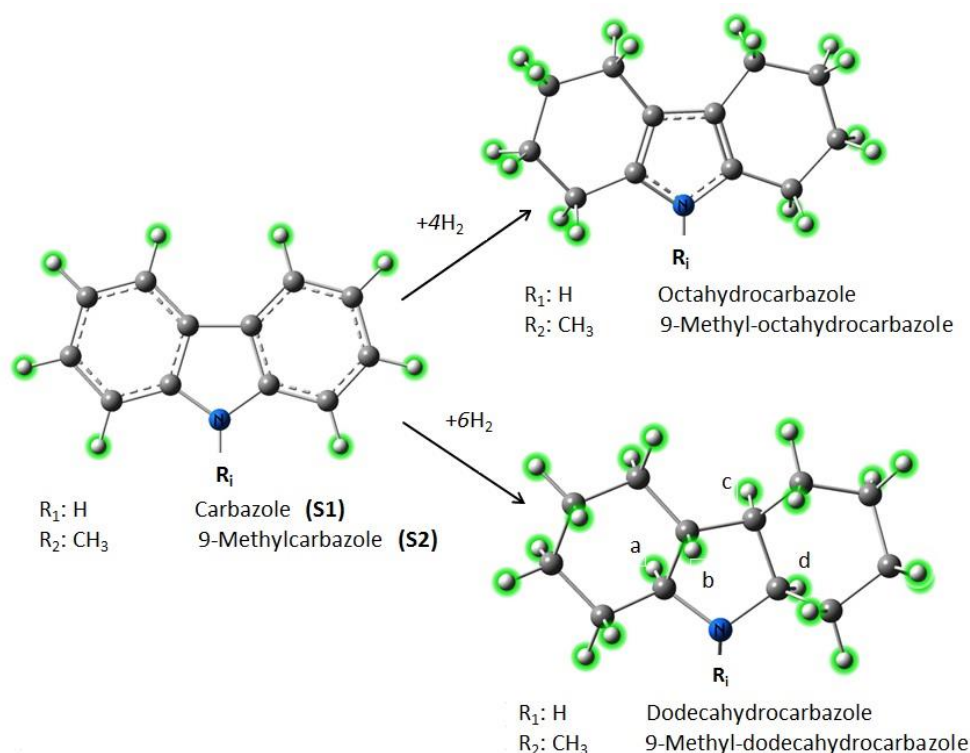


Fig. 1. Optimized structures of S1, S2 and their hydrogenated structures computed at M06-2X theory, 6-31+G (d,p) level

The average values of relative energies per hydrogen atom are 16.24 and 16.28 eV for S1+nH₂ and S2+nH₂ forms, respectively. Total binding energies for the hydrogen atoms attached to carbons have been calculated as -45.815 and -45.744 eV in the S1 and S2 structures, respectively. These values are approximately -82.979 and -82.902 eV in the S1+6H₂ and S2+6H₂ hydrogenated forms, respectively. While the binding energies per hydrogen atom are -5.727 and -5.718 eV in the S1 and S2 structures, these results are -4.149 and -4.145 eV in the S1+6H₂ and S2+6H₂, respectively.

On the other hand, the calculated BSSE energies are increasingly on the rise in hydrogenated forms of S1, S2. This situation can be attributed to positioning where there are involved fragments and of course, to the applied method and

basic set. While the number of functions included in the basic set increases, the BSSE energy is reduced. So, The BSSE energy has a small value in a large basis set. Another factor that affects the BSSE energy value is occupied or unoccupied orbitals. Unoccupied orbital's give greatly an e increasing effect in the BSSE energy.

For the dodecahydrocarbazole structures in Fig. 1, we like to examine the conformers for which the relative values between the ground state energies are many minor by calculation method. The relative energies, complexation and binding energies for the conformers of dodecahydrocarbazoles are given in Table 2. The positioning of the conformers has been identified at the bottom line of Table 2 (see also Fig. 1). Considering the total energies, we say that the most stable optimization is conformer 1 for the

both hydrogenated forms (+6H₂). The calculated energy differences between the various conformations for +nH hydrogenated forms of 9-ethylcarbazole have been calculated by Density Function Theory (DFT) method with the B3LYP hybrid functional including electron correlation in a previous study [7].

Table 1. Calculated relative and hydrogen binding energy values for substituted carbazoles and, their hydrogenated forms.

Organic Liquid Materials	Relative Energy* (eV)	Binding Energy** Per Hydrogen Atom (eV)
S1	0.000	-5.727
+2H ₂	64.822	-4.732
+4H ₂	129.592	-4.242
+6H ₂	195.785	-4.149
S2	0.000	-5.718
+2H ₂	64.783	-7.080
+4H ₂	130.559	-3.994
+6H ₂	195.795	-4.145

* Relative values between the total energy

** obtained by using CP corrected energy.

As seen in Table 2 the minimal corrected complexation energies have been computed as -84.541 (conformer 5) and -84.350 eV (conformer 2), approximately. The lower value of the complexation energy corresponds to the more stable complex [18]. Also, the conformer 5 in the S1+6H₂ and the conformer 2 in S2+6H₂ have minimal values as binding energy per hydrogen atom. In the both hydrogenation structures, the conformers 2 and 5 draw attention with their minimum complexation and binding energies. In here we take into account the conformers 1 for the dodecahydro-structures in the calculations and in the comments relating to binding energy and molecular orbitals since they have the minimum total energies.

The first and second frontier molecular orbitals and energy diagrams of S2+6H₂ hydrogenated form have been displayed in Fig. 2. The claret red and green tones represent the positive and negative wave functions, respectively, for the orbitals. The visual for the highest occupied molecular orbital is scattered over the nitrogen and the carbons close to the nitrogen. The positive wave functions for the lowest unoccupied orbitals are focused in the C-H bonds. Frontier molecular orbitals (HOMO and LUMO), act as the electron donor and acceptor, respectively, and these orbital energy values explain the optical and electrical properties of the molecules in quantum computations [19-21].

HOMO-LUMO energy gaps and chemical hardness in hydrogenated carbazoles are given in Table 3. The type of bonding interaction can be explained by the topic of the

highest occupied and lowest unoccupied orbital energies and also molecules with high HOMO energies are more reactive and of course unstable [22].

Table 2. Calculated relative, complexation and hydrogen binding energy values for conformers of dodecahydrocarbazole formed according to positions of hydrogens attached to carbons.

Conformers	Relative Energy (eV)	Complexation Energy [corrected] (eV)	Binding Energy Per Hydrogen Atom (eV)
S1+6H₂			
1	0.000	-82.975	-4.149
2	0.2060	-84.312	-4.216
3	0.2062	-83.627	-4.182
4	0.3389	-84.219	-4.211
5	0.4403	-84.541	-4.227
6	0.5453	-83.828	-4.191
S2+6H₂			
1	0.000	-82.897	-4.145
2	0.1690	-84.350	-4.218
3	0.2039	-83.862	-4.193
4	0.3860	-84.090	-4.205
5	0.5478	-84.252	-4.213
6	0.4972	-83.773	-4.189

Conformer 1= b(front),acd(back); 2= abcd(front); 3=ab(front),cd(back); 4=abc(front),d(back); 5=ac(front),bd(back); 6=bc(front),ad(back)

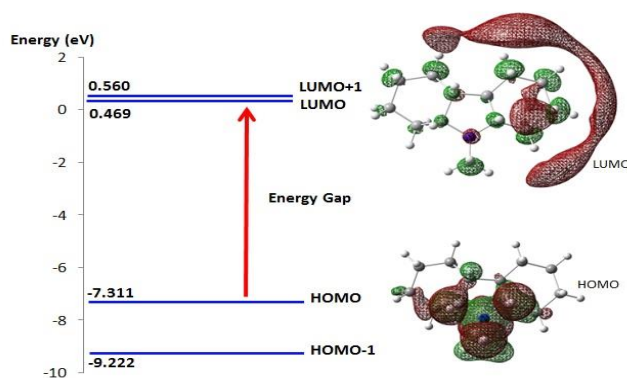


Fig. 2. Highest and lowest energy levels of occupied and unoccupied orbitals for S2+6H₂ hydrogenated forms

As seen in Table 3, the HOMO energies have been computed at the highest values in the octahydro- structures. The energy gaps in FMO's comment the intramolecular charge transfer interactions and, its lower value means a

more reactive molecule, chemically [23]. On the other hand, the higher values of hardness are directly related to the stability [23-26]. The octahydro- structures have smaller energy gaps relative to the others in this study. Conversely, the maximal energy gaps have been computed in the S1+6H₂ and S2+6H₂ hydrogenated forms. The calculation results for the chemical hardness support that the stabilities of S1+6H₂ and S2+6H₂ hydrogenated forms are highest.

Table 3. HOMO energies, energy gaps and chemical hardnesses for substituted carbazoles and their hydrogenated forms

Organic Liquid Materials	HOMO energy (eV)	Energy Gap (eV)	Chemical Hardness (eV)
S1	-6.978	6.724	3.362
+2H ₂	-6.616	6.850	3.425
+4H ₂	-6.286	6.638	3.319
+6H ₂	-7.565	7.902	3.951
<hr/>			
S2	-6.811	6.571	3.286
+2H ₂	-6.480	6.773	3.386
+4H ₂	-6.270	6.572	3.286
+6H ₂	-7.311	7.780	3.890

4. Conclusion

In present study, the hydrogenated forms of substituted carbazoles have been achieved by the output of quantum computing at M06-2X theory, 6-31+G (d,p) level. Considering the total energies, the most stable optimization is conformer 1 for the S1+6H₂ and S2+6H₂ structures. But the conformers 2 and 5 have drawn our attention with their minimum complexation (corrected) and binding energies per hydrogen atom. As for the hydrogenated forms, S1+4H₂ and S2+4H₂ are more reactive than the other forms according to the highest occupied molecular orbitals. Conversely, the stabilities of the S1+6H₂ and S2+6H₂ hydrogenated forms are highest since of their maximal energy gaps.

Acknowledgements

This study was financially supported by Sinop University with the project number of MMF-1901.14-01. The author gratefully acknowledges the support of Sinop University, the presidency of project management office.

References

[1] V. Balema, "Hydrogen Storage Materials", *Material Matters*, vol. 2, pp. 1-31, 2007.

[2] Z. Jiang, Q. Pan, J. Xu, T. Fang, "Current situation and prospect of hydrogen storage technology with new organic liquid", *Int. J. Hydrogen Energ.*, vol. 39, pp. 17442-17451, 2014.

[3] P. Chena, M. Zhu, "Recent progress in hydrogen storage", *Mater. Today*, vol. 11, pp. 36-43, 2008.

[4] S.G. Chalka, J.F. Miller, "Key challenges and recent progress in batteries, fuel cells, and hydrogen storage for clean energy systems", *J. Power Sources*, vol. 159 (1), pp. 73-80, 2006.

[5] W. Peschka, C. Carpetis, "Cryogenic hydrogen storage and refueling for automobiles", *Int. J. Hydrogen Energ.*, vol. 5(6), pp. 619-625, 1980.

[6] E. Rönnebro, "Development of group II borohydrides as hydrogen storage materials", *Curr. Opin. Solid St. M.*, vol. 15(2), pp. 44-51 2011.

[7] K.M. Eblagon, D. Rentsch, O. Friedrichs, A. Remhof, A. Zuetzel, A.J. Ramirez-Cuesta, S.C. Tsang, "Hydrogenation of 9-ethylcarbazole as a prototype of a liquid hydrogen carrier", *Int. J. Hydrogen Energ.*, vol. 35, pp. 11609-11621, 2010.

[8] N. Kariya, A. Fukuoka, T. Utagawa, M. Sakuramoto, Y. Goto, M. Ichikawa, "Efficient hydrogen production using cyclohexane and decalin by pulse spray mode reactor with Pt catalyst", *Appl. Catal. A*, vol. 247, pp. 247, 247-59, 2003.

[9] R.H. Crabtree, "Hydrogen storage in liquid organic heterocycles", *Energy Environ. Sci.*, vol. 1, pp. 134-8, 2008.

[10] F. Alhumaidan, D. Cresswell, A. Garforth, "Hydrogen storage in liquid organic hydride: producing hydrogen catalytically from methylcyclohexane", *Energy Fuels*, vol. 25, pp. 4217-34, 2011.

[11] A. Shukla, S. Karmakar, R.B. Biniwale, "Hydrogen delivery through liquid organic hydrides: considerations for a potential technology", *Int. J. Hydrogen Energ.*, vol. 37, pp. 3719-26, 2012.

[12] X. Ye, Y. An, G. Xu, "Kinetics of 9-ethylcarbazole hydrogenation over Raney Ni catalyst for hydrogen storage", *J. Alloy. Compd.*, vol. 509, pp. 152-156, 2011.

[13] F. Sotoodeh, B.J.M. Huber, K.J. Smith, "Dehydrogenation kinetics and catalysis of organic heteroaromatics for hydrogen storage", *Int. J. Hydrogen Energ.*, vol. 37, pp. 2715-2722, 2012.

[14] F. Sotoodeh, B.J.M. Huber, K.J. Smith, "The effect of the N atom on the dehydrogenation of heterocycles used for hydrogen storage", *Appl. Catal. A-Gen.*, vol. 419-420, pp. 67-72, 2012.

[15] R. Dennington, T. Keith, J. Millam, GaussView, Version 5.0.9, Semichem Inc., Shawnee Mission, KS, 2009.

- [16] M.J. Frisch, G.W. Trucks, H.B. Schlegel, G.E. Scuseria, M.A. Robb, J.R. Cheeseman et al., Gaussian 09, Revision D.01, Gaussian, Inc., Wallingford CT, 2009.
- [17] S.F. Boys, F. Bernardi, "The calculation of small molecular interactions by the differences of separate total energies. Some procedures with reduced errors", *Mol. Phys.*, vol. 19, pp. 553-566, 1970.
- [18] M.J. Jenita, A. Antony, M. Prabhu, N. Rajendiran, "Theoretical study of inclusion complexation of tricyclic antidepressant drugs with β -cyclodextrin", *Indian Journal of Chemistry*, vol. 51A, pp. 1686-1694, 2012.
- [19] I. Fleming, "Frontier orbitals and organic chemical reactions", Wiley, London, 1976.
- [20] M. Govindarajan, M. Karabacak, A. Suvitha, S. Periandy, *Spectrochim. Acta A*, vol. 89, pp. 137-148, 2012.
- [21] M.M. El-Nahass, M.A. Kamel, E.F. El-deeb, A.A. Atta, S.Y. Huthaily, *Spectrochim. Acta A*, vol. 79, pp. 443-450, 2011.
- [22] H. Ullah, A.A. Shah, S. Bilal, K. Ayub, "DFT Study of Polyaniline NH₃, CO₂, and CO Gas Sensors: Comparison with Recent Experimental Data", *J. Phys. Chem. C*, vol. 117, pp. 23701-23711, 2013.
- [23] S. Armaković, S.J. Armaković, J.P. Šetrajić, L.D. Džambas, "Specificities of boron disubstituted sumanenes", *J. Mol. Model.*, vol. 19, pp. 1153-1166, 2013.
- [24] K.R.S. Chandrakumar, T.K. Ghanty, S.K. Ghosh, "Relationship between ionization potential, polarizability, and softness: a case study of lithium and sodium metal clusters", *J. Phys. Chem. A*, vol. 108, pp. 6661-6666, 2004.
- [25] R.G. Parr, P.K. Chattaraj, "Principle of maximum hardness", *J. Am. Chem. Soc.*, vol. 113, pp. 1854-1855, 1991.
- [26] P.K. Chattaraj, H. Lee, R.G. Parr, "HSAB principle", *J. Am. Chem. Soc.*, vol. 113, pp. 1855-1856, 1991.

A New Multilevel Inverter Based Parallel Active Power Filter

Korhan Karaarslan*[‡], Birol Arifoglu*, Ersoy Beser*, Sabri Camur*

*Department of Electrical Engineering, Kocaeli University, Umuttepe Campus 41380 Izmit, Kocaeli, Turkey

(korhan.karaarslan@kocaeli.edu.tr, barif@kocaeli.edu.tr, ebeser@kocaeli.edu.tr, scamur@kocaeli.edu.tr)

[‡]Corresponding Author; Korhan Karaarslan, Department of Electrical Engineering, Kocaeli University, Umuttepe Campus 41380 Izmit, Kocaeli, Turkey, Tel: +90 542 420 2022,

Fax: +90 262 303 3003, korhan.karaarslan@kocaeli.edu.tr

Received: 14.09.2017 Accepted: 13.12.2017

Abstract- Developments in the field of power electronics have increased the use of non-linear loads. The increase in the use of these loads causes power quality to decrease and problems to appear in transmission and distribution systems. The adverse effect of passive harmonic filters and the up-growing use of modern sensitive loads in the production process have made active power filters an important area of interest in eliminating current and voltage harmonics. In this study, a multilevel inverter topology for parallel active power filter applications has been proposed. The principle of operation for the proposed multilevel inverter topology is explained in detail. The harmonic components of the grid current which has a high total harmonic distortion (THD) value, are eliminated by the proposed multilevel inverter providing a reduced number of switching elements. The generation of switching signals for parallel active power filter application is also expressed with generalized formulas. All required operating states of multilevel inverter topology are given in detail to obtain reference filter current with harmonic components. In addition, the simulation studies carried out for different number of level modules and different values of harmonic distortion are presented. The obtained results show that the proposed multilevel inverter topology is suitable for parallel active power filter applications.

Keywords Active power filter, multilevel inverter, total harmonic distortion, power quality.

1. Introduction

The widespread use of nonlinear loads such as arc and ladle furnaces, motor drivers, switched-mode power supplies, rectifiers and dc/dc converters has increased due to advances in the field of power electronics. Such loads cause power quality problems in transmission and distribution systems. Current and voltage harmonics as a problem of power quality become more considerable in parallel with the increasing use of modern sensitive loads in the production process [1].

Due to the ever-increasing power quality problems, active filtering solutions are of interest for harmonic suppression since the conventional passive filters have adverse effects such that they are affected by the grid impedance and can filter only for the specified harmonic component.

Active power filters, which can be applied to solve many problems such as filtering harmonics, reactive power

compensation, resonance suppression and voltage regulation, are mainly classified into two groups according to the grid connection modes; parallel and series active power filters. Parallel active power filters are used to eliminate problems created by non-linear loads acting as harmonic current sources, while series active power filters connected to the system via a transformer provide voltage regulation by eliminating voltage harmonics.

The operation principle of the active power filters is based on the generation of the reference current and/or voltage waveforms obtained by a set of control techniques from the sampled load current and/or voltage with the help of controlled semiconductor power switches [1]. Based on this operation, it can be said that active power filters consist of three main parts as shown in Fig.1; harmonic detection unit, control unit and inverter unit. Generally, the harmonic detection unit and the control unit are defined together. The harmonic detection unit detects the harmonics from the

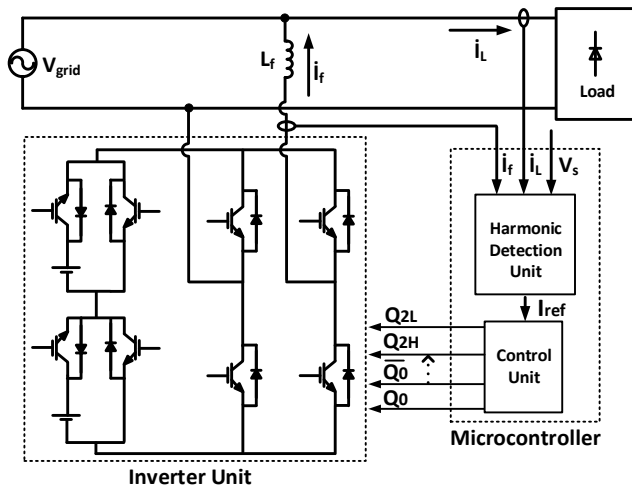


Fig. 1. The principle scheme of parallel active power filter with main parts

sampled load current and/or voltage by means of an algorithm thus determining the reference signal. Algorithms developed for the determination of harmonics are carried out in this unit. These algorithms are generally divided into two groups as frequency and time domain based methods. The frequency domain methods used to determine harmonics in active power filters are Discrete Fourier Transform (DFT), Fast Fourier Transform (FFT) and Sliding-Discrete Fourier Transform (S-DFT).

The time domain methods applied for the same purpose are instantaneous power theory (p-q theory), artificial neural network based techniques, constant reference ($\alpha\beta$) transformation, synchronous reference (dq) transformation and hybrid ($\alpha\beta/dq$) transformation [2-3].

At the input of the current and/or voltage control unit, there is the reference signal determined at the harmonic detection unit while the switching signals of the inverter unit are found at the output. The contribution of this unit to the operating principle of the active power filter is the generation of switching signals for controlled semiconductor power switches. For this purpose, it is seen that different control techniques such as Pulse Width Modulation (PWM), Sinusoidal PWM, hysteresis control and recently used "dead-beat" control are used in the literature.

The inverter unit is the part where the filter output voltage (V_{AB}) is obtained according to the reference voltage. The switching signals from the control unit are used to generate the filter output voltage of the inverter. In the literature, many studies have been carried out with different inverter units to reduce the complexity of the control method by reducing the number of semiconductor power switches [4]. When many features such as switching frequency, dv/dt voltage stress on switching elements, efficiency, electromagnetic interference, harmonic distortion and output filter requirement are taken into consideration, multilevel inverter topologies are often preferred for active power filter applications [5-7]. In the literature, although there are studies on active power filters with diode-clamped and flying-capacitor inverters, it has been determined that the most common multilevel topology in active power filter

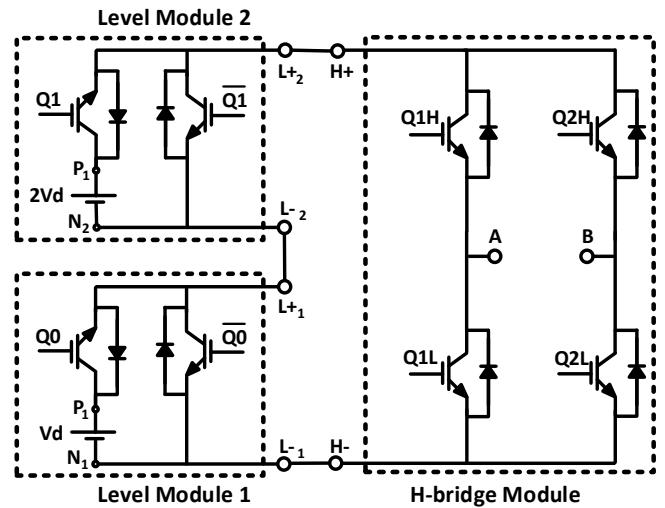


Fig. 2. The principle scheme for 7-level half-bridge cascaded inverter

applications is the cascaded H-bridge inverter, The reasons for the preference of the cascaded H-bridge inverter are that it is suitable for high voltage and high power applications, the dv/dt voltage stress on the switching elements is reduced and the THD value of the output voltage is lower [8-11].

Multilevel inverters can produce output voltage with sinusoidal form as well as output voltage with desired harmonics. In this way, multilevel inverters are used for active power filter applications [11]. In this study, a half-bridge cascaded multilevel inverter topology is proposed. The switching algorithm developed for the proposed multilevel inverter based parallel active power filter is also introduced. The switching signals to obtain the required output waveform and the other results of the filtering process are demonstrated by simulation studies. The results of the carried out simulation studies confirm that the developed strategy works properly.

2. Half-Bridge Cascaded Multilevel Inverter

Figure 2 shows the principle scheme of the 7-level half-bridge cascaded inverter to be used for parallel active power filter application. The inverter is basically composed of two different parts, the level module (LM) and the H-bridge module (HM) [12]. The required level of the inverter can be acquired by changing the number of LM. To expand the system and increase the output voltage levels of the inverter, more LMs connected in series are used.

LM comprises a dc source and two semiconductor switching elements. The voltage of dc source V_d in LM 1 is related to the required maximum value of the output voltage and the level of the inverter.

The voltage of dc sources in other LMs are scaled in power of 2. The maximum level of the inverter n can be computed as

$$n = 2^{(m+1)} - 1 \tag{1}$$

where m is the number of LMs used in the inverter.

HM shown in Fig. 2 is a conventional H-bridge inverter. HM is the constant part of the multi-level inverter. In order to increase the number of levels, HM is connected to the series-connected LMs as shown in Fig. 2.

The value of n is the maximum level number of the inverter depending on m calculated by using equation (1). However, any required level can also be acquired by the same number of LMs. For example, a number of level modules of 3, a maximum of 15 levels can be obtained, as well as 9, 11 or 13 levels. By increasing the number of LMs, any required number of level can be easily obtained by the proposed inverter since it has a simple and modular structure.

3. Switching Algorithm

The multilevel inverter used in the proposed active power filter has the capability to generate an output voltage waveform more sinusoidally. Furthermore, the multilevel inverter can produce any voltage with harmonic components. Due to this feature, it acts as a harmonic voltage source. For this purpose, it is first necessary to define the reference voltage signal which contains the desired harmonic components [13]. The reference voltage is defined as in equation (2);

$$V_{ref} = \frac{V_{dc}}{2} + \sum_{h=1}^{\infty} V_h \sin(h\omega t + \phi_h) \tag{2}$$

The reference voltage signal is present by the harmonic detection unit. A sample reference voltage signal with 3rd and 7th harmonic components is chosen to describe the proposed switching algorithm. The waveform of the sample reference voltage signal is shown in Fig.3, and the mathematical definition of this waveform is given in equation (3).

$$V_{ref} = V_3 \sin(3\omega t + \phi_3) + V_7 \sin(7\omega t + \phi_7) \tag{3}$$

Fig.3 depicts the sampling time of the switching signals (Δt). The smaller the sampling time, the more similar the output voltage is to the reference voltage signal. The sampling time depends on the frequency of the fundamental harmonic of the output voltage and the number of level modules.

$$t_{sample} = \Delta t = t_{i+1} - t_i \tag{4}$$

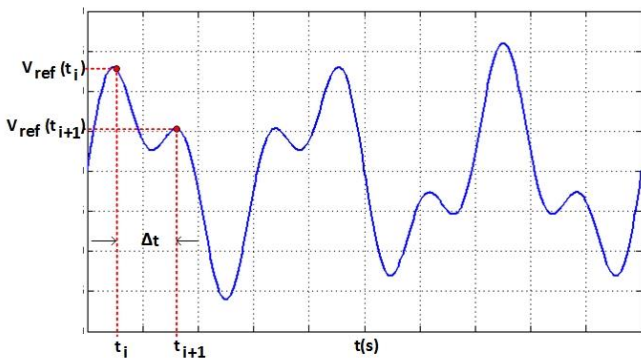


Fig. 3. The waveform of a sample reference voltage signal

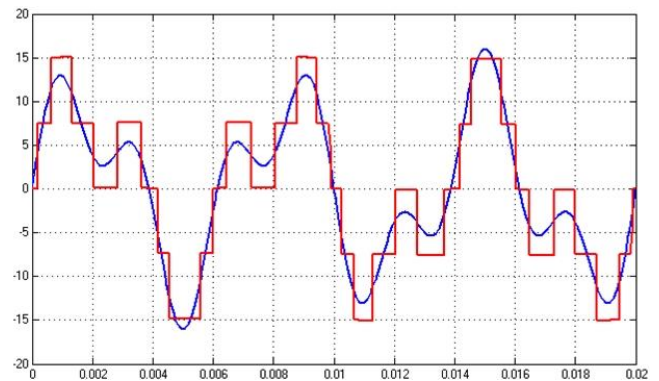
Switching signals are generated for the instantaneous values of the reference voltage signal V_{ref} . The equation for the switching signals used in the system can be generalized according to the number of level modules as follows;

$$Q_{(j-1)}(t) = \left\{ \begin{array}{l} j=1, V_{ref}(t) \bmod 2 \\ j>1, \left(\frac{V_{ref}(t) - (V_{ref}(t) \bmod 2^{(j-1)})}{2^{(j-1)}} \right) \bmod 2 \end{array} \right\} \tag{5}$$

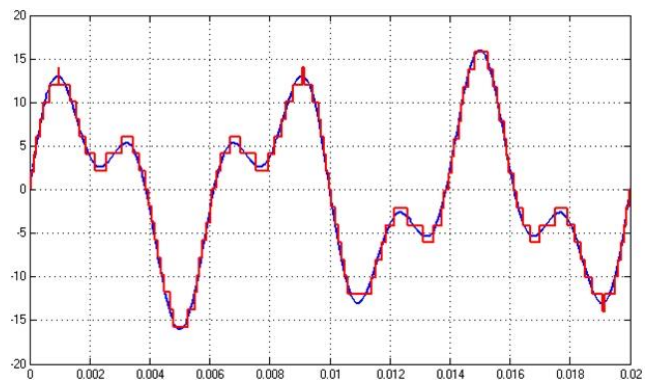
By using equation (5), the switching signals for the switching elements used in LMs are easily obtained. There are two switching elements in each level module, and these switching elements are operated as if they are the inverse of each other.

With the obtained switching signals an output voltage similar to the reference voltage signal given in Fig.3 can be produced as shown in Fig.4.

The waveforms of the inverter output voltage given in Fig.4 can converge to the reference voltage signal by increasing the number of level modules. If the inverter output voltage converges to the reference signal, the harmonic filtering capability of the parallel active power filter increases.



(a) 7-level



(b) 31-level

Fig. 4. The waveforms of reference voltage signal and output voltage of a multilevel inverter

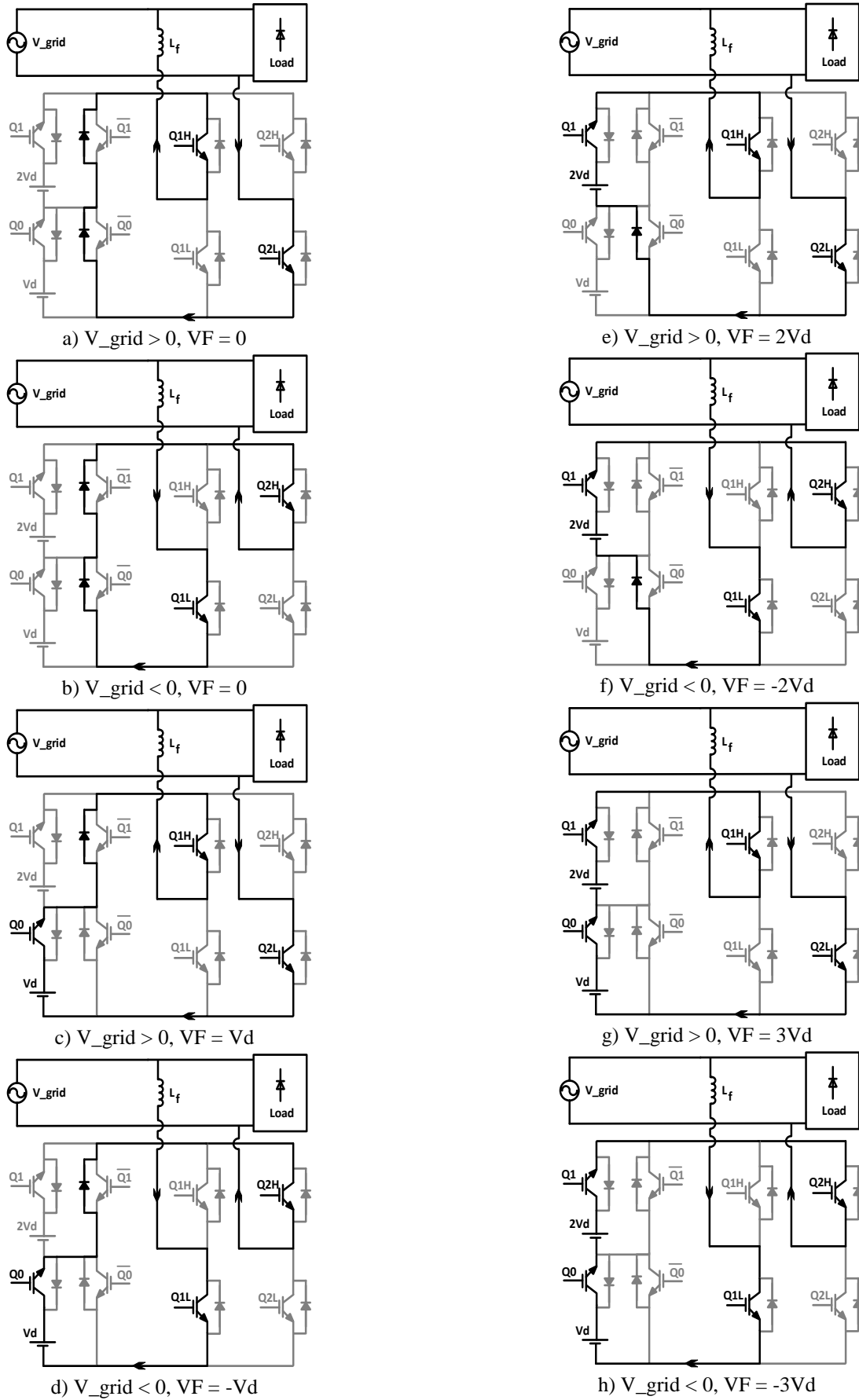


Fig. 5. The operating states of a 7-level parallel active power filter

Figure 5 shows the topology of the multilevel inverter with the ability to generate the desired voltage waveform at its output through the proposed switching algorithm, including all operating states of a parallel active power filter application. The results of this application are included in the simulation study.

4. Simulation Study

The switching algorithm proposed for parallel active power filter is applied to inverters with different number of level modules. For this purpose, a distorted grid current with a THD value of 23.43% is filtered by using 31-level inverter. The grid current consists of 5th, 7th, and 9th harmonic components with fundamental harmonic. After filtering, the grid current is nearly sinusoidal with the THD value of 0.30%. The grid current and its harmonic current components, the grid and filter currents after the parallel active power filter is applied, and switching signals are shown in Fig.6a, 6b and 6c, respectively. To demonstrate the effect of level number, in other words the number of level modules, a highly distorted grid current consisting 3rd and 7th harmonic components except fundamental with a THD value of 34.99% is filtered by using 7-level and 31-level inverter based parallel active power filters. The simulation results are shown in Fig.7 and Fig.8. The grid current and its harmonic current components are shown in Fig.7a and Fig.8a; the grid and filter currents after the parallel active power filter is applied are shown in Fig.7b and Fig.8b; and switching signals are shown in Fig.7c and Fig.8c.

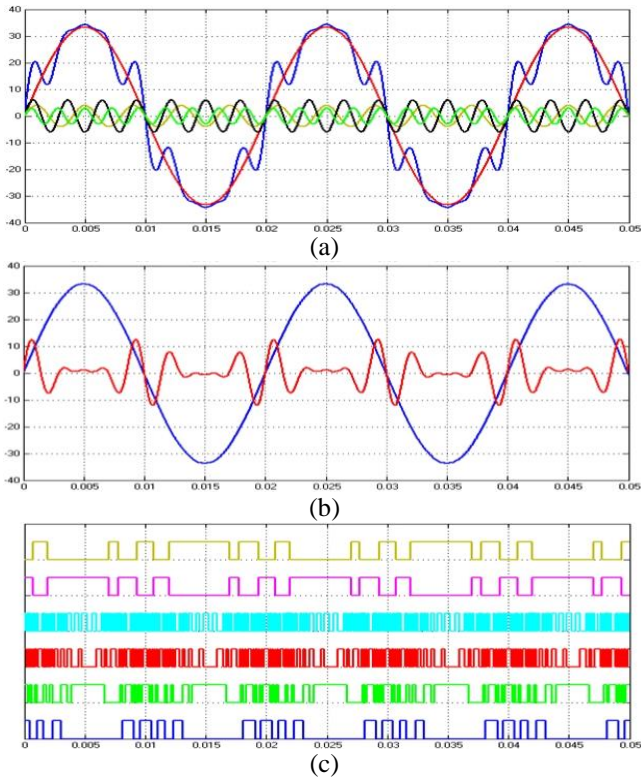


Fig. 6. The simulation results obtained from 31-level inverter based parallel active power filter, a) grid current with a THD value of 23.43% and harmonic components before filtering, b) grid current and filter current, c) switching signals

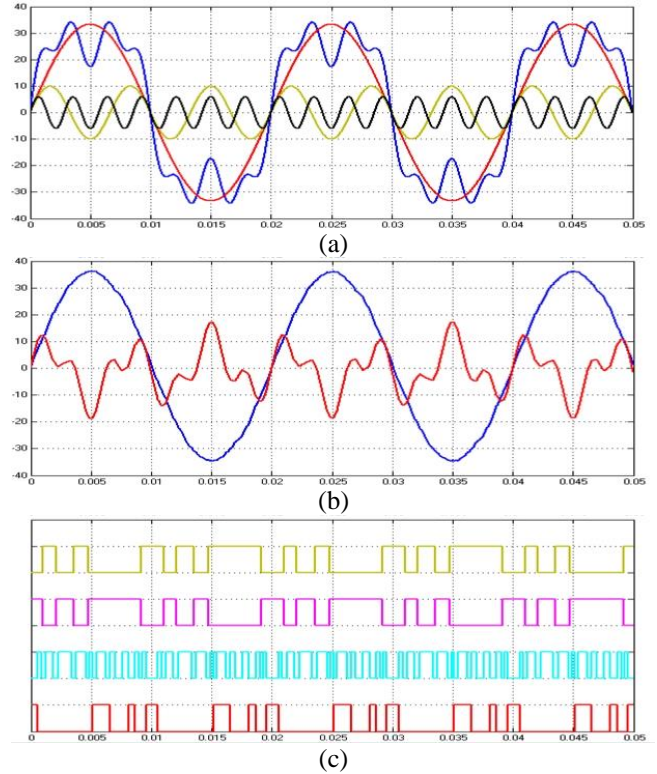


Fig. 7. The simulation results obtained from 7-level inverter based parallel active power filter, a) grid current with a THD value of 34.99% and harmonic components before filtering, b) grid current and filter current, c) switching signals

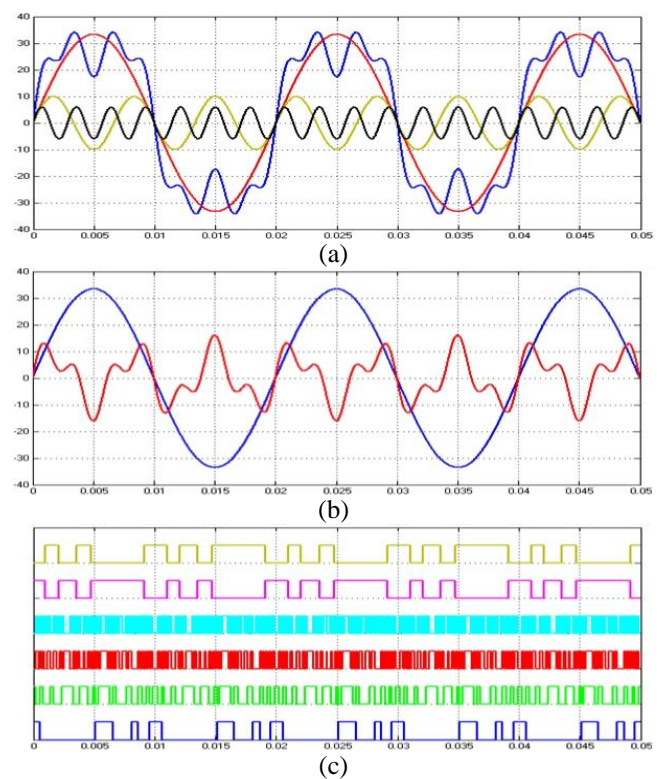


Fig. 8. The simulation results obtained from 31-level inverter based parallel active power filter, a) grid current with a THD value of 34.99% and harmonic components before filtering, b) grid current and filter current, c) switching signals

According to the simulation results, it is seen that the grid current after filtering becomes approximately sinusoidal.

5. Conclusions

Active power filters are frequently used in solving power quality problems in parallel with the increased use of non-linear loads. In this study, a switching algorithm developed for multilevel inverter based parallel active power filter is introduced. Through the switching algorithm used for the acquisition of switching signals, the total harmonic distortion of 34.99% generated by the third and seventh harmonic current component is reduced to 1.70% using two level modules and 0.27% using four level modules. The results of the simulation studies demonstrate the validity of the control algorithm and the importance of the number of level modules used in the inverter unit.

Acknowledgements

This study has been funded by Kocaeli University. Project Number: 060-2014.

References

- [1] İ. Kocabaş, O. Uçak, and A. Terciyanlı, "DSP Tabanlı Gerilim Kaynaklı Şönt Aktif Güç Filtresi Uygulaması," ELECO 2006, Bursa, Türkiye, pp. 171-175, 2006.
- [2] Y.F. Wang, and Y.W. Li, "Three-Phase Cascaded Delayed Signal Cancellation PLL for Fast Selective Harmonic Detection," IEEE Trans. on Industrial Electronics, vol. 60, no. 4, pp. 1452-1463, 2013.
- [3] Y.F. Wang, and Y.W. Li, "A Fundamental and Harmonic Component Detection Method for Single-Phase Systems," IEEE Trans. on Power Electronics, vol. 28, no. 5, pp. 2204-2213, 2013.
- [4] V. Khadkikar, "Enhancing Electric Power Quality Using UPQC: A Comprehensive Overview," IEEE Trans. on Power Electronics, vol. 27, no. 5, pp. 2284-2297, 2012.
- [5] F. S. Kang, S. J. Park, S. E. Cho, C. U. Kim, and T. Ise, "Multilevel PWM Inverters Suitable for the Use of Stand-Alone Photovoltaic Power Systems," IEEE Trans. on Energy Conversion, vol. 20, no. 4, pp. 906-915, 2005.
- [6] M. Ortuzar, R. Carmi, J. Dixon, and L. Moran, "Voltage Source Active Power Filter, Based on Multi-Stage Converter and Ultra Capacitor DC-Link," The 29th Annual Conference of the IEEE Industrial Electronics Society (IECON 2003), pp. 2300-2305, 2003.
- [7] C. Junling, L. Yaohua, W. Ping, Y. Zhizhu, and D. Zuyi, "A Closed-Loop Selective Harmonic Compensation with Capacitor Voltage Balancing Control of Cascaded Multilevel Inverter for High Power Active Power Filters," IEEE Power Electronics Specialists Conference (PESC 2008), pp. 569-573, 2008.
- [8] W. Madhukar, and P. Agarwal, "Comparison of Control Strategies for Multilevel Inverter based Active Power Filter used in High Voltage Systems," Power Electronics Drives and Energy Systems, pp. 1-6, 2010.
- [9] Z. Chen, Y. Luo, and M. Chen, "Control and Performance of a Cascaded Shunt Active Power Filter for Aircraft Electric Power System," IEEE Trans. On Industrial Electronics, vol. 59, no. 9, pp. 3617-3623, 2012.
- [10] A.A. Valdez-Fernandez, P.R. Martinez-Rodriguez, G. Escobar, C.A. Limones-Pozos, and J.M. Sosa, "A Model-Based Controller for the Cascade H-Bridge Multilevel Converter Used as a Shunt Active Filter," IEEE Trans. On Industrial Electronics, vol. 60, no. 11, pp. 5019-5028, 2013.
- [11] E. Beşer, B. Arifoğlu, S. Çamur, and E. Kandemir Beşer, "A Novel Design and Application of A Single Phase Multilevel Inverter," International Review of Electrical Engineering, vol. 4, no. 1, pp. 7-13, 2009.
- [12] E. Beşer, "Anahtarlama Elemanı Sayısı ve Harmonik Optimizasyonu ile Bir Fazlı Çok Seviyeli Evirici Tasarımı," Kocaeli Üniversitesi Fen Bilimleri Enstitüsü, Doktora Tezi, Kocaeli, 2009.
- [13] E. Beşer, B. Arifoğlu, S. Çamur, and E. Kandemir Beşer, "Design and Application of a Single Phase Multilevel Inverter Suitable for Using as a Voltage Harmonic Source," Journal of Power Electronics, vol. 10, no. 2, pp. 138-145, 2010.

Effects of Arc Voltage and Welding Current on the Arc Length of Tungsten Inert Gas Welding (TIG)

Ikpe Aniekan E.*[‡], Owunna Ikechukwu**, Ememobong Ikpe***

*[‡]Department of Mechanical Engineering, University of Benin, Nigeria.

**Department of Mechanical Engineering, University of Benin, Nigeria.

*** Electrical Electronics/Instrumentation Department, Exxon Mobile Nigeria, Nigeria

(ikpeaniekan@gmail.com, ikechukwu.owunna@uniben.edu, ememobong.e.ikpe@gmail.com)

[‡]Corresponding Author; Ikpe Aniekan, Room 142, Mechanical Engineering Department, University of Benin, Benin City,

Tel: +2349024773812, ikpeaniekan@gmail.com

Received: 10.06.2017 Accepted: 13.12.2017

Abstract- The effects of welding current and arc voltage on the arc length of Tungsten Inert Gas (TIG) welding was investigated in this study. Mild steel plates of 10mm thickness and 50mm x 100mm diameter were joined together through TIG welding process for four (4) different intervals and the welding arc lengths were measured consecutively. The measured arc length for each welding interval increased from 1.19mm, 1.93mm, 2.54mm and 3.12mm as the current increased from 50A, 100A, 150A to 190A while the voltage also maintained the same increasing trend from 200V, 240V, 280V to 320V. The minimum arc length values measured for each welding interval with the aforementioned current and voltage range also maintained an increasing trend, and that led to the conclusion that the higher the welding current and arc voltage, the longer and wider the arc length which is an influential factor to other welding attributes.

Keywords Welding, Arc voltage, Arc length, Welding current, Electrode, Mild Steel.

1. Introduction

Welding is the process of joining two or more metals together [1]. Welding processes can be classified into two major groups such as fusion welding and solid-phase welding. Fusion welding is based on the principles of heat application to join two or more materials together, and it is categorized into various types of welding operation which includes arc welding, resistance welding, oxy-fuel welding also referred to as oxyacetylene welding or oxy welding, electron beam welding and laser beam welding. Solid-phase welding which is the other group of welding classification is based on the application of pressure alone or combination of both heat and pressure to join two or more materials together, and it is categorized into diffusion welding, friction welding, forge welding and ultrasonic welding [2]. Arc is divided into four (4) major processes such as Shielded Metal Arc Welding (SMAW) also known as Manual Metal Arc Welding, Gas Metal Arc Welding (GMAW) also known as Metal Inert Gas or Active Gas Welding (MIG/MAG), Flux Core Arc Welding (FCAW) and Gas Tungsten Arc Welding or Tungsten Inert

Gas (TIG) which is the centre of focus in this study [3]. The above mentioned welding processes has not always been widely used in the past but its application and relevance in many industries in recent times has increased tremendously due to cost and reliability. Among the aforementioned welding technologies, TIG welding is gradually emerging as the process of choice for joining thin material, dissimilar and particularly suitable for welding metals and metal alloys than any other arc welding process with little smoke or fumes, neat and slag free welds and appearance that may result in ease of finishing despite its slower travel speeds than other processes, lower filler metal deposition rates and the cost of equipment which can be higher than using other welding processes [4]. Tungsten inert gas (TIG) welding also referred to as Gas tungsten arc welding (GTAW) is an electric arc welding method that applies a non-consumable tungsten electrode in the process of joining two metals together.

Weld penetration is the rate at which the fusion line extends below the surface of the welded material. Weld penetration is interrelated with arc length and welding current,

as increase or decrease in current can result in further increase or decrease in arc length and in the weld penetration depth. Studies have shown that weld penetration is influenced by welding current, polarity, arc travel speed, electrode diameter etc. [5]. Memduh et al. [6] noted that weld penetration is directly proportional to welding current, and that deep penetration can be achieved in operations where DCEP polarity is employed whereas, shallow penetration can be achieved as a result of DCEN polarity. Penetration decreases with the increase in welding speed because the time at which the arc force is allowed to penetrate into the material's surface decreases. The penetration decreases with the increase in electrode diameter due to decrease in current intensity and arc length [7]. British Standard Institution (BSI) describes arc length as the accumulative distance from the tip of the welding electrode to the adjacent surface of the weld pool [8]. According to Egerland [9], an average arc length may be expressed by equation 1,

$$l_{arc_{av}} = c_1 * L_{arc_{max}} + c_2 * L_{arc_{min}} \quad (1)$$

Where, $l_{arc_{av}}$ is the average arc length, $L_{arc_{max}}$ is the maximum arc length, $L_{arc_{min}}$ is the minimum arc length, c_1 and c_2 are constants showing current correspondence and pulse current time.

Tewari et al. [10] studied the effect of welding current, arc voltage, welding speed and heat input rate on the weldability of Mild Steel specimens of 50mm×40mm×6 mm dimensions using metal arc welding. The result obtained showed that the depth of penetration increased with increasing welding speed up to 110.39 mm/min which was optimum value to obtain maximum penetration. Therefore, increasing the speed of travel and maintaining constant arc voltage and current resulted in increased penetration until optimum speed was reached at which penetration was maximum. Increasing the speed beyond this optimum resulted in decreased penetration. Ghazvinloo et al. [11] reported that if the welding speed decreases beyond a certain point, the penetration also will decrease due to the pressure of the large amount of weld pool beneath the electrode, which will cushion the arc penetrating force. However, high welding voltage produces wider, flatter and less deeply penetrating welds than low welding voltages. Depth of penetration is maximum at optimum arc voltage [7].

Welding voltage varies with the arc length between the welding electrode and molten weld metal. An increase in arc length oftentimes lead to increase in the arc voltage because extension of the arc exposes the entire arc column to the cool boundary of the arc [12]. Similarly, the arc column continues to lose the charge carriers through radial movement into the cool boundary of the arc, thereby, introducing a higher requirement for maintaining adequate charge carriers between the welding electrode and the weld material [5]. The shape of the weld bead cross section and its physical appearance is mainly determined by the voltage. Furthermore, if the welding voltage is increased with constant welding current and welding speed, a flatter, wider, and less penetrated weld beads may be obtained which tends to reduce the porosity due to corrosion or scale on steel materials. Increasing arc voltage can equally lead to increase in the size of droplets as well as increase in the droplet transfer movement time and thus,

decreasing the number of droplets [10]. Also, the possibility of breaking the arc may increase with increasing voltage and affecting the welding process. Increasing welding voltage can increase flux consumption which in turn increases or lessens the alloying elements, thereby, affecting the mechanical and metallurgical properties of the weld metal [11, 13]. In addition, extremely high voltage has the tendency of producing wider bead geometry that is prone to cracks, increased undercut and difficulty in slag removal. Low voltage produces a stiffer arc, which improves penetration in a deep weld groove and resists arc blow, whereas, extremely low voltage produces a narrow bead geometry and results in difficulty during slag removal along the bead edges.

In a given arc welding operation carried out with constant voltage and amperage, the thermal efficiency of heat source is given [14] as shown in equation 2;

$$\eta = \frac{Q_s t_{weld}}{V I t_{weld}} = \frac{Q_s}{VI} \quad (2)$$

Where, Q_s is the rate of heat generated, t_{weld} is the welding time and η is the thermal efficiency.

For welding operations where electric arc serves as the welding source, heat conduction through the workpiece is the primary mode of heat transfer, and the partial differential equation for transient heat conduction is expressed by equation 3;

$$\rho c \frac{\partial T}{\partial t} = \nabla \cdot (k \nabla T) + f \quad (3)$$

Where ρ is the density, c the specific heat and k is the thermal conductivity which are all dependent on the temperature T . t is the welding time and f is the additional heat generated in the workpiece. Considering the heat generated as a result of arc welding process, the heat flux vector is shown in equation 4;

$$\vec{q} = -k \nabla T \quad (4)$$

The relationship between enthalpy and the temperature is expressed by equation 5;

$$H = \int_{T_{ref}}^T c(\tau) d\tau \quad (5)$$

This implies that;

$$c = \frac{dH}{dT} \quad (6)$$

From equation (3) and (6), the apparent heat capacity equation can be expressed by equation 7;

$$\rho \frac{\partial H}{\partial t} = \nabla \cdot (k \nabla T) + f \quad (7)$$

Welding current is the electrical amperage in the power equipment used in carrying out welding operation. It is usually read from the power meter, but depending on the connection could have a separate ammeter. Welding current is one of the most influential welding parameter because it has high tendency of affecting bead geometry, control the rate at which electrode is melted, controls deposition rate, heat affected zone, penetration depth and the amount of base metal melted depending on how the amperage is regulated during welding operation [15].

If the amps is too low, may result in a tall, narrow bead lacking in penetration. The weld will be difficult to start and the arc prone to straying towards one side of a joint in preference to the other. In cases where the bead is too high, the bead has a wider appearance that is flat and irregular, and a small undercut can be observed on the right hand side of the weld in the other sectioned of the image below. A deep crater forms at the end of the weld, and removing the slag from the edges of the weld may be difficult. Hence, excessive current should not be compensated by excessive travel speed [16]. This has a high tendency of resulting in slag inclusions due to rapid cooling of the weld. Moreover, with the amps correctly adjusted, a bead of smooth round shape is obtained, and the slag can be removed easily. The increase in electrode melting rate in kg/min as a result of increase in welding current is given by the relationship in equation 8,

Electrode Melting Rate =

$$\frac{1}{1000} \left[0.35 + \frac{d^2}{645} + 2.08 \times 10^{-7} \times \left(\frac{IL \times 25.4}{d^2} \right)^{1.22} \right] \quad (8)$$

Where, d = thickness of the melted electrode L = length of the melted electrode I = welding current.

2. Methodology

5 pieces of mild steel plate with 10mm thickness and dimension of 50mm x 100mm each were grinded to smoothen the surfaces and joined together in series of five (5) different welded grooves (joints), and the arc length which contributes to the depth of weld penetration was measured during the welding operation. Using TIG welding machine with AC currents of 50A and voltage ranges of 200V, 240V, 280V and 320V; 100A with the same voltage ranges; 150A with the same voltage ranges and 190A with the same voltage ranges on each welded plate; the procedure was carried out on four (4) different 10mm mild steel plate of the same specification. The welding set-up consisted of speed control unit, TIG welding touch and clamp, tungsten electrode, gas cylinder containing argon gas. Several welding variations noted during the welding experiment are reported in this study. Figure 1-4 represent the four (4) mild steel plates used for the experiment.



Fig 1. Workpiece welded with 50A Current



Fig 2. Workpiece welded with 100A Current



Fig 3. Workpiece welded with 150A Current

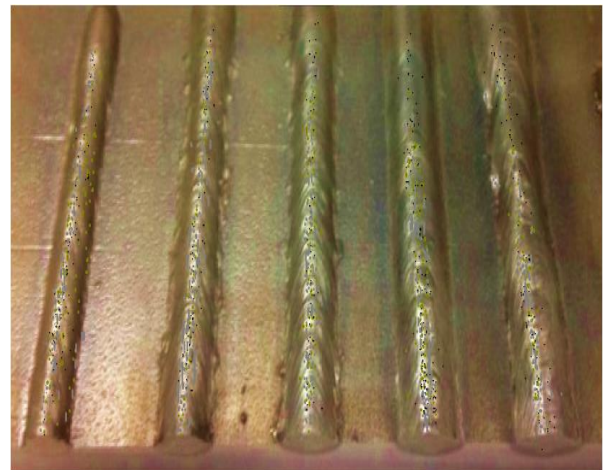


Fig 4. Workpiece welded with Current of 190A

3. Results

Results obtained from the welding conditions and process parameters stated earlier in the methodology are presented as follows;

Table 1. Result of Welding Arc Length obtained with 50A and variable Voltage Ranges

Welding Current (A)	Arc Voltages (V)			
	200V	240V	280V	320V
	Arc Lengths (mm)			
50 A	0.62	0.92	1.4	1.19
	0.68	0.83	1.1	1.11
	0.52	0.96	1.3	1.5
	0.49	0.72	1	1.12
	0.68	0.81	1.4	1.16

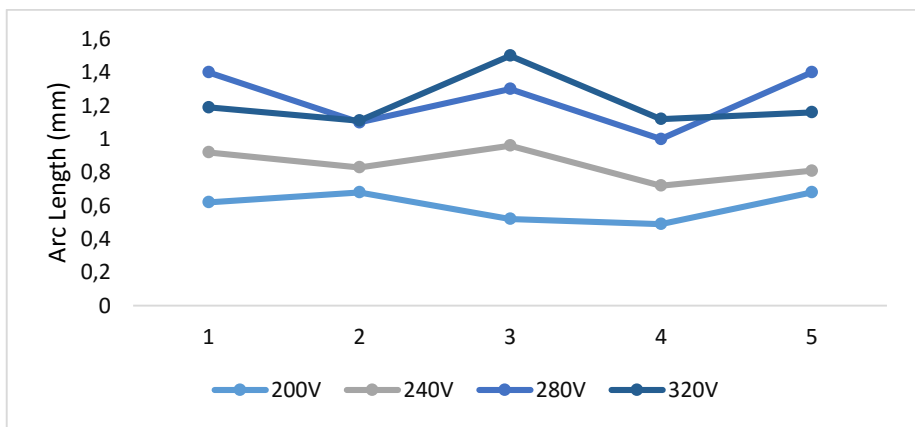


Fig 5. Trend of Arc length with 50A and Variable Voltage ranges

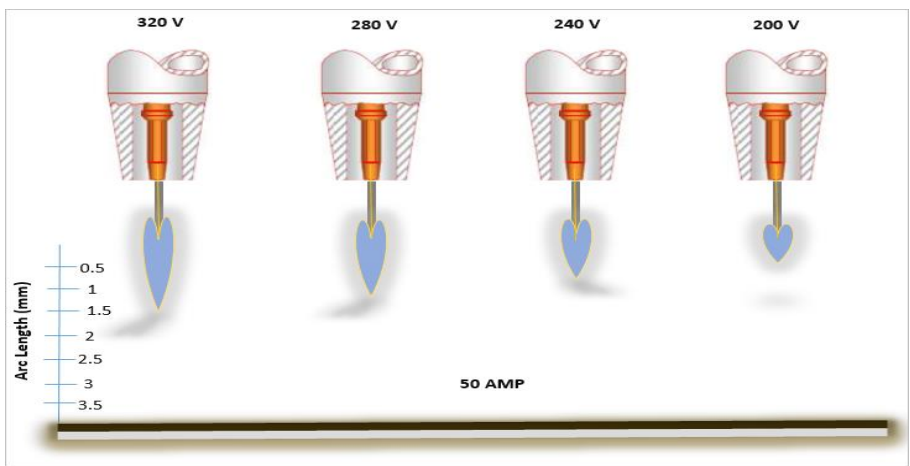


Fig 6. Measurement of Welding Arc Length with 50A and Variable Voltage Ranges

Table 2. Result of Welding Arc Length obtained with 100A and variable Voltage Ranges

Welding Current (A)	Arc Voltages (V)			
	200V	240V	280V	320V
	Arc Lengths (mm)			
100 A	1.24	1.32	1.58	1.88
	1.28	1.38	1.43	1.62
	1.2	1.36	1.49	1.93
	1.27	1.29	1.57	1.74
	1.25	1.34	1.46	1.86

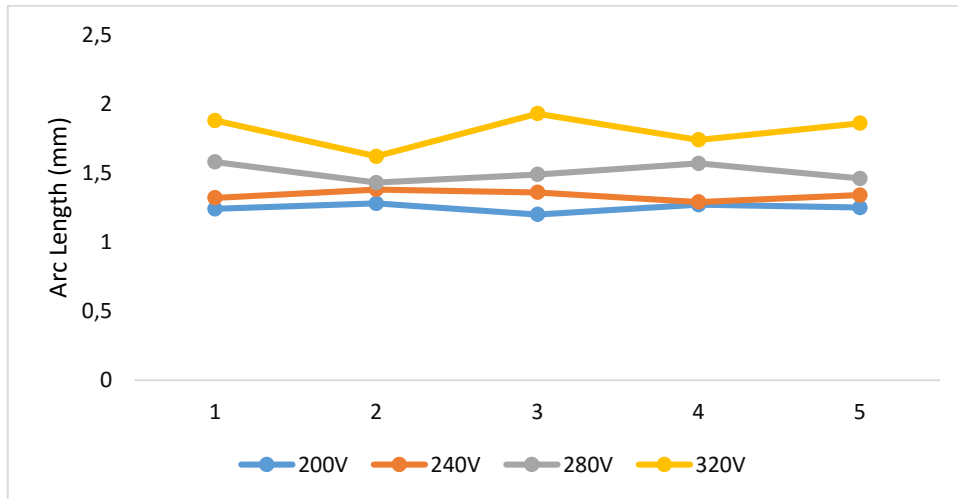


Fig 7. Trend of Arc length with 100A and Variable Voltage ranges

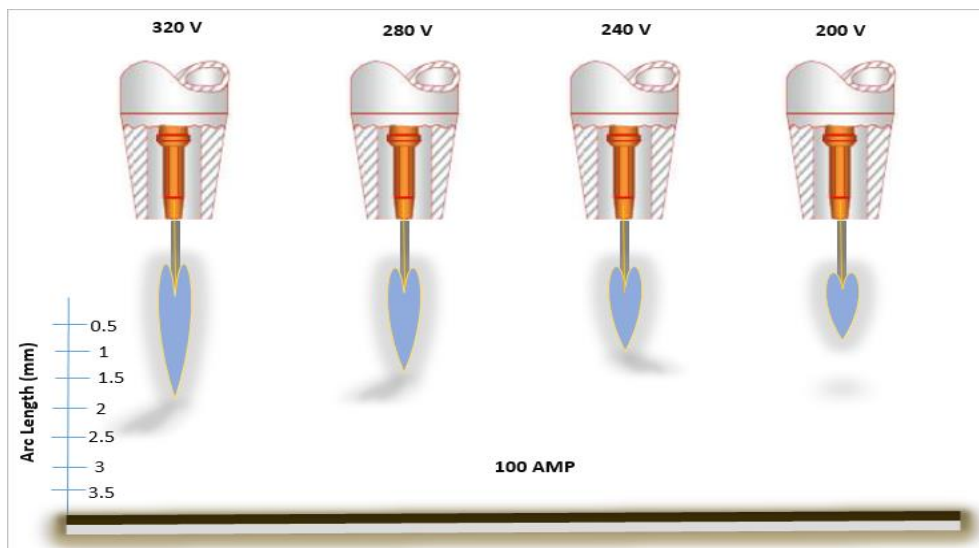


Fig 8. Measurement of Welding Arc Length with 100A and Variable Voltage Ranges

Table 3. Result of Welding Arc Length obtained with 150A and variable Voltage Ranges

Welding Current (A)	Arc Voltages (V)			
	200V	240V	280V	320V
150 A	Arc Lengths (mm)			
	1.51	1.72	2	2.51
	1.54	1.75	2.1	2.22
	1.59	1.54	1.92	2.32
	1.4	1.63	2.19	2.34
	1.46	1.6	1.84	2.54

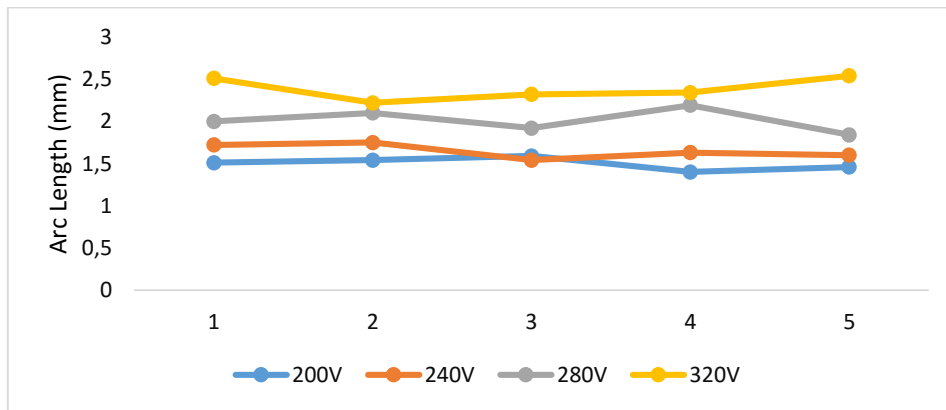


Fig 9. Trend of Arc length with 150A and Variable Voltage ranges

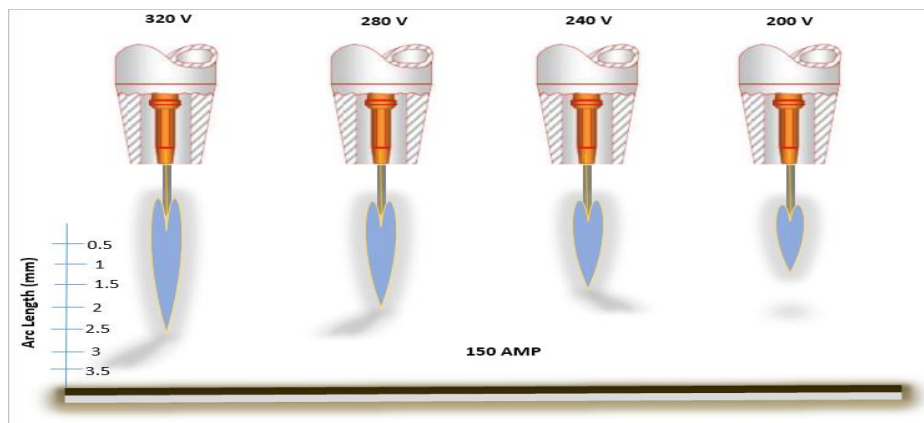


Fig 10. Measurement of Welding Arc Length with 150A and Variable Voltage Ranges

Table 4. Result of Welding Arc Length obtained with 190A and variable Voltage Ranges

Welding Current (A)	Arc Voltages (V)			
	200V	240V	280V	320V
190 A	Arc Lengths (mm)			
	2.33	2.63	2.72	2.78
	2.37	2.42	2.74	3.11
	2.26	2.54	2.63	2.91
	2.34	2.66	2.73	2.82
	2.28	2.49	2.68	3.12

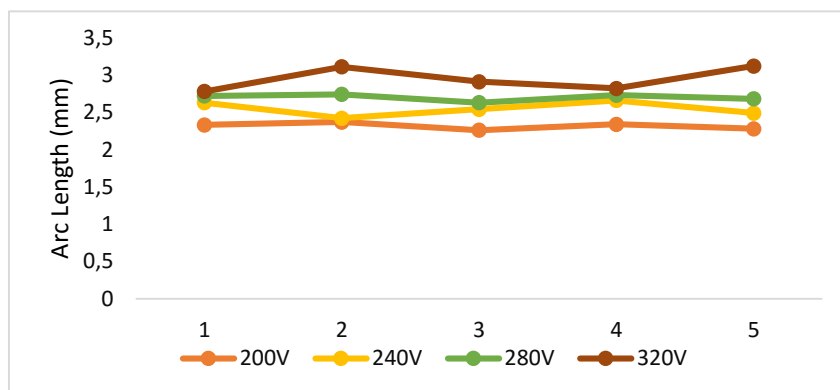


Fig 11. Trend of Arc length with 190A and Variable Voltage ranges

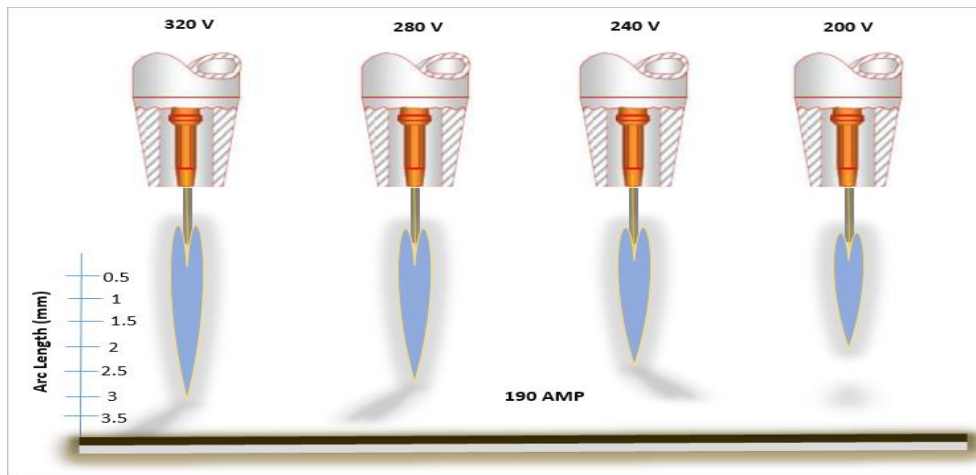


Fig 12. Measurement of Welding Arc Length with 190A and Variable Voltage Ranges

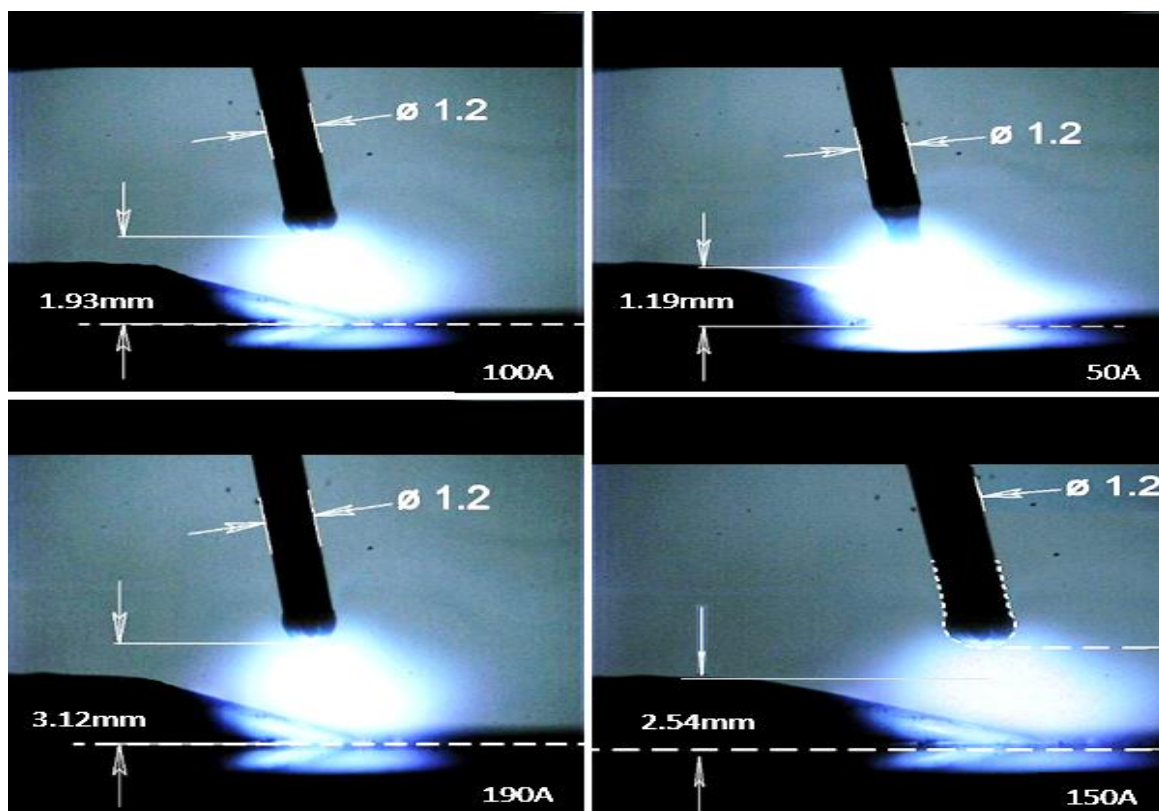


Fig 13. Maximum Arc length Measured for current applied in each of the Four (4) Welding Categories

4. Discussion

Figure 1-4 indicates behaviour of the welded material under different current and voltage ranges. It can be observed in Fig 1 that using a current of 50A with voltage ranging from 200-320, only a handful of spatters were found on the base metal and the weldment which is quite acceptable. By definition, spattering in welding application implies having tiny droplet of electrodes on or beside the weldment and may either fuse on them. In Fig 2 where current of 100A with voltage ranging from 200-320 were used, the base metal and the weldment is smoother with little or no spatters on the surface. However in Fig 3 where current of 150A with voltage ranging from 200-320 were used, microscopically black and

white spatters were found especially on the weldment with few more on the base metal. The spattering effect intensified in Fig 4 where current of 190A with voltage ranging from 200-320. The increasing number of spatters which rather produced roughness surfaces was as a result of increase in current input and vice versa. Table 1 represents the measured welding arc length obtained from a fixed current of 50A and variable voltage ranging from 200-320. It is obvious that with a fixed current and increasing voltage, the arc length is likely to increase as well. This can be observed with full clarity in Fig 5 showing the trend of Arc length with a fixed current (50A) and variable voltage ranges (200V, 240V, 280V and 320V),

and in Fig 6 depicting the measured welding arc length with the same fixed current (50A) and variable voltage ranges (200V, 240V, 280V and 320V) respectively. The same trend of increase was likewise observed for subsequent fixed currents of 100A, 150A and 190A and similar voltage ranges (200V, 240V, 280V and 320V) as shown in Table 2-4 and Fig 7-12 respectively. Fig 13 depicts the maximum Arc length measured for 50A, 100A, 150A and 190A applicable to each of the four (4) welding categories. The maximum measured arc lengths were derived from the welding operation which also correlates with some of the arc length discussed by Egerland [9].

Although the welding arc penetration was not considered in this study, several existing studies have shown that arc penetration oftentimes increase with the increase in welding current. In other words, too high a welding current at a given welding speed can influence the depth of fusion or penetration by making it so high that the resultant weldment tends to melt through the metal being welded. High current application in welding operation may result in a waste of electrodes in the form of excessive reinforcement and can as well produce digging arc and undercuts which increases distortion in weldment and shrinkage. As the welding current increases, the bead width also increase until a critical point is attained and then gradually decreases if polarity used is that of Direct Current Electrode Positive (DCEP). Also, if the polarity used is that of Direct Current Electrode Negative (DCEN), the bead width increases as current for entire range increases. For the same flux, HAZ also increases with increasing welding current.

However, if current used for the welding operation is too low, inadequate penetration or incomplete fusion may occur, and too low a welding current may equally result in inadequate penetration, unstable arc and overlapping [17]. Welding current also influences the heat requirement for desired weld pool and fusion of similar and dissimilar metals. The area of heat incident on the workpiece surface determines the heat distribution on metal surface [18]. The arc behaviour varies depending on whether the electrode is connected to the positive or negative terminal of the power source. With electrode positive (d.c.+) polarity, the electrode generates greater output heat but less penetration during welding operation than with electrode negative (d.c.-) polarity. The current-carrying capacity of an electrode of a given size will therefore be lower with positive polarity than with negative polarity [19]. Jatinder and Jagdev [20] studied the effect of welding speed and heat input rate on stress concentration factor of butt welded joint of IS 2062 E 250 A steel plates using GMAW and observed that with increase in the heat input rate, flank angle and weld bead width, reinforcement height increases, whereas notch radius decreased with an increase in the stress concentration factor increases.

5. Conclusion

The following conclusions were dawned from the experimental approach conducted in this study;

i. The measured minimum arc length was 0.49mm with current of 50A and arc voltage of 200V.

- ii. The maximum arc length measured was 3.12mm with current amperage of 190A and arc voltage input of 320V.
- iii. Slight change in arc length caused significant change in current therefore, electrode melting rate and metal deposition changed rapidly in response.
- iv. A change in welding current and arc voltage caused corresponding change in arc length.
- v. Lengthening the arc exposed the arc column to cool boundary with more heat losses, thereby, necessitating high voltage requirement.
- vi. Longer arc length produced unstable welding arc, reduced penetration, increased spatter, flatter and wider welds, and prevents shielding gas from protecting the molten puddle atmospheric contamination.
- vii. Long arc length increased puddle heat, produced flatter welds, increased penetration, reduced spatter, produced stable welding arc.
- viii. Short arc length produced flatter welds, less puddle heat, less penetration.
- ix. Shorter arc length produced less puddle heat, high tendency of electrode to stick, poor penetration, uneven beads with irregular ripples.

References

- [1] S. S. Pawale, Theoretical & experimental study of MIG/MAG welding technique. International Journal of Engineering Trends and Technology (IJETT), Vol. 24, Issue 3, pp. 142-144, 2015.
- [2] A. O. Akii Ibadode, Introduction to Manufacturing Technology, Second Edition, Benin City: Ambik Publishers, ISBN: 978-8016-34-0, 2001, pp. 553-555, 2001.
- [3] K. Weman, Welding processes handbook, ISBN 0849317738, New York: CRC Press LLC, 2003.
- [4] Miller Electric, Guidelines for Gas Tungsten Arc Welding (GTAW), Illinois Tool Works Company, Appleton, USA, Vol. 215 994 D, pp. 5, 2013.
- [5] S. Mohd, P. Mohd and K. Pratibha, Effect of MIG Welding Input Process Parameters on Weld Bead Geometry on HSLA Steel. International Journal of Engineering Science and Technology, Vol. 5, Issue1, pp. 200-212, 2013.
- [6] K. Memduh, Y. Ahmet, B. Mustafa and C. Zarif, Effects of Welding Current and Arc Voltage on FCAW Weld Bead Geometry. International Journal of Research in Engineering and Technology Vol. 4, Issue 9, pp. 23-28 2015.
- [7] P. C. Satyaduttsinh, V. Jayesh and M. Tushar, A Review on Optimization of MIG Welding Parameters using Taguchi's DOE Method. International Journal of Engineering and Management Research Vol. 4, Issue 1, pp. 16-21, 2014.

- [8] BIS-British Standards Institution, British standard BS 499-1:2009: welding terms and symbols part 1: glossary for welding, brazing and thermal cutting, BSI London, 2009.
- [9] S. Egerland, A Contribution to Arc Length Discussion, Soldagem & Inspecao, Fronius International GmbH, Wels, Austria, Vol. 20, Issue 3, 2015.
- [10] S. P. Tewari, A. Gupta, and J. Prakash, Effect of Welding Parameters on the Weldability of Material, International Journal of Engineering Science and Technology Vol. 2, Issue 4, pp. 512-516, 2010.
- [11] H. R. Ghazvinloo, A. Honarbakhsh-Raouf and N. Shadfar, Effect of arc voltage, welding current and welding speed on fatigue life, impact energy and bead penetration of AA 6061 joints produced by robotic MIG welding, Indian Journal of Science and Technology Vol. 3, Issue 2, pp. 156-162, 2010.
- [12] F. Q. Fan, Z. D. Zhang and L. M. Liu, Oxide Contribution on Arc Plasma in Tungsten Inert Gas Welding of Magnesium Alloy. Journal of Science and Technology of Welding and Joining Vol. 18, Issue 5, pp. 434-440, 2013.
- [13] Y. T. Lin, D. P. Wang, M. C. Wang, Y. Zhang and Y. Z. He, Effect of Different and Pre-and Post-Weld Heat Treatment on Microstructures and Mechanical Properties of Variable Polarity TIG Welded AA2219 Joints. Journal of Science and Technology of Welding and Joining Vol. 21, Issue 3, pp. 234-241, 2016.
- [14] M. Jeyakumar, T. Christopher, R. Narayanan and B. N. Rao, Residual Stress Evaluation in Butt-Welded Steel Plates. Indian Journal of Engineering and Material Science Vol. 18, pp. 425-434, 2011.
- [15] L. L. Wang, F. G. Lu, H. C. Cui and X. H. Tang, Investigation on Thermal Inertia of GMAW-P Welding on Al Alloy. Journal of Science and Technology of Welding and Joining Vol. 20, Issue 2, pp. 106-114, 2015.
- [16] S. Krishnan, D. V. Kulkarni and A. De, Multipass Pulsed Current Gas Metal Arc Welding of P91 Steel. Journal of Science and Technology of Welding and Joining Vol. 21, Issue3, pp. 171-177, 2016.
- [17] M. Weglowski, Y. Huang and Y. M. Zhang, Effect of welding current on metal transfer in GMAW Archives of Materials Science and Engineering Vol. 33, Issue 1, pp. 49-56, 2008.
- [18] R. Chandra, S. Arul, and R. Sellamuthu, Effect of Electrode Diameter and Input Current on Gas Tungsten Arc Welding Heat Distribution Parameters. International Conference on Advances in Manufacturing and Materials Engineering, Procedia Materials Science Vol. 5, pp. 2369-2375, 2014.
- [19] American Welding Society, Specification for Tungsten and Oxide Dispersed Tungsten Electrodes for Arc Welding and Cutting, AWS A5.12M/A5.12:2009 (ISO 6848:2004 MOD), 550 N.W. LeJeune Road, Miami, FL 33126, 2009.
- [20] G. Jatinder, and S. Jagdev, (2012) Effect of Welding Speed and Heat Input Rate on stress concentration Factor of Butt Welded Joint of Is 2062 E250 A Steel. International Journal of Advanced Engineering Research and Studies Vol. 1, Issue 3, pp. 98-100, 2012.

Interactive Fuzzy Decision Making Algorithm for Two Level Linear Fractional Programming Problems

Hasan Dalman*

*Department of Computer Engineering, Faculty of Engineering and Architecture, Istanbul Gelişim University, Avcılar, 34510, Istanbul, Turkey

(hdalman@gelisim.edu.tr)

‡Corresponding Author; Hasan Dalman, Department of Computer Engineering, Faculty of Engineering and Architecture, Istanbul Gelişim University, Avcılar, 34510, Istanbul, Turkey, Tel: +90 507 723 3421,

hdalman@gelisim.edu.tr

Received: 26.10.2017 Accepted: 13.12.2017

Abstract- This paper offers an interactive fuzzy decision-making algorithm for solving two-level linear fractional programming (TLLFP) problem which contains a single decision maker at the upper level and multiple decision makers at the lower level. In the presented interactive mechanism, the fuzzy goals and associated weight of the objective at all levels are first determined and the satisfactory solution is attained by renewing the satisfactory degrees of decision makers including the overall satisfactory balance among all levels. Moreover, the value of distance function is used in order to verify the satisfaction grades. Finally, a numerical example is given to illustrate the performance of the presented algorithm.

Keywords Two level linear fractional programming problem; fuzzy programming; fuzzy goals; Interactive methods.

1. Introduction

Multilevel programming problems usually occur in a much hierarchical system of large organizations such as government offices, profit or non-profit organizations, manufacturing plants, logistic companies, etc. Solution procedures show that all Decision Makers (DMs) has a single objective, a set of decision variables and a set of general constraints that affect all DMs. Each unit individually searches itself earnings. But each of them is affected via the actions of other units.

Multilevel programming proposed by Bracken and McGill [1] to model a decentralized noncooperative decision system with one leader and multiple followers in 1973. Multilevel programming is an NP-hard problem [5]. The Stackelberg method has been employed to solve the multilevel programming problems. It has much applicability in practical such as strategic planning (Bracken and McGill, [2]), resource allocation (Aiyoshi and Shimizu, [3]), and water management (Anandalingam and Apprey, [4]). In order to establish mathematical model of multilevel programming, many methods and algorithms have been proposed such as extreme point algorithm (Candler and Towersley, [6]), k.th best algorithm (Bialas and Karwan, [7]), branch and bound algorithm (Bard and Falk, [8]),

descent method (Savard and Gauvin, [9]). and genetic algorithm (Liu, [10]). A fuzzy multilevel programming model is presented by Gao and Liu [11]. They defined a Stackelberg–Nash equilibrium. These classical methods are based on Karush–Kuhn–Tucker conditions and/or penalty functions [12]. Furthermore, the Stackelberg method does not provide Pareto optimality because of its non-cooperative nature [13]. These solution procedures are related to Karush–Kuhn–Tucker conditions and/or penalty functions [12]. Besides, solution procedure of the Stackelberg method does not give Pareto optimality because of its noncooperative structure [13]. In such hierarchical decisions, it has been concluded that each DM should have a difficulty of motivation to cooperate with the other, and a minimum level of satisfaction of the DM at a lower level must be subject to the overall profit of the organization. In order to satisfactory solutions, fuzzy set theory to multilevel programming problems was first applied by Lai [12] in 1996. By utilizing a search procedure and fuzzy set theory, this procedure of satisfactory solution was improved by Shih et al. [14, 15]. Moreover, fuzzy programming approaches were employed by many authors for solving multiple level linear programming problems [16, 17], bilevel quadratic fractional programming problem [13, 17, 18], two-level non-convex programming problems with fuzzy parameters [18],

decentralized two-level linear programming problems [19, 20] and so on.

Recently, Baky [21] presented two fuzzy goal programming algorithm for multi-level multi-objective linear programming problems. Arora and Gupta [22] presented an interactive fuzzy goal programming algorithm connecting bilevel programming problems with the theory of dynamic programming. Wang et al. [23] introduced a concept to deal with the bilevel multilevel programming problem. A fuzzy TOPSIS algorithm is introduced in [24]. The distance function, which was introduced by Yu [24], has been widely employed to obtain compromise solutions of multi objective programming problems. Moitra and Pal [25] applied fuzzy goal programming method with the theory of distance function and produced a satisfactory balance by lessening the deviations of the leader and follower as far as for bilevel programming. However, some interesting interactive fuzzy decision making algorithms have widely been employed to obtain the efficient results of bilevel and multilevel programming problems [27, 28, 29, 30, 32]. Toksari and Bilim [31] introduced an interactive fuzzy goal method based on the Jacobian matrix for solving the multilevel fractional programming problem.

An interactive fuzzy decision making algorithm in this paper is presented for two-level linear fractional programming problems (TLLFPP) a single DM at the first level as well as multiple decision makers at the second level. Objective functions and constraint functions for DMs at both levels are fractional and linear functions, respectively. In order to solve the problem, the fuzzy goal of each of objective function is defined by getting individual optimal solutions. Thereafter, the membership function of each fractional objective for TLLFPP is constructed. Then the overall satisfactory balance between the leader and the follower is defined by introducing a new balance function. Finally, numerical examples are presented to demonstrate the feasibility of the presented interactive algorithm.

The remaining of this paper is arranged as follows. A mathematical model of bilevel fractional programming problem is given in Section 2 and an interactive fuzzy decision making algorithm is presented in Section 3. At least, two comparative examples are implemented in Section 4 and the paper is concluded in Section 5.

2. Problem Formulation

In (TLLFPP), two DMs are located at two diverse hierarchical levels including multiple objectives. Moreover, each DM independently controls a set of decision variables. The first level decision maker (DM) is known as the leader, which executes its decision in the scope of the second level DMs known as the follower. Here, each DM tries to optimize

its objective function and is affected by the activities of the other DMs.

A mathematical model of two level linear fractional programming problem is formulated as follows (see; Ahlacioglu and Tiryaki [13]):

$$\begin{aligned} \text{Upper Level: } \max_{x_0} f_0(x) &= \frac{c_0x + \alpha_0}{d_0x + \beta_0} \\ \text{Lower Level: } \max_{x_i} f_i(x) &= \frac{c_ix + \alpha_i}{d_ix + \beta_i}, i=1,2,\dots,k \end{aligned} \tag{1}$$

Subject to

$$x \in S = \{x \in \mathbb{R}^n \mid Ax \leq b, x \geq 0\}$$

where; $c_0 = (c_{00}, c_{01}, c_{02}, \dots, c_{0k}), c_i = (c_{i0}, c_{i1}, c_{i2}, \dots, c_{ik}),$
 $d_0 = (d_{00}, d_{01}, d_{02}, \dots, d_{0k})$ and
 $d_i = (d_{i0}, d_{i1}, d_{i2}, \dots, d_{ik}), i=1,2,\dots,k$ are n -dimensional fixed row vectors; $\alpha_0, \beta_0, \alpha_i$ and $\beta_i, i=1,2,\dots,k$ are reel numbers; b is m -dimensional constant column vector; A is an $m \times n$ constant matrix with full rank r . S is a non-empty, convex and compact set in \mathbb{R}^n ; $d_0x + \beta_0$ and $d_ix + \beta_i$ are greater than zero.

2.1. Construction of Membership Function

Each of the decision makers aims to minimize its own objective over the feasible region. The optimal solutions of them are found, individually and these solutions can be chosen as the best solution. Besides, the achieved value of each of objective can be admitted as the aspiration levels for the corresponding fuzzy goals. For convenience, the method given in paper [28] is used to determine membership functions. Let us $\mu(f_j), j=0,1,2,\dots,k$ to define the fuzzy goals of the leader and the follower, respectively.

$$\mu(f_j) = \begin{cases} 0 & \text{if } f_j < f_j^L \\ \frac{f_j - f_j^L}{f_j^U - f_j^L} & \text{if } f_j^L \leq f_j \leq f_j^U \\ 1 & \text{if } f_j \geq f_j^U \end{cases} \tag{2}$$

where f_j^U is called an ideal value and f_j^L is tolerance limit of j -the fuzzy goal. f_j^U and f_j^L denote the values of the objective $f_j(x), j=0,1,2,\dots,k$ such that the degrees of the membership function are 1 and 0, respectively. For the sake of simplicity, we suppose that f_j^U and f_j^L are the optimal solutions of the following fractional problems, respectively. For instance,

$$f_j^U = \max f_j(x), j=0,1,2,\dots,k \tag{3}$$

and

$$f_j^L = \min f_j(x), j=0,1,2,\dots,k \tag{4}$$

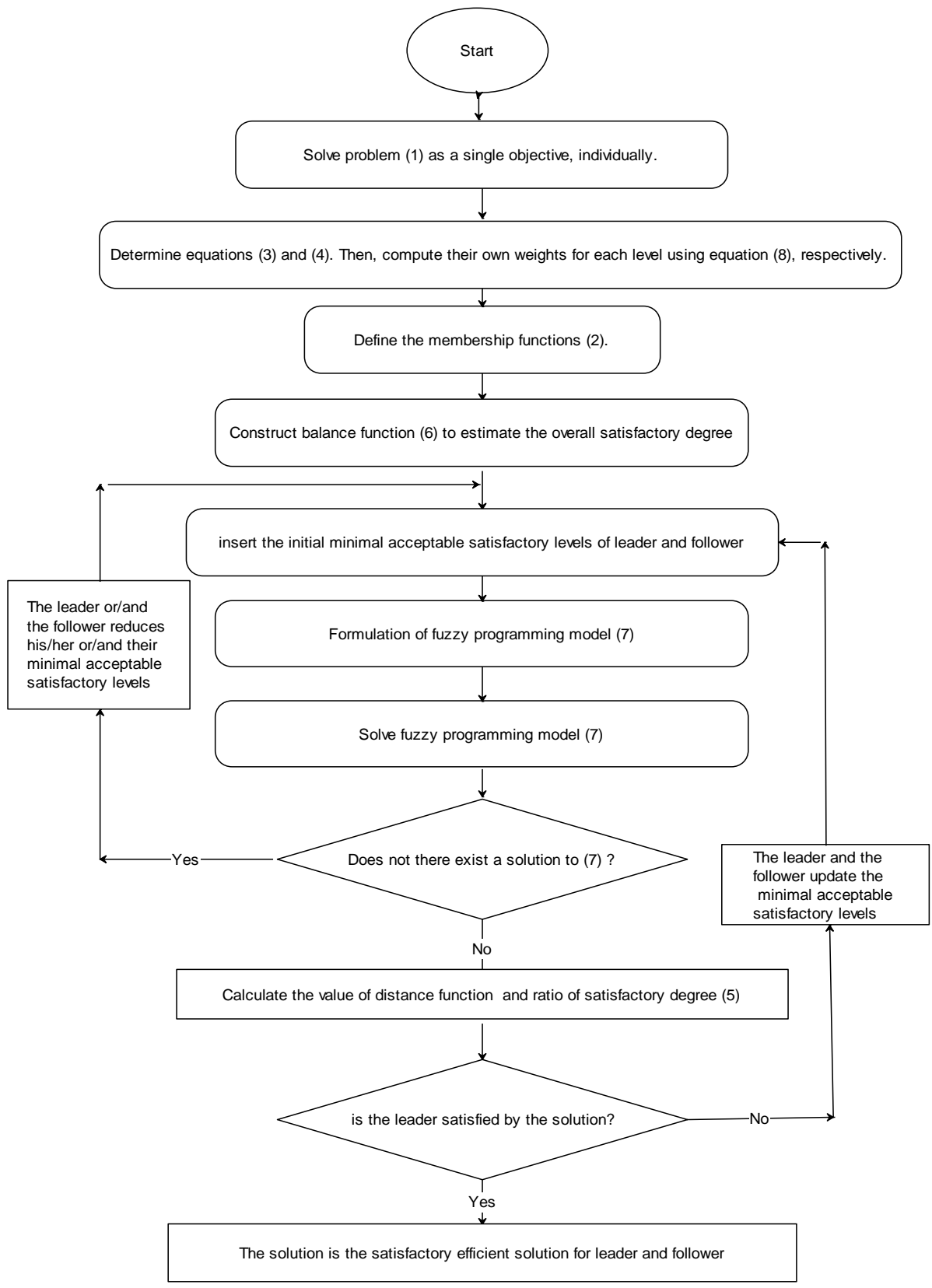


Fig. 1. Application framework of the interactive fuzzy decision making algorithm

3. Interactive Fuzzy Decision Making Method

In decision making process, achievement value of highest

membership function for a fuzzy goal is forever desired by a DM. But it is difficult to obtain the highest degree for all membership function values. Therefore, we need the theory

of the general satisfactory degree between the leader and follower. To do this, the following concept is given [12]:

$$\Delta = \frac{\sum_{i=1}^k w_i \mu(f_i)}{w_0 \mu(f_0)} \tag{5}$$

Note that, many authors implemented the notation given in above to achieve the satisfactory degree between the leader and follower at the decision making process [12, 22]. Nevertheless, this condition may result in some efficient computation. But, it can be inadequate for complex and large-scale calculations. Therefore, the following balance function is presented to estimate the overall satisfactory degree which can be characterized as the ratio of two functions:

$$d(x) = \frac{\sqrt{\sum_{j=0}^k (f_j(x) - f_j^L)^2}}{\sqrt{\sum_{j=0}^k (f_j(x) - f_j^U)^2 + \sum_{j=0}^k (f_j^U - f_j^L)^2}} \tag{6}$$

Clearly, $0 \leq d(x) \leq 1$ for all $x \in S$.

If each decision maker achieves the ideal value, $d(x)$ is equal to 1. In addition, $d(x)$ grows as the objective function values of the leader and the follower are regenerated. Therefore, we can employ the value of $d(x)$ to balance the overall satisfactory degree between the leader and follower at the two level decision making process.

Now, the formulation of the proposed method can be stated as:

$$\begin{aligned} &\max d(x) \\ &\text{subject to} \\ &\frac{\mu(f_0)}{w_0} \geq \mu_0 \\ &\sum_{i=1}^k \frac{\mu(f_i)}{w_i} \geq \mu_1 \\ &x \in S \end{aligned} \tag{7}$$

where μ_0 and μ_1 are the minimal acceptable satisfactory levels specified by the leader and the follower, respectively. w_0 and $w_i, i=1,2,\dots,k$ are importance weight of each objective. Here, lower level functions are combined using their own weights.

Furthermore, w_0 is always 1 for single decision at the upper level. Therefore, the weights are not considered and by taking into account the minimal satisfactory level of the objective at the upper level and by determining a proportional satisfaction balance among all objectives and their importance weights, we aim to achieve a satisfying solution from a Pareto optimal solution set for TLLFP problem such that the satisfactory levels of all objectives are proportional to their own weights. Here, $w_i, i=1,2,\dots,k$ is calculated as follows: (see: Kassem [33]):

$$w_i = \frac{f_i^L - f_i^U}{\sum_{k=1}^l |f_i^L - f_i^U|}, \quad i = 1, 2, \dots, l. \tag{8}$$

Theorem: If (x^*, y^*) is an optimal solution to problem (7), then it is also an efficient solution to problem (1).

Proof: If (x^*, y^*) is not an efficient solution, then there exists $(\tilde{x}, \tilde{y}) \in S$ such that $f_j(\tilde{x}, \tilde{y}) \geq f_j(x^*, y^*)$ for all $j = 0, 1, 2, \dots, k$ and $f_k(\tilde{x}, \tilde{y}) > f_k(x^*, y^*)$, $j \neq k$ for at least one index k . This contradicts that (x^*, y^*) is an optimal solution of (6).

When the leader achieves the solution of problem (7) as a satisfactory solution, the iterative process finishes. Now, we consider the following idea for refreshing the minimal acceptable satisfactory level μ_0 (see page 92 of [34]):

If the leader is not satisfied with the achieved solution and experts that it is desirable to increase the satisfactory degree of the leader at the expense of the satisfactory degree of the follower, then he/she increases the minimal acceptable satisfactory level μ_0 . Otherwise, if the leader experts that it is desirable to increase the satisfactory degree of the follower at the expense of the satisfactory degree of the leader, then he/she decreases the minimal acceptable satisfactory level μ_0 .

3.1. The proposed Interactive Fuzzy Decision Algorithm to Solve TLLFP

➤ Step 1 Solve the problem (1) as in equation (3) and (4) by taking single objective function at a time and neglecting all others.

➤ Step 2 Determine the ideal values f_j^U ($j = 0, 1, 2, \dots, k$) and tolerance limits f_j^L ($j = 0, 1, 2, \dots, k$) and weights w_i for all objective.

➤ Step 3 Construct the membership functions (2) and then combine all of objective with their own weights, respectively.

➤ Step 4 Construct balance function (6).

➤ Step 5 The leader and follower insert the initial minimal acceptable satisfactory levels μ_0, μ_1 .

➤ Step 6 Formulate the fuzzy decision making programming model (7). Then, solve problem (7) to obtain the optimal solutions.

➤ Step 7 If there does not exist a solution to (7), the leader or/and the follower reduces his/her or/and their minimal acceptable satisfactory levels, until a solution (x^*, y^*) is obtained for (7).

➤ Step 8 If the leader is satisfied by the solution in Step 7, go to Step 9, else go to Step 10.

➤ Step 9 The solution is the satisfactory efficient solution for leader and follower in problem (1).

➤ Step 10 The leader and the follower update the minimal acceptable satisfactory levels μ_0 and μ_1 , go to step (6).

A comparison of results based on linearization procedures given above is shown in Fig. 1.

In order to evaluate the satisfaction, we not only use the value of the overall satisfactory degree $d(x)$, but also the

value of distance function $D = \left\{ \sum_{j=0}^k [1 - \mu(f_j)]^2 \right\}^2$ (for details, see; [35, 36]) where $\mu(f_j)$ represents the achieved membership value of the j -th decision maker.

4. Numerical Example

The suggested interactive fuzzy decision making method will be used to a known numerical example. The following numerical example was given by Ahlatcioglu and Tiryaki [13]. They used the decentralized method to solve the following problem.

Example

Upper level:

$$\max_{x_0} f_0 = \frac{3x_{01} + 5x_{02} + x_{11} + 3x_{12} - x_{21} + 2x_{22} + x_{31} + 2x_{32}}{x_{01} + 2x_{02} + 2x_{11} + x_{12} + x_{22} + x_{31} + 2x_{32} + 1}$$

Lower level:

$$\max_{x_1} f_1 = \frac{x_{11} + x_{12}}{2x_{11} + x_{12} + 1}, \max_{x_2} f_2 = \frac{x_{21} - x_{22}}{x_{21} + x_{22} + 1}, \max_{x_3} f_3 = \frac{x_{31} + 2x_{32} + 3}{x_{32} + 1}$$

$$s.t. \begin{cases} g_1 = 2x_{01} + x_{02} + x_{11} - x_{12} + 2x_{21} - 2x_{22} - x_{31} + 3x_{32} \leq 12, \\ g_2 = -x_{01} + x_{02} + 2x_{11} + 4x_{12} + 3x_{21} - x_{22} + 2x_{31} - x_{32} \leq 24, \\ g_3 = 3x_{01} - x_{02} + 3x_{11} - x_{21} + x_{31} + 2x_{32} \leq 9, \\ g_4 = x_{01} + 2x_{02} + 5x_{12} + x_{22} - 2x_{31} - x_{32} \leq 10, \\ g_5 = x_{01} - x_{02} + x_{11} + 4x_{21} + 5x_{22} + x_{32} \leq 20, \\ g_6 = 4x_{01} + 3x_{02} + 2x_{11} - x_{12} + x_{21} + x_{22} \leq 36, \\ g_7 = 5x_{01} + 2x_{02} + x_{12} + 3x_{22} + 4x_{32} \leq 30, \\ g_8 = -2x_{01} - x_{02} + 5x_{11} + x_{21} + 2x_{32} \leq 20, \\ g_9 = x_{01} + x_{02} + 2x_{11} + x_{22} + 4x_{31} + x_{32} \leq 8, \\ g_{10} = -x_{01} - 3x_{11} + 2x_{12} + x_{21} + 4x_{31} + 2x_{32} \leq 48, \\ g_{11} = 3x_{01} - 5x_{11} + 2x_{21} + 5x_{22} - 2x_{32} \leq 15, \\ g_{12} = x_{01} + 2x_{02} + x_{11} - x_{12} + 3x_{21} + 5x_{31} - x_{32} \leq 60 \\ x_{01}, x_{02}, x_{11}, x_{12}, x_{21}, x_{22}, x_{31}, x_{32} \geq 0 \end{cases}$$

where $x_0 = (x_{01}, x_{02}), x_1 = (x_{11}, x_{12}), x_2 = (x_{21}, x_{22})$ and $x_3 = (x_{31}, x_{32})$.

Table 1 presents the individual minimum and maximum values (Step 1), the ideal values, tolerance limits and weights (Step 2) of all the objective functions in both the levels.

Step 3:

Upper level membership function:

$$\mu(f_0) = \begin{cases} 0 & \text{if } f_0 < -5 \\ \frac{f_0 - 5}{2.455 + 5} & \text{if } -5 \leq f_0 \leq 2.455 \\ 1 & \text{if } f_0 \geq 2.455 \end{cases}$$

Table 1: The individual minimum and maximum values, the ideal value and tolerance limits and weights

	f_0	f_1	f_2	f_3
max f_j	2.455	0.765	0.849	5
min f_j	-5	0	-804	2.160
f_j^U	2.455	0.765	0.849	5
f_j^L	-5	0	-804	2.160

$$= \frac{0.134(3x_{01} + 5x_{02} + x_{11} + 3x_{12} - x_{21} + 2x_{22} + x_{31} + 2x_{32})}{x_{01} + 2x_{02} + 2x_{11} + x_{12} + x_{22} + x_{31} + 2x_{32} + 1} + 0.671$$

Lower level membership functions:

$$\mu(f_1) = \begin{cases} 0 & \text{if } f_1 < 0 \\ \frac{f_1 - 0}{0.765 - 0} & \text{if } 0 \leq f_1 \leq 0.765 \\ 1 & \text{if } f_1 \geq 0.765 \end{cases}$$

$$\Rightarrow \mu(f_1) = \frac{1.307(x_{11} + x_{12})}{2x_{11} + x_{12} + 1}$$

$$\mu(f_2) = \begin{cases} 0 & \text{if } f_2 < 0.804 \\ \frac{f_2 + 0.804}{0.849 + 0.804} & \text{if } 0.804 \leq f_2 \leq 0.849 \\ 1 & \text{if } f_2 \geq 0.849 \end{cases}$$

$$\Rightarrow \mu(f_2) = \frac{0.605(x_{21} - x_{22})}{x_{21} + x_{22} + 1} + 0.486$$

$$\mu(f_3) = \begin{cases} 0 & \text{if } f_3 < 2.16 \\ \frac{f_3 - 2.16}{5 - 2.16} & \text{if } 2.16 \leq f_3 \leq 5 \\ 1 & \text{if } f_3 \geq 5 \end{cases}$$

$$\Rightarrow \mu(f_3) = \frac{0.375(x_{31} + 2x_{32} + 3)}{x_{32} + 1} - 0.873$$

and all of them are combined using their weights as:

$$\sum_{i=1}^3 \frac{\mu(f_i)}{w_i} = \frac{1.307(x_{11} + x_{12})}{0.172} + \frac{0.605(x_{21} - x_{22})}{0.371} + 0.486 + \frac{0.375(x_{31} + 2x_{32} + 3)}{0.600} - 0.873$$

Step 4:

Balance function (6) is determined as

$$d(x) = \frac{\sqrt{\left(\frac{3x_{01} + 5x_{02} + x_{11} + 3x_{12} - x_{21} + 2x_{22} + x_{31} + 2x_{32} + 5}{x_{01} + 2x_{02} + 2x_{11} + x_{12} + x_{22} + x_{31} + 2x_{32} + 1} \right)^2 + \left(\frac{x_{11} + x_{12}}{2x_{11} + x_{12} + 1} \right)^2 + \left(\frac{x_{21} - x_{22}}{x_{21} + x_{22} + 1} + 0.804 \right)^2 + \left(\frac{x_{31} + 2x_{32} + 3}{x_{32} + 1} - 2.16 \right)^2}}{\sqrt{\left(\frac{3x_{01} + 5x_{02} + x_{11} + 3x_{12} - x_{21} + 2x_{22} + x_{31} + 2x_{32} - 2.455}{x_{01} + 2x_{02} + 2x_{11} + x_{12} + x_{22} + x_{31} + 2x_{32} + 1} \right)^2 + \left(\frac{x_{11} + x_{12}}{2x_{11} + x_{12} + 1} - 0.765 \right)^2 + \left(\frac{x_{21} - x_{22}}{x_{21} + x_{22} + 1} - 0.849 \right)^2 + \left(\frac{x_{31} + 2x_{32} + 3}{x_{32} + 1} - 5 \right)^2}} + 66.024$$

Step 5: Let $\mu_0 = 1$ and $\mu_1 = 0.9$.

Step 6: Then, the corresponding problem (7) can be formulated as:

$$\max d(x) = \frac{\sqrt{\left(\frac{3x_{01} + 5x_{02} + x_{11} + 3x_{12} - x_{21} + 2x_{22} + x_{31} + 2x_{32} + 5}{x_{01} + 2x_{02} + 2x_{11} + x_{12} + x_{22} + x_{31} + 2x_{32} + 1}\right)^2 + \left(\frac{x_{11} + x_{12}}{2x_{11} + x_{12} + 1}\right)^2 + \left(\frac{x_{21} - x_{22}}{x_{21} + x_{22} + 1} + 0.804\right)^2 + \left(\frac{x_{31} + 2x_{32} + 3}{x_{32} + 1} - 2.16\right)^2}}{\sqrt{\left(\frac{3x_{01} + 5x_{02} + x_{11} + 3x_{12} - x_{21} + 2x_{22} + x_{31} + 2x_{32} - 2.455}{x_{01} + 2x_{02} + 2x_{11} + x_{12} + x_{22} + x_{31} + 2x_{32} + 1}\right)^2 + \left(\frac{x_{11} + x_{12}}{2x_{11} + x_{12} + 1} - 0.765\right)^2 + \left(\frac{x_{21} - x_{22}}{x_{21} + x_{22} + 1} - 0.849\right)^2 + \left(\frac{x_{31} + 2x_{32} + 3}{x_{32} + 1} - 5\right)^2} + 66.024}$$

Subject to

$$\frac{0.134(3x_{01} + 5x_{02} + x_{11} + 3x_{12} - x_{21} + 2x_{22} + x_{31} + 2x_{32})}{x_{01} + 2x_{02} + 2x_{11} + x_{12} + x_{22} + x_{31} + 2x_{32} + 1} + 0.671 \geq 1,$$

$$\frac{1.307(x_{11} + x_{12})}{2x_{11} + x_{12} + 1} + \frac{0.605(x_{21} - x_{22})}{x_{21} + x_{22} + 1} + 0.486 \frac{0.375(x_{31} + 2x_{32} + 3)}{x_{32} + 1} - 0.873 \geq 0.9,$$

$$\frac{0.172}{0.371} + \frac{0.600}{0.600} \geq 0.9,$$

$$g_1 = 2x_{01} + x_{02} + x_{11} - x_{12} + 2x_{21} - 2x_{22} - x_{31} + 3x_{32} \leq 12,$$

$$g_2 = -x_{01} + x_{02} + 2x_{11} + 4x_{12} + 3x_{21} - x_{22} + 2x_{31} - x_{32} \leq 24,$$

$$g_3 = 3x_{01} - x_{02} + 3x_{11} - x_{21} + x_{31} + 2x_{32} \leq 9,$$

$$g_4 = x_{01} + 2x_{02} + 5x_{12} + x_{22} - 2x_{31} - x_{32} \leq 10,$$

$$g_5 = x_{01} - x_{02} + x_{11} + 4x_{21} + 5x_{22} + x_{32} \leq 20,$$

$$g_6 = 4x_{01} + 3x_{02} + 2x_{11} - x_{12} + x_{21} + x_{22} \leq 36,$$

$$g_7 = 5x_{01} + 2x_{02} + x_{12} + 3x_{22} + 4x_{32} \leq 30,$$

$$g_8 = -2x_{01} - x_{02} + 5x_{11} + x_{21} + 2x_{32} \leq 20,$$

$$g_9 = x_{01} + x_{02} + 2x_{11} + x_{22} + 4x_{31} + x_{32} \leq 8,$$

$$g_{10} = -x_{01} - 3x_{11} + 2x_{12} + x_{21} + 4x_{31} + 2x_{32} \leq 48,$$

$$g_{11} = 3x_{01} - 5x_{11} + 2x_{21} + 5x_{22} - 2x_{32} \leq 15,$$

$$g_{12} = x_{01} + 2x_{02} + x_{11} - x_{12} + 3x_{21} + 5x_{31} - x_{32} \leq 60,$$

$$x_{01}, x_{02}, x_{11}, x_{12}, x_{21}, x_{22}, x_{31}, x_{32} \geq 0$$

Step 7: There does not exist feasible solution for the above problem with $\mu_0 = 1$ and $\mu_1 = 0.9$. So the leader adjusts the minimal acceptable level $\mu_0 = 1$ by reducing $\mu_0 = 1$ to $\mu_0 = 0.9$.

The above problem is solved with $\mu_0 = 0.9$ and $\mu_1 = 0.9$ using the Maple 18.02 software program, the optimal solutions for the above problem are $x_{01} = 2.640, x_{02} = 0., x_{11} = 0., x_{12} = 2.008,$
 $x_{21} = 0.260, x_{22} = 0., x_{31} = 1.340, x_{32} = 0.$

For this optimal solution, membership functions values are $\mu(f_0) = 0.959, \mu(f_1) = 0.873, \mu(f_2) = 0.611, \mu(f_3) = 0.753$ and objective values are $f_0 = 2.150, f_1 = 0.668, f_2 = 0.207, f_3 = 4.340.$

The ratio of satisfactory degrees is $\Delta = 0.934$.

We execute a comparison with the obtained solutions from [13] in Table 2. From the obtained solutions of $d(x)$ and D , the obtained solution of the suggested method in this paper is better than the method of Tiryaki and Ahlatcioglu [13]. Furthermore, all of the sum of the leader's values and the follower's values generated by our suggested method is greater than that generated by Ahlatcioglu and Tiryaki [13]. So, these solutions indicate that the suggested method in this paper is practicable.

Numerical results prove that the suggested method in this paper has the following interesting features.

- According to Table 2, we can observe that the value of D by the suggested method is smaller than that of other method.

It should be noted that the larger value of Δ in (5) is not the more satisfactory the solution. We can see from the distance function D .

5. Conclusion

In this paper, a new interactive fuzzy decision making method based on the idea of the membership function is suggested for solving the two-level fractional programming problem. We use the overall satisfactory balance between the leader and the follower into consideration by introducing a new balance function. Then, a satisfactory solution is achieved. This solution involves knowledge concerning importance weights of lower level objectives and the minimal satisfactory level of all objectives. Furthermore, this method has an interactive structure as it provides leader to provide the opportunity of exchange the data presented that the leader is not satisfied from this solution. Consequently, application of the suggested method is discussed with a numerical model and the effectiveness of the solutions obtained by the suggested method is verified. Moreover, from table 2, our suggested approach gives a more efficient solution comparing to the approaches of Ahlatcioglu and Tiryaki [13].

Hence, our suggested algorithm can be easily extended both the lower level and upper level with multiple objectives (for example, [31]).

Acknowledgements

The author sincerely thank the anonymous reviewers and editor-in-chief for their careful reading, constructive comments, and fruitful suggestions.

The author confirms that there is no conflict of interest regarding a financial supporter.

Table 2: Comparison of results of Example.

	f_0	f_1	f_2	f_3	$\mu(f_0)$	$\mu(f_1)$	$\mu(f_2)$	$\mu(f_3)$	$d(x)$	Δ	D
The proposed method	2.150	0.668	0.207	4.340	0.959	0.873	0.611	0.753	0.919	0.934	0.480
Method in [13]	2.082	0.655	0.510	4.22	0.950	0.856	0.601	0.709	–	0.738	0.517

References

- [1] Bracken J & McGill JM. (1973). Mathematical programs with optimization problems in the constraints. *Operational Research*, 21, 37–44.
- [2] Bracken J & McGill JM. (1974). Defense applications of mathematical programs with optimization problem in the constraints. *Operations Research*, 22, 1086–1096.
- [3] Aiyoshi E & Shimizu K (1981). Hierarchical decentralized systems and its new solution by a barrier method. *IEEE Transactions on Systems, Man, and Cybernetics*, 11(6), 444–449.
- [4] Anandalingam G & Apprey V (1991). Multi-level programming and conflict resolution. *European Journal of Operational Research*, 51, 233–247.
- [5] Ben-Ayed O & Blair CE (1990). Computational difficulties of bilevel linear programming. *Operations Research*, 38, 556–560.
- [6] Candler, W & Towersley R (1982). A linear two-level programming problem. *Computers and Operations Research*, 9, 59–76.
- [7] Bialas WF & Karwan MH (1984). Two-level linear programming. *Management Science*, 30, 1004–1020.
- [8] Bard J & Falk J (1982). An explicit solution to the multi-level programming problem. *Computers and Operations Research*, 9, 77–100.
- [9] Savard G & Gauvin J (1994). The steepest descent direction for the nonlinear bilevel programming problem. *Operations Research Letters*, 15, 275–282.
- [10] Liu B (1998). Stackelberg–Nash equilibrium for multilevel programming with multiple followers using genetic algorithms. *Computers & Mathematics with Applications*, 36(7), 79–89.
- [11] Gao J & Liu B (2005). Fuzzy multilevel programming with a hybrid intelligent algorithm. *Computers & Mathematics with Applications*, 49(9-10), 1539–1548
- [12] Lai YJ (1996). Hierarchical optimization: a satisfactory solution. *Fuzzy Sets and Systems*, 77(3), 321–335.
- [13] Ahlatcioglu M & Tiryaki F (2007). Interactive fuzzy programming for decentralized two-level linear fractional programming (DTLLFP) problems. *Omega*, 35(4), 432–450.
- [14] Shih HS, Lai YJ & Lee ES (1996). Fuzzy approach for multi-level programming problems. *Computer & Operations Research*, 23, 73–91.
- [15] Shih HS & Lee ES (2000). Compensatory fuzzy multiple level decision making. *Fuzzy Sets and Systems*, 114(1), 71–87.
- [16] Sakawa M, Nishizaki I & Uemura Y (2000). Interactive fuzzy programming for two-level linear fractional programming problems with fuzzy parameters. *Fuzzy Sets and Systems*, 115(1), 93–103.
- [17] Sakawa M & Nishizaki I (2001). Interactive fuzzy programming for two-level linear fractional programming problems. *Fuzzy Sets and Systems*, 119(1), 31–40.
- [18] Sakawa M & Nishizaki I (2002). Interactive fuzzy programming for two-level nonconvex programming problems with fuzzy parameters through genetic algorithms. *Fuzzy Sets and Systems*, 127(2), 185–197.
- [19] Sakawa M, & Nishizaki I (2002). Interactive fuzzy programming for decentralized two-level linear programming problems. *Fuzzy Sets and Systems*, 125(3), 301–315.
- [20] Tiryaki F (2006). Interactive compensatory fuzzy programming for decentralized multi-level linear programming (DMLLP) problems. *Fuzzy sets and systems*, 157(23), 3072–3090.
- [21] Baky IA (2010). Solving multi-level multi-objective linear programming problems through fuzzy goal programming approach. *Applied Mathematical Modelling*, 34(9), 2377–2387.
- [22] Arora SR & Gupta R (2009). Interactive fuzzy goal programming approach for bilevel programming problem. *European Journal of Operational Research*, 194(2), 368–376.
- [23] Wang G, Wang X & Wan Z (2009). A fuzzy interactive decision making algorithm for bilevel multi-followers programming with partial shared variables among followers. *Expert Systems with Applications*, 36(7), 10471–10474.
- [24] Yu PL (1973) A class of solutions for group decision problems. *Management Science*, 19(8), 936–946.
- [25] Pal BB & Moitra BN (2003). A fuzzy goal programming procedure for solving quadratic bilevel programming problems. *International Journal of Intelligent Systems*, 18(5), 529–540.

- [26] Baky IA & Abo-Sinna MA (2013). TOPSIS for bi-level MODM problems. *Applied Mathematical Modelling*, 37(3), 1004-1015.
- [27] Sakawa M & Nishizaki I (2012). Interactive fuzzy programming for multi-level programming problems: a review. *International Journal of Multicriteria Decision Making*, 2(3), 241-266.
- [28] Zheng Y, Liu J & Wan Z (2014). Interactive fuzzy decision making method for solving bilevel programming problem. *Applied Mathematical Modelling*, 38(13), 3136-3141.
- [29] Sakawa, M., & Matsui, T. (2013). Interactive fuzzy random two-level linear programming based on level sets and fractile criterion optimization. *Information Sciences*, 238, 163-175.
- [30] Emam, O. E. (2013). Interactive approach to bi-level integer multi-objective fractional programming problem. *Applied Mathematics and Computation*, 223, 17-24.
- [31] Toksarı, M. D., & Bilim, Y. (2015). Interactive Fuzzy Goal Programming Based on Jacobian Matrix to Solve Decentralized Bi-level Multi-objective Fractional Programming Problems. *International Journal of Fuzzy Systems*, 1-10.
- [32] Singh, S., & Haldar, N. (2015). A New Method To Solve Bi-Level Quadratic Linear Fractional Programming Problems. *International Game Theory Review*, 17(02), 1540017.
- [33] Kassem, M. A. E. H. (1995). Interactive stability of multiobjective nonlinear programming problems with fuzzy parameters in the constraints. *Fuzzy Sets and Systems*, 73(2), 235-243.
- [34] Sakawa, M., & Nishizaki, I. (2009). *Cooperative and noncooperative multi-level programming* (Vol. 48). Springer Science & Business Media.
- [35] Pramanik, S., & Roy, T. K. (2007). Fuzzy goal programming approach to multilevel programming problems. *European Journal of Operational Research*, 176(2), 1151-1166.
- [36] Biswas A & Pal BB (2005). Application of fuzzy goal programming technique to land use planning in agricultural system. *Omega*, 33(5), 391-398.

Innovative Design for a Ball Worm Gear Mechanism

Sait Koçak*[‡]

*Department of Mechatronics Engineering, Faculty of Technology, Pamukkale University, 20700 Denizli, Turkey

(skocak@pau.edu.tr)

[‡]Corresponding Author; Sait Koçak, Department of Mechatronics Engineering, Faculty of Technology, Pamukkale University, 20700 Denizli, Turkey, Tel: +90 258 296 4189, Fax: +90 258 296 41 96, skocak@pau.edu.tr

Received: 31.10.2017 Accepted: 13.12.2017

Abstract- In this study, a new mechanism was designed and presented as an alternative to the worm gear mechanism without its disadvantages. This novel mechanism is referred to as a “ball worm gear mechanism”. The force of the worm gear mechanism is transmitted by a sliding movement, which leads to high operating temperature and low efficiency as well as wear on the bronze worm wheel. Therefore, a new mechanism was designed with balls placed into the helical grooves on the worm shaft which move by rolling on the worm wheel. The worm wheel of the newly designed mechanism is made of case-hardened steel, which is less expensive than bronze. Thus, it is anticipated that not only the cost of the worm wheel will be reduced, but also its life will be extended. Greater efficiency and elimination of the high operating temperature are expected to result from the power transmission achieved by the rolling motion of the new mechanism. Modelling of the design was carried out with SolidWorks software and the feasibility of the mechanism was confirmed.

Keywords Worm gear mechanism, ball-screw mechanism, CAD, efficiency.

1. Introduction

The invention of the wheel (4000-3500 BC) made it possible to transfer rolling motion to linear movement and laid the foundations of the gear wheel system [1].

Induced gear units of electric motors or internal combustion engines that are designed to reduce high rotational speeds to the speeds required for the machines are called reducers [2]. Gearboxes are specified according to the gearwheel which is used in the gear reducers, e.g., spur gear, helical gear, bevel gear and worm gear reducers.

The present-day size of the gearbox is small when compared that of the past. At 12 horsepower, the axis-to-axis distance of a worm gear unit with a conversion ratio of 35 was 356 mm in the year 1903, but now it is around 100 mm [3].

One of the first screw profiles was invented by Archimedes in the 3rd century BC. Archimedes was able to transport water upwards, thanks to the screw known by his name – the Archimedes, or Archimedean, screw [4].

Worm gear mechanisms have very high conversion rates compared to other gear mechanisms. The conversion rates achieved in several stages with reducers made up of other gear mechanisms can be attained in one step by means of the worm gear mechanism, thus allowing for the designing of lighter and cheaper constructions requiring less space [5, 6]. The screw profile in the worm gear mechanism is usually dependent on the manufacturing process. The five most commonly used endless screws are the A, C, I, K, and N types [7]. The basic concepts needed for calculating the dimensions of the worm gear and worm wheel are shown in Figure 1 [8].

In addition to the abovementioned advantages of the worm gear mechanism, there are also disadvantages, such as low efficiency, high operating temperatures and rapid worm wheel wear [9]. Moreover, due to adhesion wear when using the same material for both components, the worm gear and the worm wheel must be fabricated from two different materials that have a low wear coefficient and are suitable for sliding. A steel-bronze material pair is preferred at the medium-high speed [6]. As bronze is expensive, it makes the cost of the endless screw mechanism high.

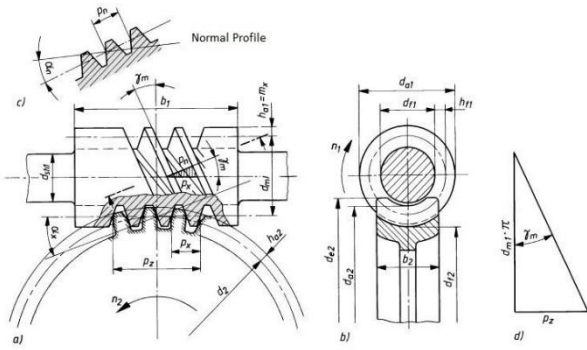


Fig. 1. Worm gear and worm wheel base

Table 1. Efficiency of gear mechanisms

Mechanism	Efficiency (%)
Cylindrical gear mechanism	0.96 – 0.98
Bevel gear mechanism	0.95 – 0.97
Worm gear locking ($\gamma m > \rho$)	0.6 – 0.8
Worm gear anti-locking ($\gamma m \leq \rho$)	0.25 – 0.4

The efficiency differences in various gear mechanisms are given in Table 1. The efficiency of the other gear mechanisms is around 95-98%, while for the worm gear mechanism type without locking it is as low as 25% [5].

Worm gear mechanisms are currently used in lifts and elevators, crane rope drums, textile machines, automobile and ship steering mechanisms, conveyors (banded, grided and helical) and machine tools [3,10].

The worm gear mechanism has disadvantages which include low efficiency, rapid wear, overheating during operation and high cost. However, it is the advantage of its very wide field of application that led to the idea of a ball worm gear mechanism.

In this study, a new mechanism was designed to overcome the disadvantages of the worm gear mechanism. The newly designed mechanism was given the name of “ball worm gear mechanism”. The design of the mechanism was implemented using the SolidWorks package program and the mechanics were tested via the SolidWorks Motion Study module.

2. Design of the ball worm gear mechanism

The design of gear mechanisms is a research area that has attracted many scientists and engineers over a number of years [11-21].

The design of the ball worm gear mechanism was inspired by the ball screw. The transmission of the force between the

screw and the nut in the ball screw is achieved by the balls. A sectional view of the ball screw is given in Figure 2 [22].

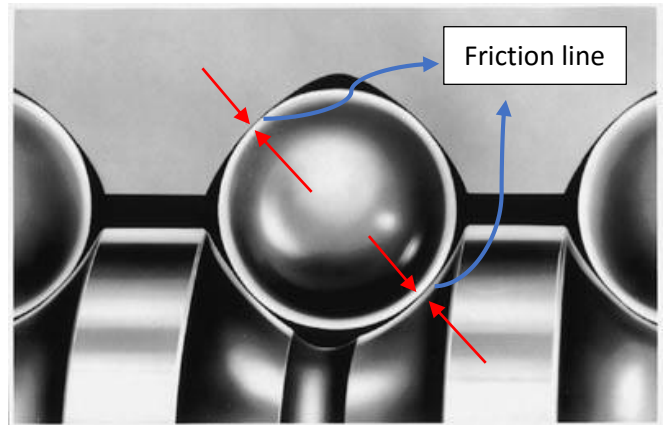


Fig. 2. Ball screw mechanism section

The balls in the ball screw roll away along the helical grooves opened on the shaft. Thus, the sliding movement between the screw and the nut in the transmission shaft is converted into a rolling motion in the ball screw resulting in lower friction coefficients because rolling friction requires much less force than sliding friction. The difference between rolling and sliding friction is illustrated in Figure 3 [22].

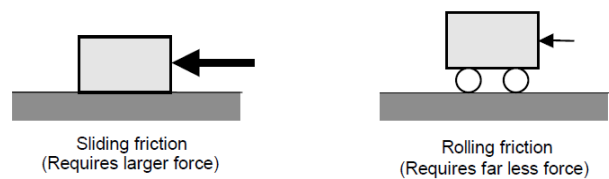


Fig. 3. Difference between sliding friction and rolling friction

In the designing of the ball worm gear mechanism, the concept of the rolling motion of balls in a nest on the shaft and the rolling motion on the worm wheel was addressed. In order to make comparisons during the designing of the worm gear mechanism, commercially available measurements were taken into consideration. To this purpose, a worm gear mechanism with an axis distance (e) of 80 mm and a cycle ratio (i) of 30 was taken as a reference.

2.1. Ball screw shaft design

In the design of the ball screw shaft, hemispherical cavities with a diameter (dw) of 8 mm were formed on a helical 13 mm pitch (pa). In the design phase it was noted that the distance between the axes (e) was 80 mm and the cycle ratio (i) was 30. A technical drawing of the ball screw shaft is given in Figure 4.

The use of cementation steel was planned for the production of the ball screw shaft and in the manufacturing stage, a lathe and vertical milling machine would be used. Shaft diameters were to be made on the lathe. To open the

grooves on the shaft, a spherical end-mill cutter would be used in a vertical milling machine.

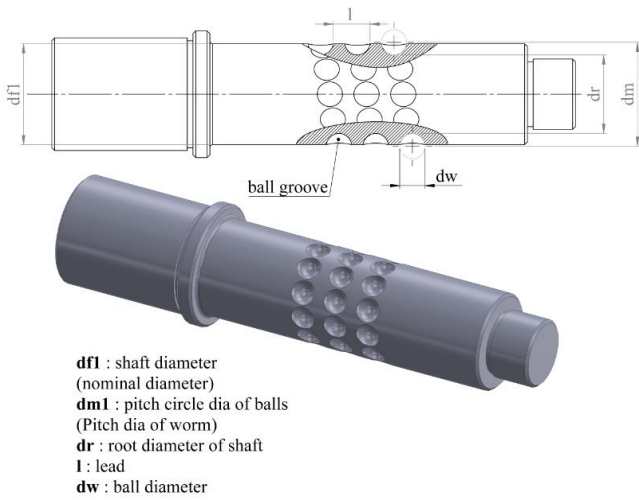


Fig. 4. Technical drawing of ball screw shaft

2.2. Ball worm wheel design

In the design of the ball worm wheel, semi-circular profiles were used instead of module teeth. These profiles, through which the balls will roll, will be slightly larger than the ball diameter to allow the mechanism to work more smoothly. Relevant information about the size of the opening will be provided by future experimental work. A technical drawing of the ball worm wheel is shown in Figure 5.

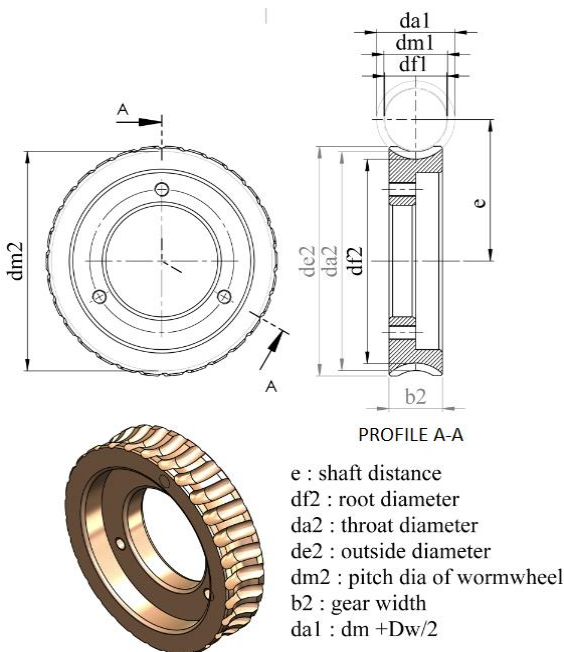


Fig. 5. Technical drawing of ball worm wheel

Cementation steel was planned for use in the manufacture of the ball worm wheel. In the production of the ball worm

wheel, firstly the material was to be brought to the desired length and diameter measurements on the lathe, and then the teeth would be formed with a specially designed milling cutter (Fig. 6).

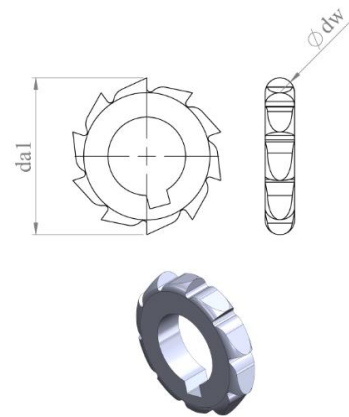


Fig. 6. Special semi-circular mouthed milling cutter

Commercially available milling cutters cannot be used in the manufacture of the ball worm wheel as they are module-mouthed. For this reason, a milling cutter with a semi-circular rim similar to that shown in Figure 6 was selected.

2.3. Guide sleeve design

The guide sleeve in the ball worm gear mechanism was designed to guide the balls within the ball screw mechanism like a ball nut and prevent the balls from spreading around during operation. A hemispherical gap was opened on the guide sleeve to allow for the working zones of the ball screw shaft and ball worm wheel equivalent gear. At the same time, the guide sleeve was fixed in the frame to accommodate axial reaction forces. A technical drawing of the guide sleeve is given in Figure 7.

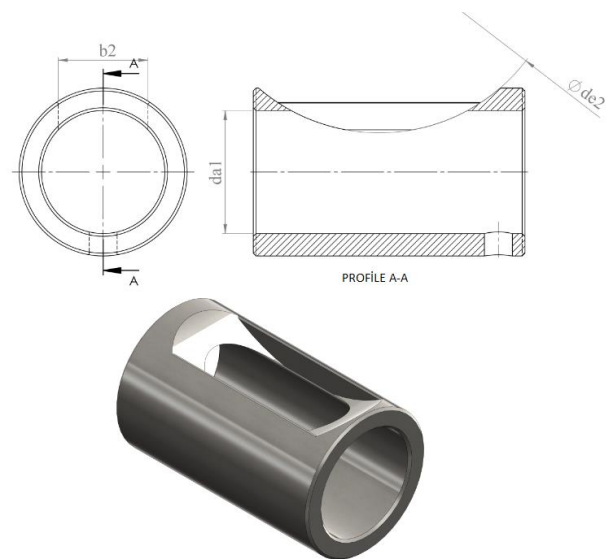


Fig. 7. Technical drawing of the guide sleeve

Conventionally produced steel was used as guide sleeve material. During the manufacturing phase, first, the inside and outside of the steel tube diameter will be machined on the lathe, then the hemispherical spaces will be formed using an end milling cutter on a machining center. An alternative technique would be to manufacture the part by the casting method and machining the necessary features on the side.

2.4. Body design

For the ball worm gear mechanism, in place of a new body design, a commercially available worm gear gearbox body with an 80 mm distance between axes and a conversion ratio of 30 was used. The ball screw shaft clearance of the ready-made body was designed so that the guide sleeve had a smooth fit. In addition, the radial screw holes were drilled on the body to secure the guide sleeve axially. Current worm gear mechanisms have cooling fins on the gearbox body because the operating temperatures are very high. This requirement is expected to be omitted in the newly designed mechanism.

2.5. Assembly of the ball worm gear mechanism

In the installation of the ball screw mechanism, the guide is first placed in the housing and fixed axially and radially. The ball worm screw shaft, on which the ball bits are attached, is then inserted into the guide sleeve. In practice, the holding of the balls onto the shaft will be carried out with the aid of high lubricicity. Deep-grooved ball bearings are installed on both sides of the assembled ball worm screw shaft. The assembly of the ball worm wheel is carried out in the same way. A cross-section view of the assembled ball endless screw mechanism is given in Figure 8.

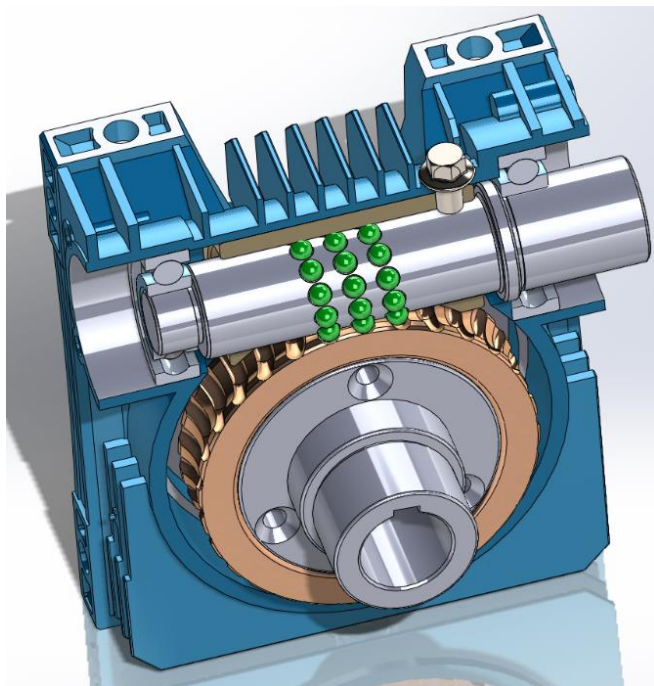


Fig. 8. Cross-section view of the assembled ball worm gear mechanism

The ball worm wheel was designed as two parts for easy assembly and disassembly. The operation of the mechanics was tested through the SolidWorks design program.

In the Motion Study Module of the SolidWorks program, it was observed that the mechanism worked smoothly when contact was established between all parts and the rotational moment was provided via the input shaft.

2.6. Sizing of the ball worm gear mechanism

The pitch / pi connection was used instead of the module to size the ball worm gear mechanism.

The pitch diameter of the worm wheel was calculated using equation (1).

$$d_{m2} = m_a \cdot z_2 = \frac{p_a}{\pi} \cdot z_2 \quad (1)$$

The shaft distance was calculated using equation (2).

$$e = \frac{d_{m1} + d_{m2}}{2} \quad (2)$$

Givens:

Pitch, $p_a = 13 \text{ mm}$

Shaft distance, $e = 80 \text{ mm}$

Number of teeth, $z_1 = 1, z_2 = 30$

Ball diameter, $d_w = 8 \text{ mm}$

Sizes:

Pitch diameter of the ball worm wheel from equation (1)

$$d_{m2} = 124.14 \text{ mm}$$

Pitch diameter of the ball worm shaft from equation (2)

$$d_{m1} = 35.86 \text{ mm}$$

3. Conclusion

In the newly designed ball worm gear mechanism, the ball pieces slide on the worm screw shaft and proceed to move by rolling on the ball worm wheel. Since rolling friction requires less force than sliding friction, the ball worm gear mechanism will have higher efficiency than the conventional worm gear mechanism.

In the ball worm gear mechanism, as the force transmission between the ball worm shaft and the ball worm

wheel is effected by rolling, the mechanism will not generate very high temperatures during operation. This situation will allow the gearbox oil to retain its long-term properties and make the mechanism more durable.

In the worm gear mechanism, since the force is transmitted by sliding, the worm wheel is usually produced from bronze, which is a softer material than that used for the worm shaft. Bronze is expensive and exhibits rapid wear. In the newly designed ball worm gear mechanism, the ball worm wheel will be manufactured from cementation steel, which is much cheaper than bronze. This will both reduce the cost of the mechanism and extend its life.

Acknowledgments

This study was performed in the framework of The Scientific Research Projects Unit of Pamukkale University, Project No: 2013FBE034. The author gratefully acknowledges the support of this institution.

References

- [1] B. Salman, Sonsuz Vidalar ve Sonsuz Vida Karşılık Dişlisi Helisel Dişli Matematik Modellemesi, İstanbul Teknik Üniversitesi Fen bilimler Enstitüsü, İstanbul, 2009.
- [2] J. J. Uicker, G. R. Pennock, J. E. Shigley, Theory of Machines and Mechanisms, 3rd ed., Oxford University Press, New York, 2003.
- [3] P. W. Crosher, Design and Application of the Worm Gear, ASME Press, New York, 2002.
- [4] P. J. Kantert, Manual for Archimedean Screw Pump, Hirshammer Verlag, 2008.
- [5] T. Şekercioğlu, Makine Elemanları Hesap Şekillendirme, 1st ed. Birsen Yayınevi, 2013, pp.327.
- [6] F.C. Babalık, Makine Elemanları ve Konstrüksiyon Örnekleri, 3rd ed., Nobel Yayınevi, 2008.
- [7] ISO/TR 10828-1997, Worm Gears – Geometry of worm profiles, 1997.
- [8] D. Muhns, H. Wittel, D. Jannasch, J. Vobiek, Rolof / Matek Maschinenelemente, 19th, Vieweg Verlag, Wiesbaden, 2011.
- [9] S. Koçak, Bilyeli Sonsuz Vida Mekanizması Tasarımı ve İmalatı, Pamukkale Üniversitesi Fen bilimler Enstitüsü, Denizli, 2014.

- [10] M. Pak, Sonsuz Vidalı Redüktörlerin Bilgisayar Yardımıyla Parametrik Tasarımı, Sakarya Üniversitesi Fen bilimler Enstitüsü, Sakarya, 1998.
- [11] J.R. Colbourne, The use of oversize hobs to cut worm gears, American Gear Manufacturers Association, 1989, pp 89.
- [12] M. De Donno, F.L. Litvin, Computerized design and generation of worm gear drives with stable bearing contact and low transmission errors, ASME Journal of Mechanical Design, vol.121, No. 4, pp. 573–578, 1999.
- [13] D.B. Dooner, A.A. Seirig, The Kinematic Geometry of Gearing: a concurrent engineering approach, 3rd ed. John Wiley and Sons, New York, 1995.
- [14] H. S. Fang, C. B. Tsay, Mathematical model and bearing contacts of the zn-type worm gear set cut by oversize hob cutters, Mechanism and Machine Theory vol. 35, pp. 1689–1708, 2000.
- [15] S.A. Lagutin, Synthesis and application of general type worm gears with localized contact, Tech. Univ., Rektor, 1998.
- [16] F.L. Litvin, Development of gear technology and theory of gearing, NASA Reference Publication pp.1406-1500, 1998.
- [17] I.H. Seol, Design, generation and simulation of meshing of worm-gear drive with longitudinally localized contacts, ASME Journal of Mechanical Design vol.122, no.2, pp. 201–206, 2000.
- [18] V.V. Simon, Computer aided loaded tooth contact analysis in cylindrical worm gears, Journal of Mechanical Design vol.127, pp.973 – 981, 2005.
- [19] V.V. Simon, Influence of tooth errors and shaft misalignments on loaded tooth contact in cylindrical worm gears, Mechanism and Machine Theory vol.41, pp.707–724, 2006.
- [20] D.P. Townsend, Dudley's Gear Handbook, 2nd ed., McGraw-Hill Inc., New York, 1992.
- [21] C. Zanzi, J.I. Pedrero, Application of modified geometry of face gear drive, Computer Methods in Applied Mechanics and Engineering, vol. 194, pp. 3047–3066, 2005.
- [22] Ball Screw. <http://www.nsk.com/products/precision-machine/ballscrew/index.html#tab2> (accessed 07.08.17).

INTERNATIONAL JOURNAL OF ENGINEERING TECHNOLOGIES-IJET

Guide for Authors

The **International Journal of Engineering Technologies (IJET)** seeks to promote and disseminate knowledge of the various topics of engineering technologies. The journal aims to present to the international community important results of work in the fields of engineering such as imagining, researching, planning, creating, testing, improving, implementing, using and asking. The journal also aims to help researchers, scientists, manufacturers, institutions, world agencies, societies, etc. to keep up with new developments in theory and applications and to provide alternative engineering solutions to current.

The *International Journal of Engineering Technologies* is a quarterly published journal and operates an online submission and peer review system allowing authors to submit articles online and track their progress via its web interface. The journal aims for a publication speed of **60 days** from submission until final publication.

The coverage of IJET includes the following engineering areas, but not limited to:

All filed of engineering such as;

Chemical engineering

- Biomolecular engineering
- Materials engineering
- Molecular engineering
- Process engineering

Civil engineering

- Environmental engineering
- Geotechnical engineering
- Structural engineering
- Transport engineering
- Water resources engineering

Electrical engineering

- Computer engineering
- Electronic engineering
- Optical engineering
- Power engineering

Mechanical engineering

- Acoustical engineering
- Manufacturing engineering
- Thermal engineering
- Vehicle engineering

Systems (interdisciplinary) engineering

- Aerospace engineering
- Agricultural engineering
- Applied engineering
- Biological engineering
- Building services engineering
- Energy engineering
- Railway engineering
- Industrial engineering
- Mechatronics
- Military engineering
- Nano engineering
- Nuclear engineering
- Petroleum engineering

Types of Articles submitted should be original research papers, not previously published, in one of the following categories,

- Applicational and design studies.
- Technology development,
- Comparative case studies.
- Reviews of special topics.
- Reviews of work in progress and facilities development.
- Survey articles.
- Guest editorials for special issues.

Editor-in-Chief and Associate Editors

Editor-in-Chief:

Prof. Dr. Mustafa BAYRAM

Associate Editors:

Prof. Dr. A. Burak POLAT

Assoc. Prof. Dr. Baris SEVIM

Asst. Prof. Dr. Ahmet AKTAS

Asst. Prof. Dr. Yalcin CEKIC

Asst. Prof. Dr. Ali ETEMADI

Ethic Responsibilities

The publication of an article in peer-reviewed “*International Journal of Engineering Technologies*” is an essential building block in the development of a coherent and respected network of knowledge. It is a direct reflection of the quality of the work. Peer-reviewed articles support and embody the scientific method. It is therefore important to agree upon standards of expected ethical behavior for all parties involved in the act of publishing: the author, the journal editor, the peer reviewer, the publisher and the society of society-owned or sponsored journals.

All authors are requested to disclose any actual or potential conflict of interest including any financial, personal or other relationships with other people or organizations within three years of beginning the submitted work that could inappropriately influence, or be perceived to influence, their work.

Submission of an article implies that the work described has not been published previously that it is not under consideration for publication elsewhere. The submission should be approved by all authors and tacitly or explicitly by the responsible authorities where the work was carried out, and that, if accepted, it will not be published elsewhere in the same form, in English or in any other language, including electronically without the written consent of the copyright-holder.

Upon acceptance of an article, authors will be asked to complete a “Copyright Form”. Acceptance of the agreement will ensure the widest possible dissemination of information. An e-mail will be sent to the corresponding author confirming receipt of the manuscript together with a “Copyright Form” form or a link to the online version of this agreement.

Author Rights

As a journal author, you retain rights for a large number of author uses, including use by your employing institute or company. These rights are retained and permitted without the need to obtain specific permission from *IJET*. These include:

- ❖ The right to make copies (print or electronic) of the journal article for your own personal use, including for your own classroom teaching use;
- ❖ The right to make copies and distribute copies (including via e-mail) of the journal article to research colleagues, for personal use by such colleagues for scholarly purposes;
- ❖ The right to post a pre-print version of the journal article on internet web sites including electronic pre-print servers, and to retain indefinitely such version on such servers or sites for scholarly purposes
- ❖ the right to post a revised personal version of the text of the final journal article on your personal or institutional web site or server for scholarly purposes
- ❖ The right to use the journal article or any part thereof in a printed compilation of your works, such as collected writings or lecture notes.

Article Style

Authors must strictly follow the guide for authors, or their articles may be rejected without review. Editors reserve the right to adjust the style to certain standards of uniformity. Follow Title, Authors, Affiliations, Abstract, Keywords, Introduction, Materials and Methods, Theory/Calculation, Conclusions, Acknowledgements, References order when typing articles. The corresponding author should be identified with an asterisk and footnote. Collate acknowledgements in a separate section at the end of the article and do not include them on the title page, as a footnote to the title or otherwise.

Abstract and Keywords:

Enter an abstract of up to 250 words for all articles. This is a concise summary of the whole paper, not just the conclusions, and is understandable without reference to the rest of the paper. It should contain no citation to other published work. Include up to six keywords that describe your paper for indexing purposes.

Abbreviations and Acronyms:

Define abbreviations and acronyms the first time they are used in the text, even if they have been defined in the abstract. Abbreviations such as IEEE, SI, MKS, CGS, sc, dc, and rms do not have to be defined. Do not use abbreviations in the title unless they are unavoidable.

Text Layout for Peer Review:

Use single column layout, double spacing and wide (3 cm) margins on white paper at the peer review stage. Ensure that each new paragraph is clearly indicated. Present tables and figure legends in the text where they are related and cited. Number all pages consecutively; use 12 pt font size and standard fonts; Times New Roman, Helvetica, or Courier is preferred.

Research Papers should not exceed 12 printed pages in two-column publishing format, including figures and tables.

Technical Notes and Letters should not exceed 2,000 words.

Reviews should not exceed 20 printed pages in two-column publishing format, including figures and tables.

Equations:

Number equations consecutively with equation numbers in parentheses flush with the right margin, as in (1). To make equations more compact, you may use the solidus (/), the exp function, or appropriate exponents. Italicize Roman symbols for quantities and variables, but not Greek symbols. Use an dash (–) rather than a hyphen for a minus sign. Use parentheses to avoid ambiguities in denominators. Punctuate equations with commas or periods when they are part of a sentence, as in

$$C = a + b \tag{1}$$

Symbols in your equation should be defined before the equation appears or immediately following. Use “Eq. (1)” or “equation (1),” while citing.

Figures and Tables:

All illustrations must be supplied at the correct resolution:

- * Black and white and colour photos - 300 dpi
- * Graphs, drawings, etc - 800 dpi preferred; 600 dpi minimum
- * Combinations of photos and drawings (black and white and color) - 500 dpi

In addition to using figures in the text, upload each figure as a separate file in either .tiff or .eps format during submission, with the figure number.

Table captions should be written in the same format as figure captions; for example, “Table 1. Appearance styles.”. Tables should be referenced in the text unabbreviated as “Table 1.”

References:

Please ensure that every reference cited in the text is also present in the reference list (and viceversa). Any references cited in the abstract must be given in full. Unpublished results and personal communications are not recommended in the reference list, but may be mentioned in the text. Citation of a reference as “in press” implies that the item has been accepted for publication. Number citations consecutively in square brackets [1]. Punctuation follows the bracket [2]. Refer simply to the reference number, as in [3]. Use “Ref. [3]” or Reference [3]” at the beginning of a sentence: “Reference [3] was ...”. Give all authors’ names; use “et al.” if there are six authors or more. For papers published in translated journals, first give the English citation, then the original foreign-language citation.

Books

- [1] J. Clerk Maxwell, *A Treatise on Electricity and Magnetism*, 3rd ed., vol. 2. Oxford:Clarendon Press, 1892, pp.68-73.

Journals

- [2] Y. Yorozu, M. Hirano, K. Oka, and Y. Tagawa, “Electron spectroscopy studies on magneto-optical media and plastic substrate interface”, *IEEE Transl. J. Magn. Japan*, vol. 2, pp. 740-741, August 1987.

Conferences

- [3] Çolak I., Kabalci E., Bayindir R., and Sagiroglu S, “The design and analysis of a 5-level cascaded voltage source inverter with low THD”, *2nd PowerEng Conference*, Lisbon, pp. 575-580, 18-20 March 2009.

Reports

- [4] IEEE Standard 519-1992, Recommended practices and requirements for harmonic control in electrical power systems, *The Institute of Electrical and Electronics Engineers*, 1993.

Text Layout for Accepted Papers:

A4 page margins should be margins: top = 24 mm, bottom = 24 mm, side = 15 mm. Main text should be given in two column. The column width is 87mm (3.425 in). The space between the two columns is 6 mm (0.236 in). Paragraph indentation is 3.5 mm (0.137 in). Follow the type sizes specified in Table. Position figures and tables at the tops and bottoms of columns. Avoid placing them in the middle of columns. Large figures and tables may span across both columns. Figure captions should be centred below the figures; table captions should be centred above. Avoid placing figures and tables before their first mention in the text. Use the abbreviation “Fig. 1,” even at the beginning of a sentence.

Type size (pts.)	Appearance		
	Regular	Bold	<i>Italic</i>
10	Authors’ affiliations, Section titles, references, tables, table names, first letters in table captions, figure captions, footnotes, text subscripts, and superscripts	Abstract	
12	Main text, equations, Authors’ names, ^a		<i>Subheading (1.1.)</i>
24	Paper title		

Submission checklist:

It is hoped that this list will be useful during the final checking of an article prior to sending it to the journal's Editor for review. Please consult this Guide for Authors for further details of any item. Ensure that the following items are present:

- ❖ One Author designated as corresponding Author:
- E-mail address
- Full postal address
- Telephone and fax numbers

❖ All necessary files have been uploaded

- Keywords: a minimum of 4
- All figure captions (supplied in a separate document)
- All tables (including title, description, footnotes, supplied in a separate document)

❖ Further considerations

- Manuscript has been "spellchecked" and "grammar-checked"
- References are in the correct format for this journal
- All references mentioned in the Reference list are cited in the text, and vice versa
- Permission has been obtained for use of copyrighted material from other sources (including the Web)
- Color figures are clearly marked as being intended for color reproduction on the Web (free of charge) and in print or to be reproduced in color on the Web (free of charge) and in black-and-white in print.

Article Template Containing Author Guidelines for Peer-Review

First Author*, Second Author**‡, Third Author***

*Department of First Author, Faculty of First Author, Affiliation of First Author, Postal address

**Department of Second Author, Faculty of First Author, Affiliation of First Author, Postal address

***Department of Third Author, Faculty of First Author, Affiliation of First Author, Postal address

(First Author Mail Address, Second Author Mail Address, Third Author Mail Address)

‡Corresponding Author; Second Author, Postal address, Tel: +90 312 123 4567, Fax: +90 312 123 4567,corresponding@affl.edu

Received: xx.xx.xxxx Accepted:xx.xx.xxxx

Abstract- Enter an abstract of up to 250 words for all articles. This is a concise summary of the whole paper, not just the conclusions, and is understandable without reference to the rest of the paper. It should contain no citation to other published work. Include up to six keywords that describe your paper for indexing purposes. Define abbreviations and acronyms the first time they are used in the text, even if they have been defined in the abstract. Abbreviations such as IEEE, SI, MKS, CGS, sc, dc, and rms do not have to be defined. Do not use abbreviations in the title unless they are unavoidable.

Keywords- Keyword1; keyword2; keyword3; keyword4; keyword5.

2. Introduction

Authors should any word processing software that is capable to make corrections on misspelled words and grammar structure according to American or Native English. Authors may get help by from word

processor by making appeared the paragraph marks and other hidden formatting symbols. This sample article is prepared to assist authors preparing their articles to IJET.

Indent level of paragraphs should be 0.63 cm (0.24 in) in the text of article. Use single column layout, double-spacing and wide (3 cm) margins on white paper at the peer review stage. Ensure that each new paragraph is clearly indicated. Present tables and figure legends in the text where they are related and cited. Number all pages consecutively; use 12 pt font size and standard fonts; Times New Roman, Helvetica, or Courier is preferred. Indicate references by number(s) in square brackets in line with the text. The actual authors can be referred to, but the reference number(s) must always be given. Example: "..... as demonstrated [3, 6]. Barnaby and Jones [8] obtained a different result"

IJET accepts submissions in three styles that are defined as Research Papers, Technical Notes and Letter, and Review paper. The requirements of paper are as listed below:

- Research Papers should not exceed 12 printed pages in two-column publishing format, including figures and tables.
- Technical Notes and Letters should not exceed 2,000 words.
- Reviews should not exceed 20 printed pages in two-column publishing format, including figures and tables.

Authors are requested write equations using either any mathematical equation object inserted to word processor or using independent equation software. Symbols in your equation should be defined before the equation appears or immediately following. Use "Eq. (1)" or "equation (1)," while citing. Number equations consecutively with equation numbers in parentheses flush with the right margin, as in Eq. (1). To make equations more compact, you may use the solidus (/), the exp function, or appropriate exponents. Italicize Roman symbols for quantities and variables, but not Greek symbols. Use an dash (–) rather than a hyphen for a minus sign. Use parentheses to avoid ambiguities in denominators. Punctuate equations with commas or periods when they are part of a sentence, as in

$$C = a + b \tag{1}$$

Section titles should be written in bold style while sub section titles are italic.

3. Figures and Tables

3.1. Figure Properties

All illustrations must be supplied at the correct resolution:

- Black and white and colour photos - 300 dpi
- Graphs, drawings, etc - 800 dpi preferred; 600 dpi minimum
- Combinations of photos and drawings (black and white and colour) - 500 dpi

In addition to using figures in the text, Authors are requested to upload each figure as a separate file in either .tiff or .eps format during submission, with the figure number as Fig.1., Fig.2a and so on. Figures are cited as “Fig.1” in sentences or as “Figure 1” at the beginning of sentence and paragraphs. Explanations related to figures should be given before figure. Figures and tables should be located at the top or bottom side of paper as done in accepted article format.



Figure 1. Engineering technologies.

Table captions should be written in the same format as figure captions; for example, “Table 1. Appearance styles.”. Tables should be referenced in the text unabbreviated as “Table 1.”

Table 1. Appearance properties of accepted manuscripts

Type size (pts.)	Appearance		
	Regular	Bold	<i>Italic</i>
10	Authors’ affiliations, Abstract, keywords, references, tables, table names, figure captions, footnotes, text subscripts, and superscripts	Abstract	
12	Main text, equations, Authors’ names, Section titles		<i>Subheading (1.1.)</i>
24	Paper title		

4. Submission Process

The *International Journal of Engineering Technologies* operates an online submission and peer review system that allows authors to submit articles online and track their progress via a web interface. Articles that are prepared referring to this template should be controlled according to submission checklist given in “Guide f Authors”. Editor handles submitted articles to IJET primarily in order to control in terms of compatibility to aims and scope of Journal.

Articles passed this control are checked for grammatical and template structures. If article passes this control too, then reviewers are assigned to article and Editor gives a reference number to paper. Authors registered to online submission system can track all these phases.

Editor also informs authors about processes of submitted article by e-mail. Each author may also apply to Editor via online submission system to review papers related to their study areas. Peer review is a critical element of publication, and one of the major cornerstones of the scientific process. Peer Review serves two key functions:

- Acts as a filter: Ensures research is properly verified before being published
- Improves the quality of the research

5. Conclusion

The conclusion section should emphasize the main contribution of the article to literature. Authors may also explain why the work is important, what are the novelties or possible applications and extensions. Do not replicate the abstract or sentences given in main text as the conclusion.

Acknowledgements

Authors may acknowledge to any person, institution or department that supported to any part of study.

References

- [1] J. Clerk Maxwell, *A Treatise on Electricity and Magnetism*, 3rd ed., vol. 2. Oxford:Clarendon Press, 1892, pp.68-73.
(Book)
- [2] H. Poor, *An Introduction to Signal Detection and Estimation*, New York: Springer-Verlag, 1985, ch. 4. (Book Chapter)
- [3] Y. Yorozu, M. Hirano, K. Oka, and Y. Tagawa, "Electron spectroscopy studies on magneto-optical media and plastic substrate interface", *IEEE Transl. J. Magn. Japan*, vol. 2, pp. 740-741, August 1987. (Article)
- [4] E. Kabalcı, E. Irmak, I. Çolak, "Design of an AC-DC-AC converter for wind turbines", *International Journal of Energy Research*, Wiley Interscience, DOI: 10.1002/er.1770, Vol. 36, No. 2, pp. 169-175. (Article)
- [5] I. Çolak, E. Kabalci, R. Bayindir R., and S. Sagiroglu, "The design and analysis of a 5-level cascaded voltage source inverter with low THD", *2nd PowerEng Conference*, Lisbon, pp. 575-580, 18-20 March 2009. (Conference Paper)
- [6] IEEE Standard 519-1992, Recommended practices and requirements for harmonic control in electrical power systems, *The Institute of Electrical and Electronics Engineers*, 1993. (Standards and Reports)

Article Template Containing Author Guidelines for Accepted Papers

First Author*, Second Author**‡, Third Author***

*Department of First Author, Faculty of First Author, Affiliation of First Author, Postal address

**Department of Second Author, Faculty of First Author, Affiliation of First Author, Postal address

***Department of Third Author, Faculty of First Author, Affiliation of First Author, Postal address

(First Author Mail Address, Second Author Mail Address, Third Author Mail Address)

‡Corresponding Author; Second Author, Postal address, Tel: +90 312 123 4567,

Fax: +90 312 123 4567,corresponding@affl.edu

Received: xx.xx.xxxx Accepted:xx.xx.xxxx

Abstract- Enter an abstract of up to 250 words for all articles. This is a concise summary of the whole paper, not just the conclusions, and is understandable without reference to the rest of the paper. It should contain no citation to other published work. Include up to six keywords that describe your paper for indexing purposes. Define abbreviations and acronyms the first time they are used in the text, even if they have been defined in the abstract. Abbreviations such as IEEE, SI, MKS, CGS, sc, dc, and rms do not have to be defined. Do not use abbreviations in the title unless they are unavoidable.

Keywords Keyword1, keyword2, keyword3, keyword4, keyword5.

1. Introduction

Authors should use any word processing software that is capable of making corrections on misspelled words and grammar structure according to American or British English. Authors may get help from word processor by making visible the paragraph marks and other hidden formatting symbols. This sample article is prepared to assist authors preparing their articles to IJET.

Indent level of paragraphs should be 0.63 cm (0.24 in) in the text of article. Use single column layout, double-spacing and wide (3 cm) margins on white paper at the peer review stage. Ensure that each new paragraph is clearly indicated. Present tables and figure legends in the text where they are related and cited. Number all pages consecutively; use 12 pt font size and standard fonts; Times New Roman, Helvetica, or Courier is preferred. Indicate references by number(s) in square brackets in line with the text. The actual authors can be referred to, but the reference number(s) must always be

given. Example: "... as demonstrated [3,6]. Barnaby and Jones [8] obtained a different result"

IJET accepts submissions in three styles that are defined as Research Papers, Technical Notes and Letter, and Review paper. The requirements of paper are as listed below:

➤ Research Papers should not exceed 12 printed pages in two-column publishing format, including figures and tables.

➤ Technical Notes and Letters should not exceed 2,000 words.

➤ Reviews should not exceed 20 printed pages in two-column publishing format, including figures and tables.

Authors are requested write equations using either any mathematical equation object inserted to word processor or using independent equation software. Symbols in your equation should be defined before the equation appears or immediately following. Use "Eq. (1)" or "equation (1),"

while citing. Number equations consecutively with equation numbers in parentheses flush with the right margin, as in Eq. (1). To make equations more compact, you may use the solidus (/), the exp function, or appropriate exponents. Italicize Roman symbols for quantities and variables, but not Greek symbols. Use an dash (-) rather than a hyphen for a minus sign. Use parentheses to avoid ambiguities in denominators. Punctuate equations with commas or periods when they are part of a sentence, as in

$$C = a + b \quad (1)$$

Section titles should be written in bold style while sub section titles are italic.

6. Figures and Tables

6.1. Figure Properties

All illustrations must be supplied at the correct resolution:

- Black and white and colour photos - 300 dpi
- Graphs, drawings, etc - 800 dpi preferred; 600 dpi minimum
- Combinations of photos and drawings (black and white and colour) - 500 dpi

In addition to using figures in the text, Authors are requested to upload each figure as a separate file in either

Table 1. Appearance properties of accepted manuscripts

Type size (pts.)	Appearance		
	Regular	Bold	<i>Italic</i>
10	Main text, section titles, authors' affiliations, abstract, keywords, references, tables, table names, figure captions, equations, footnotes, text subscripts, and superscripts	Abstract-	<i>Subheading (1.1.)</i>
12	Authors' names,		
24	Paper title		

6.2. Text Layout for Accepted Papers

A4 page margins should be margins: top = 24 mm, bottom = 24 mm, side = 15 mm. The column width is 87mm (3.425 in). The space between the two columns is 6 mm (0.236 in). Paragraph indentation is 3.5 mm (0.137 in). Follow the type sizes specified in Table. Position figures and tables at the tops and bottoms of columns. Avoid placing them in the middle of columns. Large figures and tables may span across both columns. Figure captions should be centred below the figures; table captions should be centred above. Avoid placing figures and tables before their first mention in

.tiff or .eps format during submission, with the figure number as Fig.1., Fig.2a and so on. Figures are cited as "Fig.1" in sentences or as "Figure 1" at the beginning of sentence and paragraphs. Explanations related to figures should be given before figure.



Fig. 1. Engineering technologies.

Figures and tables should be located at the top or bottom side of paper as done in accepted article format. Table captions should be written in the same format as figure captions; for example, "Table 1. Appearance styles.". Tables should be referenced in the text unabbreviated as "Table 1."

the text. Use the abbreviation "Fig. 1," even at the beginning of a sentence.

7. Submission Process

The International Journal of Engineering Technologies operates an online submission and peer review system that allows authors to submit articles online and track their progress via a web interface. Articles that are prepared referring to this template should be controlled according to submission checklist given in "Guide f Authors". Editor handles submitted articles to IJET primarily in order to control in terms of compatibility to aims and scope of Journal. Articles passed this control are checked for

grammatical and template structures. If article passes this control too, then reviewers are assigned to article and Editor gives a reference number to paper. Authors registered to online submission system can track all these phases. Editor also informs authors about processes of submitted article by e-mail. Each author may also apply to Editor via online submission system to review papers related to their study areas. Peer review is a critical element of publication, and one of the major cornerstones of the scientific process. Peer Review serves two key functions:

- Acts as a filter: Ensures research is properly verified before being published
- Improves the quality of the research

8. Conclusion

The conclusion section should emphasize the main contribution of the article to literature. Authors may also explain why the work is important, what are the novelties or possible applications and extensions. Do not replicate the abstract or sentences given in main text as the conclusion.

Acknowledgements

Authors may acknowledge to any person, institution or department that supported to any part of study.

References

- [7] J. Clerk Maxwell, A Treatise on Electricity and Magnetism, 3rd ed., vol. 2. Oxford:Clarendon Press, 1892, pp.68-73. (Book)
- [8] H. Poor, An Introduction to Signal Detection and Estimation, New York: Springer-Verlag, 1985, ch. 4. (Book Chapter)
- [9] Y. Yorozu, M. Hirano, K. Oka, and Y. Tagawa, "Electron spectroscopy studies on magneto-optical media and plastic substrate interface", IEEE Transl. J. Magn. Japan, vol. 2, pp. 740-741, August 1987. (Article)
- [10] E. Kabalcı, E. Irmak, I. Çolak, "Design of an AC-DC-AC converter for wind turbines", International Journal of Energy Research, Wiley Interscience, DOI: 10.1002/er.1770, Vol. 36, No. 2, pp. 169-175. (Article)
- [11] I. Çolak, E. Kabalcı, R. Bayindir R., and S. Sagiroglu, "The design and analysis of a 5-level cascaded voltage source inverter with low THD", 2nd PowerEng Conference, Lisbon, pp. 575-580, 18-20 March 2009. (Conference Paper)
- [12] IEEE Standard 519-1992, Recommended practices and requirements for harmonic control in electrical power systems, The Institute of Electrical and Electronics Engineers, 1993. (Standards and Reports)

**INTERNATIONAL JOURNAL OF ENGINEERING TECHNOLOGIES (IJET)
COPYRIGHT AND CONSENT FORM**

This form is used for article accepted to be published by the IJET. Please read the form carefully and keep a copy for your files.

TITLE OF ARTICLE (hereinafter, "The Article"):

.....
.....
.....

LIST OF AUTHORS:

.....
.....
.....

CORRESPONDING AUTHOR'S ("The Author") NAME, ADDRESS, INSTITUTE AND EMAIL:

.....
.....
.....

COPYRIGHT TRANSFER

The undersigned hereby transfers the copyright of the submitted article to International Journal of Engineering Technologies (the "IJET"). The Author declares that the contribution and work is original, and he/she is authorized by all authors and/or grant-funding agency to sign the copyright form. Author hereby assigns all including but not limited to the rights to publish, distribute, reprints, translates, electronic and published derivatives in various arrangements or any other versions in full or abridged forms to IJET. IJET holds the copyright of Article in its own name.

Author(s) retain all rights to use author copy in his/her educational activities, own websites, institutional and/or funder's web sites by providing full citation to final version published in IJET. The full citation is provided including Authors list, title of the article, volume and issue number, and page number or using a link to the article in IJET web site. Author(s) have the right to transmit, print and share the first submitted copies with colleagues. Author(s) can use the final published article for his/her own professional positions, career or qualifications by citing to the IJET publication.

Once the copyright form is signed, any changes about the author names or order of the authors listed above are not accepted by IJET.

Authorized/Corresponding Author

Date/ Signature